

Emil Spreitzer, BSc

Regulation of Cellular Senescence

MASTERARBEIT

zur Erlangung des akademischen Grades

Master of Science

Masterstudium Biochemie und Molekulare Biomedizin

eingereicht an der

Technischen Universität Graz

Betreuer

Assoz. Prof. Priv.-Doz. Mag. Dr.rer.nat. Tobias Madl

Medizinische Universität Graz
Gottfried Schatz Forschungszentrum

EIDESSTATTLICHE ERKLÄRUNG

Ich erkläre an Eides statt, dass ich die vorliegende Arbeit selbstständig verfasst, andere als die angegebenen Quellen/Hilfsmittel nicht benutzt, und die den benutzten Quellen wörtlich und inhaltlich entnommenen Stellen als solche kenntlich gemacht habe. Das in TUGRAZonline hochgeladene Textdokument ist mit der vorliegenden Masterarbeit identisch.

11.10.2018

Datum



Unterschrift

ABSTRACT	6
ZUSAMMENFASSUNG	8
INTRODUCTION	10
Aging	10
Cellular Senescence	12
Induction of Senescence	12
Cell Cycle Arrest	13
Apoptosis Resistance	14
Cellular tumor antigen p53	16
Functions	16
Structure	17
Regulation	20
FOXOs	22
Function	22
Structure	23
Regulation	23
p53 – FOXOs	24
OBJECTIVES	25
MATERIAL AND METHODS	27
Expression and purification of human p53 and FOXO4 proteins	27
Site-directed mutagenesis	28
Transformation	30
Amplification and isolation of plasmid DNA	31
Protein expression	31
Harvesting and lysis of <i>E.coli</i> cells	32
Protein purification	32
TEV cleavage	33

Size exclusion chromatography	33
Sodium dodecyl sulfate polyacrylamide gel electrophoresis	33
Nuclear Magnetic Resonance spectroscopy	34
Basic principles of Nuclear Magnetic Resonance	34
NMR for interaction studies	36
NMR assignment strategies	39
NMR Molecular dynamics	43
NMR for detection of post-translational modifications	44
Small-Angle X-ray Scattering	45
Basic principle of SAXS	45
Microscale Thermophoresis	46
RESULTS	48
Expression and Purification	48
Identification of Binding sites on p53	48
p53 physically interacts with FOXO4 Forkhead Domain with high nanomolar affinity	49
The DNA Binding Domain of p53 does not physically interact with FOXO4 Forkhead Domain	51
FOXO4 - p53 Interaction is mediated by two subdomains within the N-terminal Transactivation Domain of p53	53
SAXS confirms that two molecules of FOXO4 Forkhead Domain can bind to the N-terminal Transactivation Domain of p53	59
Transactivation domain 2 of p53 can individually bind FOXO4 Forkhead domain	61
Regulation of FOXO4 – p53 Interaction	63
Serine 15 of p53 Transactivation Domain is phosphorylated in HEK293T cells	63
Phosphorylation mimicking S46E mutation does not change binding of p53 Transactivation domain to FOXO4 Forkhead Domain	65
DISCUSSION	67
ACKNOWLEDGEMENTS	73
APPENDIX	75
Buffers and Solutions	75
Alignments	79

BIBLIOGRAPHY	80
TABLE OF FIGURES	84
ABBREVIATIONS	86
APPENDIX II	88
Figure Licences	88

Abstract

Aging is the process of getting older and is characterized by a decline of physiological mechanisms. It is also major risk factor for age-related diseases such as cancer, cardiovascular and neurodegenerative disorders. One reason that we age, is the accumulation of senescent cells over time. Upon DNA-damage they undergo senescence and are trapped in a stable cell cycle arrest.

Pivotal part in deciding the cell's fate is the interaction of the "guardian of the genome" cellular tumor antigen p53 (p53) and the "longevity gene" Forkhead box protein O4 (FOXO4). The de Keizer group designed a FOXO4-derived peptide, called FOXO4-DRI in order to dissociate the FOXO4 – p53 complex. Senescent IMR90 fibroblasts were efficiently and selectively targeted and eliminated by the peptide. Furthermore, treatment of fast-aging and naturally aged mice with FOXO4-DRI restored their fitness, fur density and renal function.

Targeting the FOXO4 – p53 interaction is a promising way to cure age-related diseases and eventually "cure" aging. Molecular details of the FOXO4 – p53 interaction are essential to understand regulation of senescence and apoptosis and are key for optimizing or finding drugs to eliminate senescent cells. In this perspective, this thesis aims to identify the yet unknown binding site of FOXO4 on p53, which is necessary to determine the atomic structure of the complex and indispensable for understanding the regulatory mechanisms deciding the cell's fate.

An *in-vitro* approach using Nuclear Magnetic Resonance (NMR) spectroscopy, complemented with other molecular biological and biophysical methods was applied to gain insight into the p53 – FOXO4 interaction. Human protein constructs of p53 and FOXO4 were heterologously expressed in *Escherichia coli* cells and purified using immobilized metal ion affinity chromatography and Size Exclusion Chromatography.

We identified the disordered N-terminal region of p53 as binding site for the FOXO4 Forkhead domain. Both of the subdomains, Transactivation domain 1 (TAD1) and Transactivation domain 2 (TAD2) are involved in binding. Based on chemical shift perturbation analysis the Transactivation domain 2 is the main binding site. Small-angle X-ray experiments revealed that two molecules of FOXO4 Forkhead bind to one molecule of the p53 N-terminal region.

Within the main binding site is the phosphorylation site for Homeodomain-interacting protein kinase 2 (HIPK2), which was shown to promote apoptosis. Mutation of Serine

46 to Glutamine, which mimics the phosphorylation, did not alter binding of p53 transactivation domain to FOXO4 Forkhead domain.

Furthermore, we demonstrate a proof-of-principle experiment using *in-cell* phosphorylation to identify two phosphorylation sites of p53 transactivation domain in HEK293T cell lysate.

These findings allow to put the FOXO4 - p53 interaction in context with already known regulatory networks and interaction partners of both proteins. Additionally, the results obtained in this study can be used as starting point to determine the atomic resolution structure of the complex.

Zusammenfassung

Altern ist ein unwiderruflich fortschreitender Prozess, der durch den Verlust von physiologischen Mechanismen gekennzeichnet ist. Altern ist der beim weiten wichtigste Risikofaktor für diverse Erkrankungen wie Krebs, Kardiovaskuläre- oder Neurodegenerative Erkrankungen. Einer der Ursachen der dem Altern zu Grunde liegt ist die Anhäufung von seneszenten Zellen im Laufe der Zeit. In Folge von DNA Schäden werden diese Zellen in einem stabilen Zellzyklus-Arrest gehalten (1).

Die Interaktion des „Wächters des Genoms“ p53 und des „Langlebigkeits-Gens“ FOXO4 von zentraler Rolle, das Schicksal der Zelle zu entscheiden. Die de Keizer Gruppe entwarf basierend auf FOXO4 ein Peptide, namens FOXO4-DRI, um die Formation des FOXO4 – p53 Komplexes zu unterbinden. Seneszente IMR90 Fibroblasten wurden effizient und selektive durch das Peptide eliminiert. Des Weiteren konnte in natürlich gealterten Mäusen und in einem schnell alternden Mausmodell die Fitness, Felddichte und Nierenfunktion wiederhergestellt werden durch Behandlung mit FOXO4-DRI (2).

Unterbindung der FOXO4-DRI Interaktion ist ein vielversprechendes Ziel für Therapien um altersbedingte Erkrankungen und das Altern an sich „zu heilen“. Molekulare Details der FOXO4 – p53 sind essenziell um die Regulation von Seneszenz und Apoptose zu verstehen und notwendig um Medikamente zu entwickeln oder zu verbessern.

In meiner Arbeit versuche ich die noch unbekanntenen Bindestellen für FOXO4 an p53 zu identifizieren. Die Identifikation der Bindestellen sind Voraussetzung um die atomare Struktur des FOXO4 – p53 Komplexes mittels NMR zu lösen und unabdingbar um die regulatorischen Mechanismen zu verstehen, die über das Schicksal von Zellen entscheiden.

Um Einblick in die FOXO4 – p53 Interaktion zu erhalten, wurde Kernspinresonanz Spektroskopie angewendet. Diese Technik wurde von weiteren molekularbiologischen und biophysikalischen Methoden ergänzt. Humane Proteinkonstrukte wurden heterolog in *Escherichia coli* Zellen exprimiert und mittels immobilisierter Metallionenaffinitätschromatographie und Größenausschlusschromatographie aufgereinigt.

Die unstrukturierte N-terminale 1-94 Region von p53 wurde als Bindestelle für FOXO4 identifiziert. Beide der Subdomänen, die Transaktivierungsdomäne 1 und die Transaktivierungsdomäne 2 sind in die Bindung involviert. Basierend auf der Änderung der chemischen Verschiebungen konnte die Transaktivierungsdomäne 2 als

Hauptbindestelle identifiziert werden. Röntgen-Kleinwinkelstreuung Experimente zeigen, dass zwei FOXO4 Forkhead Moleküle an ein Molekül p53 1-94 binden.

Innerhalb der Hauptbindestelle befindet sich die Phosphorylierungsstelle für HIPK2, die im Zusammenhang mit Induktion von Apoptose beschrieben wurde. Eine Phosphorylierung-simulierende Mutante von Serin 46 veränderte das Bindevverhalten von p53 an FOXO4 Forkhead nicht im Vergleich zu Wild-Typ p53.

Desweiteren, zeigen wir den Konzeptnachweis von in-Zell Phosphorylierung, um Phosphorylierungsstellen der Transaktivierungsdomäne von p53 in HEK293T Zelllysat zu identifizieren.

Ergebnisse dieser Studie ermöglichen es die FOXO4 – p53 in Kontext schon bekannter Regulationsnetzwerke zu setzen. Außerdem können die Ergebnisse als Startpunkt die Bestimmung der atomaren Struktur verwendet werden.

Introduction

Aging

Aging is an issue with which scientists, artists or philosophers have been involved throughout history (me too). The desire for old age and longevity really is not new. It would be nice if a legend like the one of the “fountain of youth” would be true. The fountain of youth is a very special spring: everyone who drinks from its water or bathes in it gets back his youth. (We can read about a magical fountain in writings by Herodotus (5th century BC) or the Alexander romance.)

In the 16th century the Spanish explorer Juan Ponce de León (1474 - 1521) shall have searched the fountain of youth. (His life was not very long, so I think he did not find it.) And I am sure, I am not the one to find the fountain of youth.

But the desire for longevity is still alive.

“Old age is the supreme evil, because it deprives us of all pleasures, leaving us only the appetite for them, and brings with it all sufferings. Nevertheless, we fear death, and we desire old age” (3). This is how Giacomo Leopardi (1798 - 1837) described the ambivalent human perception of aging.

Not long ago, 1999 US president Bill Clinton said at the Millennium evening at the White House: “We want to live forever, and we're getting there.” (<http://smapp.rand.org/ise/ourfuture/Rosetta/millennium.html>, called up 28.09.2018).

I do not believe in legends and wishes not always come true. So, I decided to try the long and hard way of scientific work.

Biologically the process of aging can be described as functional decline of physiological mechanisms, which strictly depends on the passage of time (1). This refers to changes, which are not malicious, such as wrinkles and graying hair, but also to changes which are key risk factors for age-related diseases such as cancer, cardiovascular or neurodegenerative disorders (1, 4).

Aging has long been considered a process of decline of physiologic functions in random fashion, leading to accumulation of cellular damage in stochastic fashion and consequently tissue decline and finally death (1). However, it is known today that aging can be regulated by evolutionary conserved biochemical and genetic processes and pathways (1). This does not implicate that aging is a programmed process, but rather a consequence of genetic programs that determine developmental growth early in life and processes which allow the organism to adopt to the environment and withstand harmful influences (1).

Lopez-Otin et al listed, based on the model of Hanahan and Weinberg's Hallmarks of Cancer, 9 distinct cellular and molecular mechanism that contribute to the aging process and together determine the aging phenotype (5, 6).

- Genomic Instability
- Telomer Attrition
- Epigenetic Alterations
- Loss of Proteostasis
- Deregulated Nutrient Sensing
- Mitochondrial Dysfunction
- Cellular Senescence
- Stem Cell Exhaustion
- Altered Intercellular Communication

Anti-aging therapies target those hallmarks in order to slow down and even prevent aging. For almost all of the hallmarks there is a compound described, in various phases of trial, dedicated to interfere with the mechanism and aging (7). Antioxidants target reactive oxygen species (ROS), which are one the reasons for genomic instability and DNA damage, caloric restriction mimetics reduce the calorie intake to compensate and prevent deregulated nutrient sensing and there are pharmacologic inducers of

autophagy, telomerase activators and epigenetic drugs (7). Despite all different efforts we are still aging.

One promising approach was described by Baar et al. in targeting senescent cells, resulting in restored juvenile phenotype of aged mice (2)

Cellular Senescence

Cellular senescence can be defined as stable arrest of the cell cycle, which is coupled to characteristic phenotypic changes (8).

DNA damage accumulates in all organisms throughout life and is usually dealt with by sophisticated DNA repair machineries. But in case of unresolved DNA damage, cells can either undergo apoptosis, where they are removed by programmed-cell death or they can undergo senescence where they are trapped in stable cell cycle arrest, to prevent propagation of the damage. Cellular senescence is therefore considered a stress response to protect against cancer. Senescence has also beneficial effect in development to build up body mass and in regenerative processes such as wound healing (9). But on the negative side senescence may also contribute to organismal aging (10). Excessive accumulation of senescent cells can negatively affect regenerative capacities and generate a proinflammatory milieu, also known as senescence associated secretory phenotype (SASP), creating a favorable environment for onset and progression of age-related diseases (8). Diverse stimuli including oxidative stress, genotoxic damage, cytokines, chromatin disorganization, oncogene activation and various mitogens can induce senescence (11).

Characteristic for senescence is the stable cell cycle arrest, that is unresponsive to extrinsic or environmental growth factor induction (11). This is achieved via activation of various cycle dependent kinase inhibitors and the induction of anti-apoptotic genes (8). Upon Oncogene-induced senescence cells stopped dividing even when Ras/MAPK pathway is constitutively active, thus acting as a checkpoint against neoplastic transformation (11).

Induction of Senescence

Shortening of telomeres is one molecular mechanism, that can induce a stable cell cycle arrest and triggers senescence (10). Telomeres consist of repetitive DNA elements at the end of linear chromosomes that protect DNA ends from degradation and recombination. Replicative DNA polymerases lack the ability to replicate completely to the terminal ends of linear DNA molecules. This can only be

accomplished by a specialized DNA polymerase known as telomerase. However, many mammalian somatic cells do not express telomerase, which leads to progressive and cumulative telomere shortening (5). Once telomeres reach a critical short length either senescence or apoptosis, depending on the cell type and context, is initiated via activation of cellular tumor antigen p53 (p53) and the cyclin-dependent kinase inhibitor p21. Many studies linked telomere length with aging and age-related diseases (10, 12, 13). Another form of DNA damage, DNA double-strand breaks can activate senescence via DNA-damage-response in consequence of phosphorylation of histone H2A histone family member X (H2AX) by Ataxia Telangiectasia mutated kinase (ATM) (8). The induced DNA-damage-response involves degradation of methyltransferases, causing a reduction in H3K9 dimethylation at promoter sites of Interleukin-6 and Interleukin-8, which are associated with the SASP (8). Persistence of DNA-damage-response results in phosphorylation of multiple serine residues of p53 and thereby in stabilization and activation of p53 (8).

DNA mutations of oncogenes as for example Ras or B-Raf proto-oncogen (BRAF) can trigger oncogene-induced senescence (10). Oncogenic Ras inactivates Breast cancer 1 (BRCA1) DNA repair complex, causing accumulation of DNA damage (14). In consequence Ras associated domain-containing protein (NORE1A), a Ras associated domain family member, regulates senescence by interacting with p53 and retinoblastoma protein (RB). NORE1A enhances stabilizing phosphorylation of p53 by HIPK2 and promotes the acetylation of p53, thereby inhibiting proapoptotic phosphorylation of p53 (Details described below in the p53 chapter) (14-16).

Also other mechanisms can induce senescence as for example chemotherapeutic agents can cause so called therapy-induced senescence, which enhances the side effects of cancer treatments (11). It was shown in cell culture and mice that inflammatory environment created by senescent cells can induce new senescent cells via the Transforming growth factor β (TGF- β) pathways (17).

Cell Cycle Arrest

Focal point for the stable cell cycle arrest during senescence is the INK4a/ARF locus, encoding two critical tumor suppressors, p16INK4 and ARF and the cyclin dependent kinase inhibitor p21 (10). p16INK4 is an inhibitor of the cyclin-dependent kinases CDK4 and CDK6 and acts by imposing a G1 cell cycle arrest, ARF regulates the stability of p53 by inactivating the p53-degrading ubiquitin ligase mouse double minute 2 homolog

(MDM2) (10). In most tissues of young organisms INK4a/ARF locus is very low expressed but becomes de-repressed with aging (10).

It was shown that via knockout of p16, senescent cells can be eliminated, resulting in a delayed onset of age-related phenotypes (18). Regulation of p16 is achieved at epigenetic level via methyltransferases DNA Methyltransferase 3 β (DNMT3 β) and DNA Methyltransferase 1 (DNMT1) as well as at transcriptional level by transcription factors specificity protein 1 (Sp1), E26 transformation-specific (Ets), activator protein 1 (AP1) and Peroxisome proliferator-activated receptor γ (PPAR γ) (8). In consequence of ARF-mediated stabilization of p53, p53 activates the expression of the cyclin-dependent kinase inhibitor p21. p21 is capable of inhibiting a range of CDKs, but paradoxically is also necessary for cell cycle progression (8). Transactivation of p21 is mainly mediated by p53, but also TNF- β pathway can activate p21. A complex regulatory network controls p21 function involving various transcription factors, microRNAs, RNA-binding proteins or kinases (8).

Apoptosis Resistance

Senescence cells choose upon irresolvable DNA damage to undergo senescence instead of apoptosis. In transient senescence, senescent cells are eliminated via the immune system and not via apoptosis (11). Reason for this, is the activation of several pro-survival factors that allow senescent cells to resist apoptosis.

Even apoptosis inducers are not able to downregulate the anti-apoptotic protein B-cell CLL/lymphoma 2 (BCL2) due to chronic activation of the transcription factor cAMP response element binding protein (CREB). Enrichment of repressive histone methylation of H4K20 represses the pro-apoptotic gene Bax. Additional pro-survival networks have been associated with senescence involving Phosphatidylinositol-4,5-bisphosphate 3-kinase (PI3K), p21, BCL-XL and plasminogen activated inhibitor-2 (8). Especially the anti-apoptotic factors BCL-XL and BCL-W are essential for survival of senescent cells.

The cyclin-dependent kinase inhibitor p21 maintains the viability of senescent cells. p21 prevents c-Jun N-terminal kinases (JNK) and caspase signaling under persistent DNA damage, stopping cell death. Knockdown of p21 causes multiple DNA lesions, which activates ATM and NF- κ B leading to cell death in a caspase- and JNKdependent manner. In mice p21 knockout eliminates liver senescent cells and alleviates liver fibrosis (19).

Together with the de Keizer group, our group recently identified another mechanism deciding cell's fate between apoptosis and senescence (2).

RNA sequencing experiments of senescent IMR90 fibroblasts induced by ionizing radiation surprisingly revealed upregulation of pro-apoptotic genes PUMA and BIM and downregulation of anti-apoptotic genes BCL-2. This suggested that the senescent cells are primed to undergo apoptosis, but the death program is restricted. Among the overexpressing genes are the FOXO transcription factors, which were described as longevity genes. Senescence-inducing ionizing radiation had mild effect on FOXO1 and FOXO3 expression, but FOXO4 expression increased. FOXO4 inhibition in senescent cells reduced their viability, but not the one of control cells. This indicates that FOXO4 favors senescence over apoptosis and helps repressing apoptosis to maintain viability (2).

Another protein, which was described to control both apoptosis and senescence is p53. In senescent cells p53 localizes to DNA segments with chromatin alterations reinforcing senescence (DNA-SCARS), which are nuclear substructures with persistent DNA damage and associated proteins. Interestingly FOXO4 is also localized there, interacting with p53 and trapping it in the nucleus (2).

Based on previous findings on the FOXO3 – p53 interaction a peptide containing D-aminoacids in a retro-reversed sequence, called FOXO4-DRI, was designed to interfere with the FOXO4 – p53 interaction (2, 20). Using NMR spectroscopy, it was shown that FOXO4 and p53 indeed interact and that the interaction can be inhibited using FOXO4-DRI (2).

In senescent cells, FOXO4-DRI treatment resulted in decreased viability, whereas control cells were not affected by the treatment. Interference of FOXO4 – p53 interaction releases p53 from the nucleus. Consequently, p53 translocates to mitochondria and subsequently induces apoptosis. Most striking were the results of *in-vivo* studies using fast aging *Xpd*^{TTD/TTD} mice and naturally aged mice at 115 – 130 weeks, showing restored fitness, fur density and renal function after FOXO4-DRI treatment (2).

Cellular tumor antigen p53

A key player in regulation of apoptosis as well as senescence is the tumor suppressor p53. p53 is often designated as “guardian of the genome” (21) or “cellular gatekeeper” (22) indicating its importance in health and disease (23). Since the first description in 1979, p53 is probably the most studied protein with over 35 000 linked publications. First described as a virus-associated antigen, then as an oncogene p53 is now regarded as a tumor suppressor gene (24).

Mutations of the p53 gene are the most common genetic alteration in human cancer, affecting more than 50% of all tumors (25). Mutations are widely spread over the p53 gene, but 90% are missense mutations in the DNA-binding domain, causing loss of DNA binding ability therefore affecting p53 tumor suppressive function (26).

The complex role of p53 is described by Vousden and Prives as follows: “If genius is the ability to reduce the complicated to the simple, then the study of p53 makes fools of us all.” (27). Besides the function as tumor suppressor, orchestrating apoptosis, cell-cycle arrest and senescence (23), p53 regulates metabolism, longevity, reproduction, differentiation and development (27, 28). These diverse and important functions of a single protein require a tight and complex regulation.

Functions

p53 has diverse functions, but the most important ones are regulation of the cell cycle, apoptosis and senescence thereby deciding the cell’s fate (23).

p53 can act either act as a transcription factor or function transcription-independent (23). Cell-cycle checkpoints ensure the fidelity of each cell cycle phase before proceeding. Cellular stress can cause growth arrest of cells at these checkpoints to prevent the propagation of mutations in the DNA (23). Even low levels of p53 can temporary block the cell cycle by activating the transcription of the cyclin-dependent kinase inhibitor p21 (27). Additionally, p53 can transcriptionally activate the signal transducing protein 14-3-3 after DNA damage, which in turn prevents proper nuclear localization of cyclin B1/cdc2 and thereby inhibiting cell cycle progression (23).

Cell cycle arrest can be induced by mild damage or stress and persists until the damage has been resolved or the stress removed (27). However, what if the situation cannot be resolved?

There are two possible solutions to that problem: either cells can undergo apoptosis and be removed via programmed-cell death or they can undergo senescence and be trapped in a stable cell cycle arrest (27). Both solutions are regulated by p53.

Establishment of senescence in p53-dependent manner is likely a result of changes in the expression of a number of proteins (27). The p53-target gene p21 inhibits various cyclin-dependent kinases, thereby inducing a G1 arrest after DNA damage. Lack of p21 prevents p53-dependent G1 arrest and abrogates senescence in several settings (23, 28). The activation of p21 alone is not sufficient to explain p53 dependent senescence (28). Aksoy et al. identified E2F7, a member of the E2F family, as new p53 target. E2F7 was upregulated during proliferative as well as oncogene-induced senescence thereby repressing cyclin A, cyclin B and cdc2/cdk1 which are essential for mitosis (29).

p53 can be activated by metabolic adversity causing interplay with another regulator of cellular senescence, the kinase mechanistic target of rapamycin (mTOR), which acts at the interface of growth and starvation (27, 28). Interactions with the mTOR pathway occur in several ways: (i) p53-regulated sestrins and AMP-activated protein kinase (AMPK) repress mTOR (ii) p53 upregulates Phosphatase and tensin homolog (PTEN), an inhibitor of the PI3K pathway, which is an upstream-positive regulator of TOR (28). Interplay of p53 and mTOR pathway was shown to be anti-senescent, as p53 triggers inhibition of mTOR after irreversible senescent arrest, induced by p21, to switch to a reversible cell cycle arrest (30, 31).

Besides senescence, cells can resolve irreparable DNA-damage via apoptosis. Most of the p53-target genes are implicated in apoptosis. Bax, PIG3, Killer/DR5 (fas), p53AIP1, Perp and BH3-only proteins Noxa and PUMA are all target genes of p53 and involved in apoptosis (23). Besides its nuclear activity, p53 can translocate to the mitochondria where it induces mitochondrial outer membrane permeabilization, thus leading to the release of pro-apoptotic factors from the mitochondrial intermembrane (23). Both transcription-dependent and transcription-independent mechanisms are linked through PUMA. Upon cellular stress p53 activates PUMA, which binds Bcl-X_L at the mitochondria releasing p53 to activate Bax (23).

Structure

To understand functions and regulatory mechanisms of p53 it is important to know about the structure of the protein.

p53 α , the main isoform of p53, is built up by 393 amino acids, which form well-defined domains as well as unfolded regions and adopt a tetrameric quaternary structure (25). The domain architecture is shown in Figure 1.

The intrinsically disordered N-terminus contains the transactivation domain (residues 1-62) comprising two sub-domains, Transactivation domain 1 (19-26) and Transactivation domain 2 (46-55). This region is known to interact with various regulatory proteins such as MDM2, TFIID, CBP/p300 and TFIIH thereby forming temporary secondary structure elements (25, 26). This domain is followed by a proline rich region (residues 62-94) containing SH3-domain binding motifs (PXXP) (25). DNA-binding of p53 is facilitated by the DNA-binding domain (residues 94-292) which is well folded. It specifically binds to double-stranded target DNA that contains two-decameric motifs: 5'- Pu – Pu -Pu – C – (AT) – (T/A) – G- Py – Py -Py -Py -3' (Pu = A/G, Py = T/C). A tetramer of p53 DNA-binding domains binds DNA in a cooperative manner to give a 4:1 complex. The affinity of the binding varies depending on the sequence, but is generally higher for genes involved in cell-cycle arrest and lower for genes involved in apoptosis (25).

Following the core domain is the nuclear localization signal containing region (residues 303-323) (32).

The C-terminal region includes the tetramerization domain (residues 325-356), which regulates the oligomerization state of p53, and a regulatory domain at the C-terminus which contains acetylation sites and can bind DNA non-specifically (25). The disordered C-terminal domain is also binding site for many proteins such as 14-3-3, GSK3beta, PARP1, TAF and TAF1 (26).



Figure 1: Domain architecture of p53:

TAD: Transactivation Domain, PP: Poly-Proline Region, DBD: DNA-binding Domain, TD: Tetramerization Domain, CD: C-Terminal Domain

Studying full-length p53 proves to be complicated as it is too disordered for crystallography and too large (and tetrameric) for NMR analysis (26).

The quaternary structure of human p53 was solved by Tidow et al. 2007 by a combinatory approach of NMR, SAXS and electron microscopy (32).

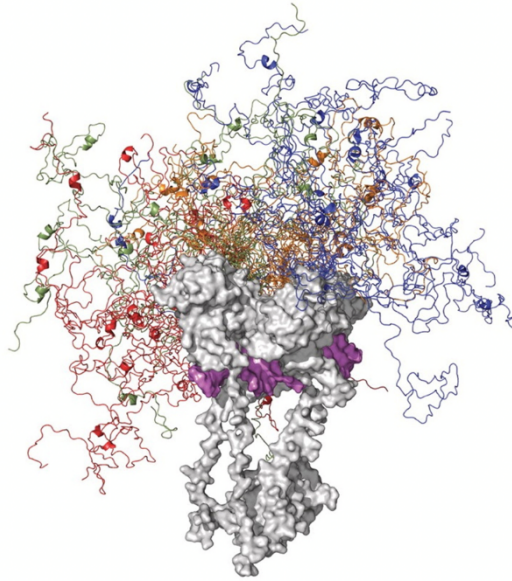


Figure 2: Model structure of p53¹⁻³⁶⁰ bound to DNA.
Average ensemble structure of the N-terminal Transactivation Domain (colored)
grafted to the DNA-Binding Domain (grey) (26)

Figure 2 shows a model of p53⁹⁶⁻³⁶⁰ bound to DNA and average ensemble structures of the intrinsically disordered N-terminal domain, illustrating the amount of different conformations the N-terminal transactivation domain can adapt (26). Structure of the individual domains are shown in Figure 3.

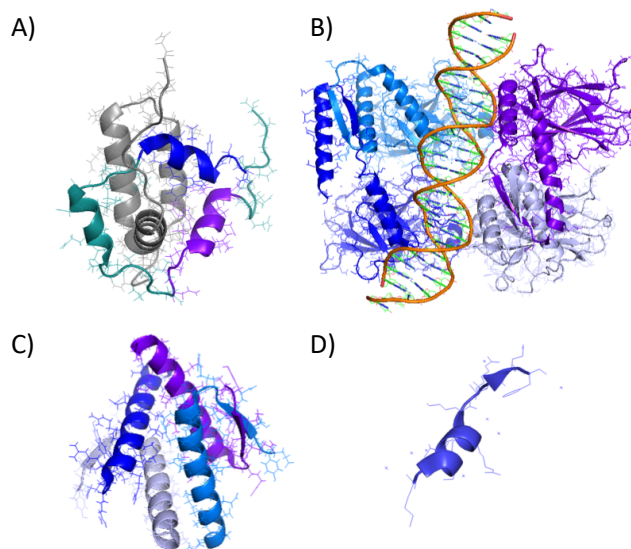


Figure 3: Structures of the individual domains of p53
A) p53 Transactivation domain bound to CBP/p300 (pdb: 2L14)
B) Tetramer of p53 DNA-binding domain bound to DNA (pdb: 3Q05)
C) Tetramer of p53 Tetramerization domain (pdb: 2j0Z)
D) C-terminal regulatory domain of p53 (pdb: 2H2D)

Regulation

In physiological conditions, cellular levels of p53 are kept low. MDM2 binds and ubiquitinates p53, which is subsequently degraded by the proteasome. Six lysine residues in the C-terminal regulatory domain of p53 are main subject for ubiquitination. Polyubiquitination promotes proteasomal degradation, mono-ubiquitination facilitates different events such as nuclear export of p53 (33). MDM2 and p53 interact sequentially through several points of contact. The main docking points for MDM2 is the N-terminal transactivation domain 1 of p53. Association of MDM2 and p53 leads to conformational changes and allows ubiquitination of the C-terminal regulatory domain of p53 (33).

Upon various cellular stress signals p53 is activated. The first step of p53 activation involves uncoupling of p53 from MDM2-mediated degradation (33). The stabilization of p53 can be achieved by phosphorylation of the N-terminal transactivation domain, interfering with MDM2 binding. Ser15 and Ser20 are phosphorylated after DNA damage or cellular stress by ATM, ATR, DNA-PK, Checkpoint kinase 1 (Chk1) and 2 (Chk2) and inhibit binding of MDM2 (34). ATM phosphorylates not only p53 but also MDM2. The main phosphorylation site is Ser395, but also Ser386, Ser407, Ser425, Ser429 and Thr419 are substrate of ATM. Those modifications allosterically inhibit MDM2 dimer formation, which is necessary for polyubiquitination of p53 (33). In consequence of oncogene activation p14, an inhibitor of MDM2, is expressed and stabilized and directly interacts with MDM2 interrupting MDM2 function. There are also drugs, such as Nutlin, that bind to MDM2 by mimicking the transactivation domain of p53, thereby preventing MDM2 – p53 interaction and stabilizing p53. Nutlin treatment was demonstrated to enhance p53-dependent apoptosis in combination with chemo – or radiotherapies (33).

Once p53 is stabilized the different effector functions are regulated by post-translational modifications and other interaction partners (33). The cyclin-dependent kinase-activating kinase usually activates the cyclin-dependent kinase – cyclin complex but was also shown to phosphorylate p53 at Ser33 regulating p53 function in response to DNA damage, thereby coupling p53 with the DNA repair machinery (35). In consequence of oncogene induced senescence by oncogenic Ras, MAP kinase-activated protein kinase 5 (PRAK) was shown to activate p53 by phosphorylating at Ser37. Also DNA-PK and ATR were reported to phosphorylate Ser37 of p53 (36, 37). Phosphorylation of Ser37 was shown to interfere with the p53 – replication protein A

interaction, thereby promoting homologous recombination (33, 38). HIPK2 phosphorylates p53 at Ser46 and thereby promotes apoptosis via p53 through selective gene expression (39). Phosphorylation of Ser46 can also be catalyzed by Protein Kinase C in response to genotoxic stress inducing cell death via apoptosis (40). Opposite effects were observed for phosphorylation of Thr55 by the largest subunit of TFIID, TAF1, resulting in p53 degradation and cell cycle progression (41). Figure 4 provides an overview of important post-translational modification sites of p53.

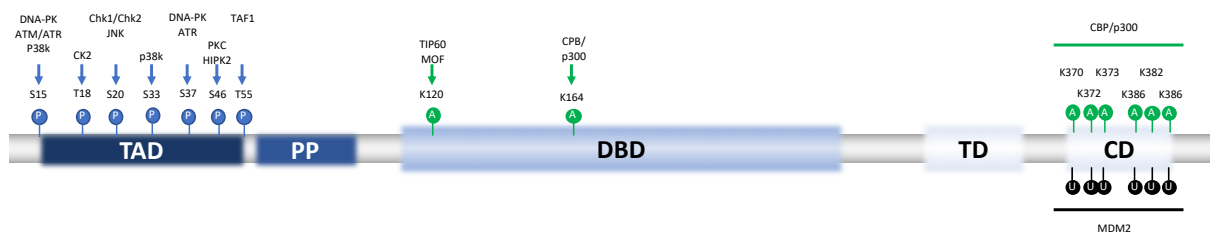


Figure 4: Schematic representation of p53 with selected important post-translational modification sites

However, understanding p53 is extremely complicated, as there are over 900 interactions with 260 proteins linked with p53 (42). Of those proteins 28 are linked to DNA repair, 62 to cell cycle arrest, 68 to cellular senescence, 42 to angiogenesis and 118 to apoptosis (42). Of the apoptotic nodes 45 have anti-apoptotic and 73 have pro-apoptotic functions. This again highlights the diverse functions of p53 (42). Recently the direct interactions of p53 with FOXO3 and FOXO transcription factors of the Forkhead box O family were described, which might decide cell's fate by discriminating between apoptosis and senescence (2, 20).

FOXOs

The FOXO family represents a subclass of Forkhead transcription factors. They are characterized by a winged helix DNA-binding domain known as Forkhead box (43). More than 100 members of Forkhead family are known in humans, from FOXA to FOXS (1). The FOXO family is conserved from *C.elegans* to mammals. *C.elegans* and *Drosophila* each only possess one FOXO gene, whereas mammals own four FOXO factors (FOXO1, FOXO3, FOXO4 and FOXO6), which differ in their tissue-specific expression and in their function (43). The functions range from regulating stress resistance, metabolism, cell cycle arrest to induction of apoptosis (1, 44). FOXO transcription factors are denoted as “longevity genes”, as they were found to extend lifespan and delay signs of age-related diseases (43, 45-48). FOXO1, FOXO3 and FOXO4 are ubiquitously expressed in mammals, FOXO6 is predominantly expressed in the brain and nervous system (49). Mutations and dysregulations of FOXO proteins are found in various cancers, for example lymphoblastic leukemia, rhabdomyosarcomas and mixed lineage leukemia (49).

Function

Members of the FOXO family are pivotal for the maintenance of tissue homeostasis in organs, mediating cell cycle arrest, DNA repair and apoptosis.

Triple knockout mouse models of FOXO1, FOXO3 and FOXO4 isoforms exhibit tumor growth, underscoring the anti-tumoral activity of FOXOs (49).

FOXOs fulfil their function by directly interacting with two consensus DNA sequences: Daf-16 family member-binding element and the insulin-responsive sequence (44). During cell cycle arrest FOXOs are localized within the nucleus, where they bind to the cyclin dependent kinase inhibitor p27 promoter and initiate p27 transcription (49). Another target gene of FOXOs that is involved in cell cycle arrest is p21, which can be targeted by FOXO1, FOXO3 and FOXO4 in complex with Smad3 and Smad4 (49). These interactions and subsequent p21 expression lead to cell cycle arrest. Furthermore, FOXOs can promote cell cycle arrest by repressing cyclin D1 and D2 expression, which are positive regulators of the cell cycle (49).

Several studies assessed FOXOs role in oncogene induced senescence. The oncogenic form of BRAF phosphorylates the JNK kinase via the MAPK/ERK pathway, which in turn phosphorylates FOXO4 leading to cell cycle arrest and cellular senescence. The activation of FOXO4 via phosphorylation, results in increased

transcription of p21 (44, 50). Opposite effects on senescence were described for FOXO1 and FOXO3. In senescent cells, phosphorylation of FOXO3 by AKT/PKB results in its nuclear exclusion and therefore inactivation of its transcriptional activity (44). FOXOs can induce the intrinsic apoptotic pathway mediated by mitochondria. Constitutively nuclear forms of FOXOs trigger cell death by transactivation of pro-apoptotic proteins (Bim and BNIP3) (49).

In response to cytokine or growth factor deprivation FOXO3-dependent expression of Puma is upregulated and might play a role in regulation of apoptosis (49). FOXO4 can indirectly repress the activity of pro-survival Bcl-XL, regulating expression of the transcriptional repressor Bcl-6.

Another function that might contribute to FOXOs reputation as longevity gene is the induction of autophagy in specific cell types and the regulation of cellular quality control and protein homeostasis (43).

Structure

The common feature of proteins of the FOX family is the Forkhead domain (51). This domain consists of three alpha helices and two disordered loops that resemble the wings of a butterfly (51). The difference of FOXO proteins from the other FOX family member is a “GDSNS” insertion within the Forkhead domain (51). The Forkhead domain of all FOXO protein recognizes the DNA sequence motif: 5'-(G/C/A) (T/C/A) AAA(T/C) A-3' (51). Besides the Forkhead domain FOXO proteins consist of long stretches, which are intrinsically disordered. Three regions of those disordered part are well conserved and were described to have a propensity to form alpha-helical structures (51). The N-terminal conserved region 1 (CR1) contains many proline. Conserved region 2 and conserved region 3 were described to be involved in transcriptional activation of respective FOXO proteins (51) (Figure 5).



Figure 5: Domain architecture of FOXO4:
 CR1: Conserved Region 1, FH: Forkhead Box, CR2: Conserved Region 2, CR3: Conserved Region 3

Regulation

The regulatory pathway of FOXO transcription factors can be triggered by growth factors such as insulin or insulin-like growth factor 1 (IGF-1). The serine/threonine kinase AKT/PKB phosphorylates FOXOs at three conserved regions within the FOXO

proteins (1). Phosphorylation by AKT/PKB results in nuclear exclusion, interfering with their transcriptional activity (49). Upon stress or in absence of growth factor signaling FOXOs are imported in the nucleus and transcribe their target-genes (49). For example, upon oxidative stress FOXO4 and nuclear import factor Transportin-1 can be oxidized by ROS and in consequence form a covalent complex involving disulfide-bridge formation. FOXO4 is then translocated to the nucleus where it can act as transcription factor (44).

Not only AKT but also other cellular kinases are involved in the regulation of FOXO activity. AMPK, JNK, MST1, ERK and p38 MAPK are known to phosphorylate different residues of FOXOs (49). JNK promotes oncogene induced senescence by phosphorylation of FOXO4 threonine 223, 447 and 451 and serine 226, resulting in p21 upregulation (50).

Besides phosphorylation, other PTM allow tight regulation of FOXOs. Mono-ubiquitination of FOXOs by low amount of MDM2 resulted in an increase in transcriptional activity of FOXO4, whereas high MDM2 amounts showed opposite effects (44). Figure 6 shows known post-translational modification sites of FOXO4.

For FOXO3 a closed conformation in which the C-terminal CR3 domain folds back to the Forkhead domain was found, providing a regulatory mechanism for transcriptional activity (20).

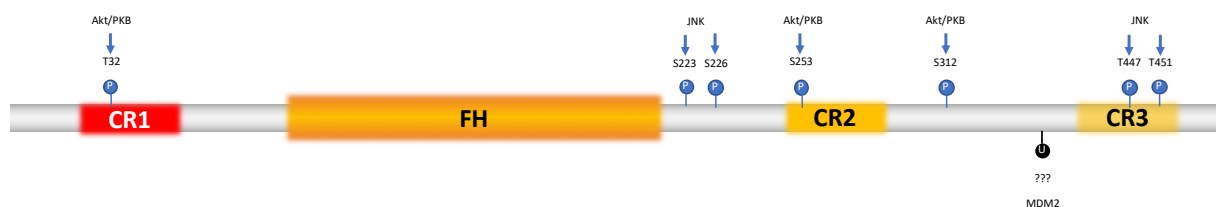


Figure 6: Schematic representation of FOXO4 with post-translational modification sites

p53 – FOXOs

Given the overlapping functions and modes of regulation of p53 and FOXOs it raises the question whether they act redundantly or cooperate to decide cell's fate (44).

Transgenic p53 knockout mice are prone to develop lymphoma and hemangionomas, which can also be observed for FOXO1, 3 and 4 triple knockout mice (44, 49).

Furthermore, p53 and FOXOs share downstream targets such as FASLG, GADD45, PA26 and p21 (44). The different sequence-specific DNA-binding elements on the

promotor site of the target genes would allow them to act in cooperative manner in order to regulate gene transcription (44).

FOXO3 was described before to interact with p53 thereby forming a strong tumor suppressor network to protect cells from damage (49). More recent work also identifies FOXO4 – p53 interaction as pivot for regulation of cellular senescence (2, 44, 52).

There are tight and complex regulatory mechanisms for p53 and FOXOs. MDM2 is not only controlling the expression levels of p53 but also the expression and activity of FOXO proteins (44).

First evidence of direct FOXO – p53 interaction was observed by investigating the effect of nutritional stress on SIRT1 expression. Under starvation FOXO3, activates the transcription of SIRT1, which is controlled by a p53-dependent promoter, suggesting a physical connection between FOXO3 and p53. This was confirmed by co-immunoprecipitation of both proteins (44). Interestingly SIRT1 is a NAD⁺ dependent deacetylase, which deacetylates and regulates the transcriptional activity of p53 and FOXOs, suggesting an autoregulatory mechanism (44).

The FOXO3-p53 interaction was further characterized using NMR spectroscopy and pull-down experiments, showing that the C-terminal transactivation domain and the Forkhead domain of FOXO3 contribute to the interaction with the DNA binding domain of p53 (44).

Recently Baar et al. demonstrated the interaction of FOXO4 and p53 and the significance for regulation of cellular senescence (2).

The direct interaction of FOXO4 with p53 was proven using NMR spectroscopy. However, the distinct binding sites and regulatory mechanisms are yet unknown.

Objectives

The central aim of my thesis is to provide insights into key molecular mechanisms regulating senescence and apoptosis, thereby contributing to the process of aging.

Aging is major risk factor for age-related diseases, such as cancer, cardiovascular - and neurodegenerative disorders.

Recent results revealed the FOXO4 – p53 interaction as central regulatory axis for promoting senescence over apoptosis (2). By designing a cell-penetrating peptide called FOXO4-DRI, that targets senescent cells by interfering the FOXO4 – p53 interaction, senescent cells can be specifically eliminated, whereas control cells are not affected. Even more striking are the *in-vivo* after FOXO4-DRI treatment of fast-

aging and naturally aged mice, showing restored renal function, overall fitness and fur density (2). Those results highlight the immense importance of this interaction for regulation of senescence and for aging in general. Targeting the FOXO4 – p53 axis is seen as a prominent way to cure age-related diseases and provide “eternal life”. However, molecular understanding of the FOXO4 – p53 interaction is essential in order to optimize existing drugs and to design new drugs with higher potency. Besides the therapeutic application to eliminate senescent cells investigation of the FOXO4 – p53 interaction is key to understand probably the most important mechanism in deciding the cell's fate.

In this way, the aim of my master's thesis is to identify the yet unknown binding site of FOXO4 on p53, which is (i) a prerequisite to determine the atomic resolution 3D structure of the complex using NMR and (ii) indispensable for a better understanding of this binary interaction in the regulation of cellular senescence.

p53 and FOXO4 are both controlled by a complex regulatory network, involving post-translational modifications, miRNAs, protein-interaction partners, acting in concert to control subcellular localization and transcriptional activity.

A large number of kinases, among them ATM, ATR, DNA-PK, Chk1, HIPK2 and Chk2 is known to phosphorylate p53 at various sites (34). It was shown that phosphorylation of p53 regulates its activity and function. Phosphorylation of Ser15 is linked with cell cycle arrest and p21 expression, phosphorylation of Thr18 and Ser20 with stabilization of p53 and Ser46 with promotion of apoptosis (34). Given the importance of the FOXO4 – p53 interaction it is likely that post-translational modifications, such as phosphorylation control the complex formation.

In this regard, my study also aims to identify potential phosphorylation sites of p53 and to investigate the impact of phosphorylation on the interaction. Both p53 and FOXO4 are subject to many post-translational modifications. This changes the binding behavior of potential drugs and has to be taken in account to efficiently target senescent cells via the FOXO4 – p53 axis. Therefore, it is essential to understand the setting within senescent cells, the pattern of post-translational modifications and their impact on the FOXO4 – p53 interaction.

Material and Methods

In order to investigate the p53 – FOXO interaction, we choose an *in-vitro* approach using purified proteins and biophysical techniques, namely Nuclear Magnetic Resonance spectroscopy (NMR) and Small-Angle X-ray Scattering (SAXS). These techniques are complemented by other molecular biological and biophysical methods. Expression and purification of recombinant expressed proteins represents the basis to all subsequent experiments.

Buffers and solutions used for preparation and experiments are listed in the appendix.

Expression and purification of human p53 and FOXO4 proteins

DNA encoding human p53 and FOXO4 protein constructs were purchased from Genscript (Piscataway, New Jersey, USA), in order to have access to an *E.coli* codon optimized version of the corresponding genomic DNA. Different organisms show particular preferences for using several codons coding for the same amino acid. As *E.coli* was used as expression system for the proteins investigated in this study, the DNA sequences were optimized for *E.coli* expression to obtain a higher yield of protein expression.

The DNA sequences were ordered already within pETM11 as cloning vector, containing a T7 promotor, a N-terminal Polyhistidine Tag, a protein A tag as well as a Tobacco Etch Virus (TEV) cleavage site for purification (Z-Tag) (As seen in Figure 7).

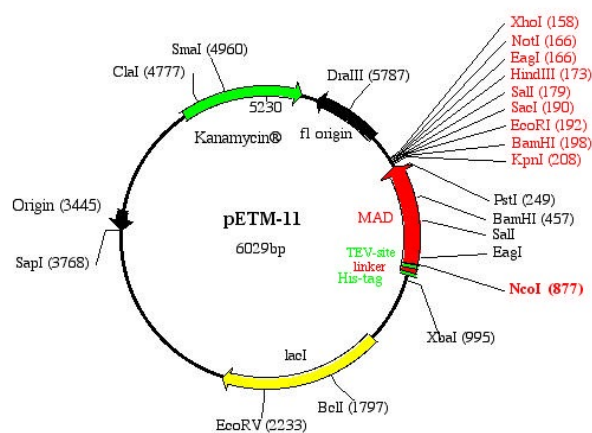


Figure 7: pETM-11 vector for expression of proteins containing Z-Tag in *E.coli*

Table 1: List of protein constructs used during the project

Protein	Synonym	Region / Mutation
p53	p53 FL	1-312
p53	p53 DBD	94-312
p53	p53 TAD	1-94
p53	p53 TAD S46E	1-94 S46E
p53	p53 TAD1	14-37
p53	p53 TAD2	37-57
FOXO4	FOXO4 FH	86-208

Site-directed mutagenesis

Site-directed mutagenesis polymerase chain reaction (PCR) served to create point mutations, which mimic the phosphorylation of a serine or to obtain shorter constructs of p53, by introducing a premature stop codon.

This method follows the same principle as common PCR reaction, but uses primers, which carry the mutation that causes the point mutation on the template DNA. The basic setup involves a DNA template, DNA polymerase, primers complementary to the target DNA, that carrying the point mutation, desoxynucleoside triphosphates (dNTPs) and a buffer containing magnesium and potassium ions. Typically, PCR reactions consist of following steps characterized by temperature changes, which are repeated in cycles:

Table 2: Primer for p53 mutagenesis

Mutation	Sequence	Annealing Temperature
p53 1-94 S15E	Fw: ACCGCCGCTGGAACAGGAAACCTTTAGC Rev: TCCACGCTCGGATCGCTC	68°C
p53 1-94 S20E	Fw: GGAAACCTTTgaaGATCTGTGGAAACTGCTGCCGAAAAC Rev: TGGCTCAGCGGCGTTCC	70°C
p53 1-94 S33E	Fw: CAACGTGCTGgaaCCGCTGCCGA Rev: TTTTCCGGCAGCAGTTTC	64°C
p53 1-94 S37E	Fw: CCCGCTGCCGGAACAGGCGATGG Rev: CTCAGCACGTTGTTTTCCG	65°C

p53 1-94 S46E	Fw: TCTGATGCTGgaaCCGGATGATATTGAACAGTG Rev: TCATCCATCGCCTGGCTC	65°C
------------------	--	------

Denaturation: In this step the sample is heated to 94-98°C for seconds, causing the DNA double-strand to melt, resulting in two molecules of single-stranded DNA molecules.

Annealing: The reaction temperature is lowered to 50-65°C for 20-40 seconds, allowing the primers to anneal to the complementary region on the single-stranded DNA. The annealing temperature depends on the primers (especially GC content and length) and should be similar for forward and reverse primer.

Elongation: Temperature of the extension step depends on the optimal activity of the DNA polymerase used. The DNA polymerase is an enzyme, which synthesizes a new DNA strand complementary to the DNA template, by adding free dNTPs in the 5'- to 3' direction. The time for the synthesis of the new strand depends on the length of the DNA fragment and the synthesis rate of the DNA polymerase.

Denaturation, annealing and elongation constitute a cycle, which is repeated multiple times to amplify the target DNA.

The PCR reaction was prepared according site-directed mutagenesis protocol NEB method.

Table 3: PCR Reaction Mix

Reagent	50µl	Concentration
Q5 High-Fidelity DNA Polymerase 10x Buffer (NEB)	10x	1x
DNTPs mix (10 µM) (NEB)	1 µl	0.2 µM
Forward Primer (10 µM)	2.5 µl	0.5 µM
Reverse Primer (10 µM)	2.5 µl	0.5 µM
Q5 High-Fidelity DNA Polymerase 2 U/µl (NEB)	0.25 ul	0.5 U
Template DNA	1 µl	20 ng
Nuclease free water	Up to 50 µl	

Table 4: PCR Reaction Setup

Step	Temperature	Time
Initial Denaturation	98°C	2 minutes

25 Cycles	98°C	30 seconds
	Annealing (60-72°C)	30 seconds
	72°C	30 seconds/kb
Final Extension	72°C	2 minutes
Hold	4°C	

The product of the PCR was analyzed using agarose electrophoresis. This method separates DNA fragments according to their size. The agarose gel was prepared at a concentration of 1% agarose in TAE buffer solution. TAE buffer was also used as running buffer. 4 µl of loading buffer were added to 6 µl sample DNA. To estimate the DNA length a DNA ladder was used.

PCR products with the desired size were then subjected to DpnI treatment. During one hour at 37°C DpnI (NEB) cleaves the methylated DNA of the old DNA strand without the desired mutations.

2 µl of DpnI treated PCR product were mixed with 15 µl of Nuclease-free water and heated for 20 minutes at 80°C. 2 µl of 10X T4 Ligase buffer (NEB) and 1 µl of T4 polynucleotide Kinase (PNK-NEB) were added to the chilled tube and incubated for 30 minutes at 37°C. The PCR product was ligated for 2 hours at room temperature by adding 1 µl of T4 Ligase (NEB).

Transformation

Plasmid DNA can be taken up by cells in a process called transformation. Those cells can either be transformed via electroporation or via chemical transformation. We employed two different chemically competent *E.coli* strains (*E.coli* BL21(DE3) for protein expression and *E.coli* TOP10 for amplification of plasmid DNA).

50 ng of plasmid DNA were added to chemically competent BL21(DE3) or TOP10 cells respectively. After incubation on ice for 10 minutes, a heat shock at 42°C was performed for 45 seconds using an Eppendorf thermomixer. During this step the membrane of bacterial cells is permeabilized and plasmid DNA can enter cells. This was followed by incubation on ice for 2 minutes. To allow the cell to express the gene responsible for antibiotic resistance and divide 1 ml of LB medium was added and cells were incubated at 37°C for 45 to 60 minutes.

300 µl of cell suspension were plated on kanamycin containing LB agar plates and incubated at 37°C overnight.

Amplification and isolation of plasmid DNA

Colonies from the LB agar plate of *E.coli* TOP10 cells were separately inoculated in 10 ml LB medium containing kanamycin and grown at 37°C overnight.

For isolation of plasmid DNA the Wizard® Plus SV Minipreps DNA Purification System (Promega) was used and performed according to protocol.

Concentration of plasmid DNA was measured using NanoDrop™ (Peachlab). Isolated plasmid DNA was sent to GATC for sequencing with the primers T7minus1 and pET-RP.

Protein expression

For protein expression of p53 and FOXO4 constructs we used cells from the *E.coli* BL21(DE3) strain. This strain is a widely used bacterial gene expression host, that is able to grow in minimal medium, which is essential for NMR studies, and deficient in key proteases (especially important for expression of proteins with long disordered stretches). BL21(DE3) cells use the T7 promoter expression system. In this strain the T7 gene has been inserted in the *E.coli* genome under control of the lac promoter. In absence of lactose and the lactose analogue Isopropyl-β-D-thiogalactopyranosid (IPTG) the lac repressor is bound to the lac promoter preventing the expression of T7 RNA polymerase.

In presence of IPTG, IPTG binds to the lac repressor, thereby displacing it from the lac promoter and allowing expression of T7 polymerase. The T7 polymerase in turn transcribes the target gene on the plasmid, which is under control of the T7 promoter. For preparation of the preculture either 500 µl of the cell suspension after transformation or one colony of a LB agar plate containing kanamycin were added to 20 ml of LB medium containing 50 mg/l kanamycin and incubated overnight.

To prepare the main culture, 10 ml of the preculture were inoculated in 1 l of LB containing 50 mg/l kanamycin. Cells were grown at 37°C until they reached an optical density (OD) of 0.8 to 1.2. Once the cells were dense enough, protein expression was induced by adding 1 mM IPTG. Depending on the protein construct expression conditions might vary, therefore an expression test to find optimal conditions for expression in *E.Coli* BL21(DE3) cells was performed. The main culture was grown at 37°C until an OD₆₀₀ of 0.8 to 1.2 and protein expression was induced via IPTG at three different temperatures, 30°C, 25°C and 20°C. 200µl of cells were taken after 1, 2, 4, 8, 16 and 24 hours incubation for all respective temperatures. After the cells were

pelleted, the supernatant was discarded, and the pellet was dissolved in Sodium dodecyl sulfate polyacrylamide gel electrophoresis (SDS-PAGE) loading buffer. After heating the sample at 95°C it was subjected to SDS-PAGE.

For expression of isotope labeled proteins a minimal medium containing either ¹⁵N ammonium chloride alone or both ¹⁵N ammonium chloride (Cortecnet) and ¹³C glucose (Cambridge Isotope) were used for cell growth (for composition see Appendix)

Harvesting and lysis of *E.coli* cells

After protein expression, cells were harvested by centrifugation (10 minutes, 6 000 rpm, 4°C). Subsequently the pelleted cells had to be lysed in order to access recombinantly expressed proteins for isolation. Therefore, the pellet was resuspended in 20 ml of lysis buffer (either native buffer for folded proteins or urea buffer for unfolded proteins).

The cell lysate was sonicated for 10 minutes (1 sec on/1 sec off; 70 % intensity) on ice and centrifuged for 30-45 minutes (12 000 rpm). The supernatant should contain all the soluble cellular proteins including the recombinant overexpressed protein and *E.coli* proteins.

Protein purification

For further purification, the supernatant was separated from the pellet. The first step of protein purification involved nickel affinity chromatography using Ni-NTA Agarose (Macherey Nagel). This method is based on binding of His-tagged proteins to Ni²⁺ residues in the gravity column. Indeed, the histidine repeat from the tag can directly bind to Ni²⁺ residues, whereas *E.coli* proteins are less likely to bind (Histidine residues of *E.coli* proteins also bind to Ni²⁺ residues but with less affinity).

First, the column was equilibrated with one column volume Buffer A. Subsequently the supernatant of the cell lysate was applied, and the column was washed with three column volumes of different washing buffers (A, A' and A'). The flow-through of the cell lysate and of the washing steps were collected. The protein-of-interest was eluted using Buffer B'. This buffer contains high concentrations of imidazole, which is part of histidine and also interacts with Ni²⁺ residues. This causes competition between imidazole and histidine for Ni²⁺ binding.

The concentration of the eluted protein was determined using NanoDrop™ (Peqlab) by measuring the absorbance at 280 nm. According to the law of Lambert Beer the

absorption at 280 nm was divided by the molar extinction coefficient ϵ of the protein to calculate the molar concentration.

TEV cleavage

To avoid a non-native conformation of proteins, the tag was removed. The N-terminal fused tag contains the Tobacco etch virus (TEV) protease recognition site ENLYFQS. This allows to remove the tag from the protein-of interest. 2% (w/w) of TEV protease was added to the protein solution and incubated at 4°C overnight.

After cleavage the buffer was exchanged to Buffer A. This was achieved using the Äkta pure Fast protein liquid chromatography (FPLC) system (GE Healthcare) with the HiPrep 26/10 (GE Healthcare) desalting column.

To separate the tag from the cleaved protein, the mixture was applied to the Ni-NTA column a second time. After successful cleavage the tag interacts with the beads, whereas the cleaved protein goes directly in the flow-through.

Size exclusion chromatography

To ensure the purity of the proteins and to remove contaminants, size-exclusion chromatography was performed. Size-exclusion chromatography separates molecule by size given their molecular weight. Size exclusion was performed on Äkta pure FPLC system using Superdex 75 10/300 (GE Healthcare) columns and Superdex peptide 10/300 (GE Healthcare). The columns differ in their pore sizes. During the separation process some proteins interact with the pores of the columns. Smaller molecules interact longer with the column and are therefore eluted later.

FOXO4⁸⁶⁻²⁰⁸, p53¹⁻³¹², p53⁹⁴⁻³¹² and p53¹⁻⁹⁴ were purified using Superdex 75 10/300 column at a flow rate of 0.7 ml/min. For smaller proteins (p53¹⁴⁻³⁷, p53³⁷⁻⁵⁷) the Superdex peptide 10/300 was used at a flow rate of 0.5 ml/min. Sample volumes of 0.5 to 2 ml were applied to the respective columns. Size-exclusion was performed in the respective buffer used for further experiments. Further settings were adjusted according to the specifications of the respective column.

Sodium dodecyl sulfate polyacrylamide gel electrophoresis

SDS-Page was performed to control the purification process and to ensure, that samples used for measurement are not contaminated by other proteins or degradation products. 20% polyacrylamide gels were placed in the SDS-PAGE Gel chambers.

20 x MES SDS running buffer was diluted to 1 x with desalted H₂O and filled in gel chamber.

Samples were mixed with Laemmli Loading dye in a ratio of 1:6.

Proteins were separated at a constant voltage of 150 V for approximately 45 minutes. To visualize the proteins on the SDS gel they were stained with Coomassie staining, which unspecifically binds to basic side chains of amino acids. The gels were incubated 30 minutes with Coomassie staining solution and destained in destaining solution for 2 hours, on a shaker at room temperature.

Nuclear Magnetic Resonance spectroscopy

Nuclear magnetic resonance (NMR) spectroscopy is one of the main methods to determine a protein structure at an atomic level besides X-ray crystallography and electron microscopy. Structure determination using NMR spectroscopy is limited to small proteins (up to a size approximately 30 kDa), due to the fact that in large proteins the magnetization relaxes faster, thus the signals become broader and weaker and eventually disappear.

However, there also substantial advantages of NMR spectroscopy, as it allows to carry out measurements in solution under near native conditions. Furthermore, NMR spectroscopy allows to access information of dynamics of proteins, which not accessible in X-ray crystallography or electron microscopy.

NMR involves the quantum mechanical properties of the nucleus of the atoms. These properties depend on the local molecular environment of a given atom.

Basic principles of Nuclear Magnetic Resonance

NMR spectroscopy studies transitions of atomic nuclear spins excited by radiofrequency pulses. In order to be observable, atomic nuclei have to possess a nonzero spin number I . Common nuclei used in NMR spectroscopy are ^1H , ^{13}C and ^{15}N (listed in Table 5), with a spin quantum number of $I = 1/2$. Placed in an externally applied magnetic field B_0 nuclei will align along or opposing B_0 . The interaction of the nuclear magnetic momentum μ of the spin with the magnetic field leads to a splitting of the energy levels (Zeeman splitting) (53).

Table 5: List of common NMR observable isotopes

Isotope	Spin I	Gyromagnetic ratio (MHz·T ⁻¹)	Natural abundance (%)
¹ H	½	+42,576	99.98
¹³ C	½	+10,705	1.108
¹⁵ N	½	-4,316	0.37

$$E = -\mu B = -\mu_z B_0 = -\gamma I_z B_0 = -\gamma m \hbar B_0$$

Where γ is the gyromagnetic ratio and \hbar is the reduced Planck constant ($6.626070040 \cdot 10^{-34}$ J·s). The magnetic quantum number m can take values $m=+\frac{1}{2}$ and $m=-\frac{1}{2}$ for nuclei with spin $\frac{1}{2}$.

The energy difference between the two Zeeman energy levels is given by:

$$\Delta E = -\gamma \hbar B_0 = \hbar \omega_0$$

Where ω_0 is the characteristic NMR frequency (Larmor frequency) of a nuclear spin at a given magnetic field.

The population difference of the two states can be calculated from the Boltzmann distribution:

$$\frac{N_\beta}{N_\alpha} = e^{-\frac{\Delta E}{kT}}$$

Where T is the temperature and k the Boltzmann constant ($1.38064852(79) \cdot 10^{-23}$ J/K). This is important as the NMR signal is proportional to the magnetization, which depends on the population differences between the two states.

The difference in population is in general very low, therefore only a small fraction of the spins present in the sample contributes to the observed NMR signal. This explains the sensitivity issues of NMR spectroscopy. In addition to that the very low natural abundance of ¹³C and ¹⁵N makes isotope enrichment techniques necessary to enhance the sensitivity of heteronuclear NMR experiments.

The position of the peaks within the spectra depends on the Larmor frequency of respective nuclei and on the chemical environment within the molecule. In a protein, chemical shifts can be characteristic for different amino acids. The three-dimensional structure creates a unique local environment explaining different positions within the

spectra. This fact makes NMR useful for binding studies, identification of binding sites and for determining the three-dimensional structure of proteins (53).

NMR for interaction studies

Interaction studies using NMR spectroscopy are based on changes in the chemical environment upon binding due to an altered protein conformation. This can influence peaks within the spectra in three different properties:

- I. The position of the peak (chemical shift) is result of the local chemical environment
- II. The peak intensity depends on the relative concentration, which is given by the population size of nuclei resonating at a given frequency.
- III. The line width is inversely correlated with the T_2 relaxation time, which in turn depends on the on the tumbling time of molecules

Investigation of those properties can be used to report ultra-strong (μM) to ultra-weak (mM) binding events. This makes NMR spectroscopy an immense versatile and powerful technique to study protein interactions (54).

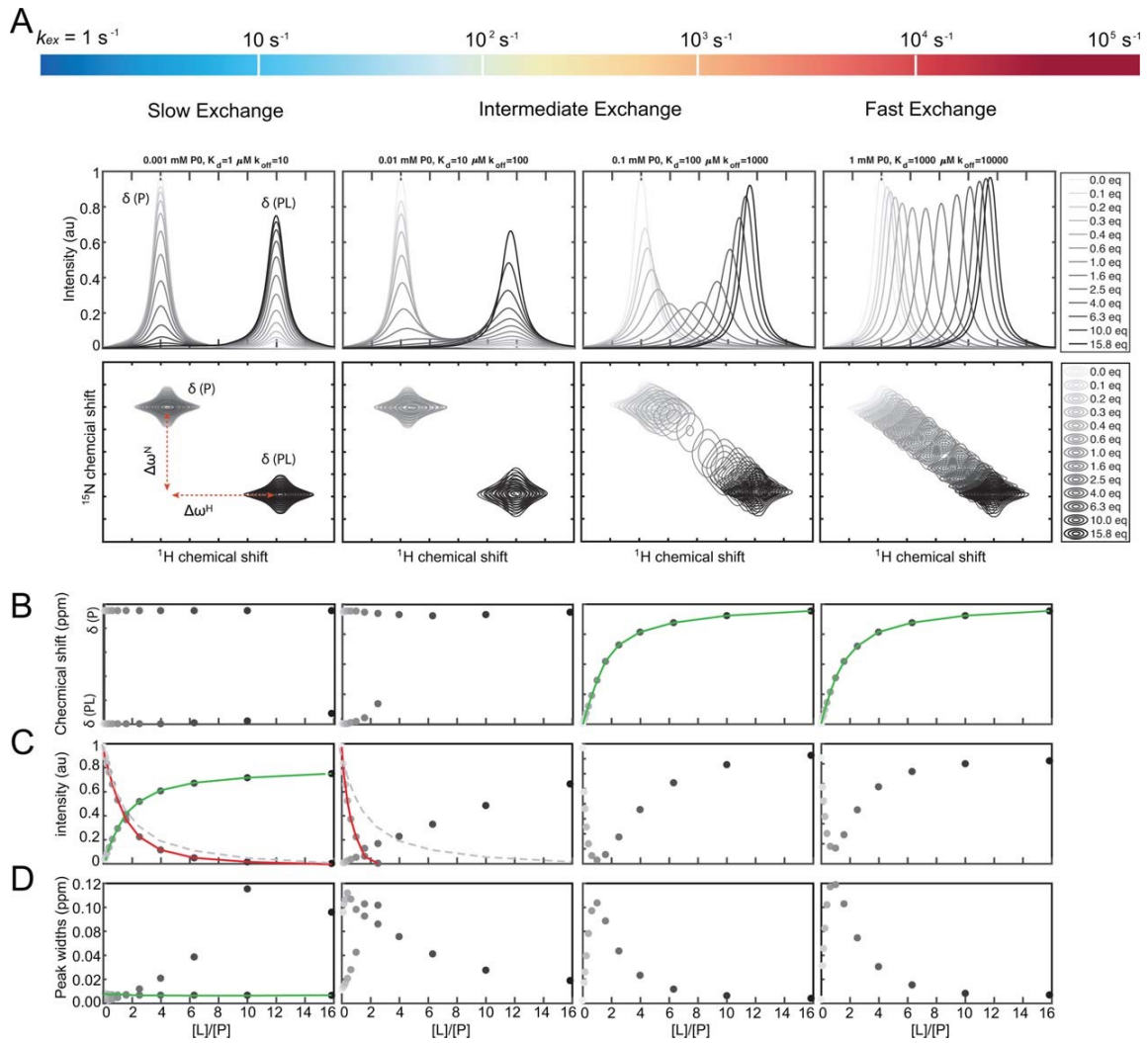


Figure 8: Schematic representation of different NMR exchange regimes.

A: Changing the exchange rate from slow to fast (left to right) changes the appearance of the spectra. In slow and intermediate exchange peaks at population weighted intensity will be visible. In fast exchange a single peak at the weighted average population of the two states will be visible.

B-D: Indicate the extractable parameters obtainable during the titration. B: Chemical shift, C: normalized Intensity, D: Peak line width at half height measured in ppm. (54)

Binding of two proteins results in different resonance frequencies ω_{free} and ω_{bound} and their difference $\Delta\omega = \omega_{bound} - \omega_{free}$. How the different species appear in a spectrum depends on the dissociation constant (K_d) and the exchange rate (k_{ex}) which is given by:

$$k_{ex} = k_{on}[P] + k_{off}$$

The population size of free protein (free) and bound protein (bound) can be calculated as follows:

$$P_{free} = \frac{k_{off}}{k_{on}[P] + k_{off}}$$

$$P_{bound} = \frac{k_{on}[P]}{k_{on}[P] + k_{off}}$$

In NMR spectroscopy there are three different exchange regimes based on k_{ex} and the difference in resonance frequency ($\Delta\omega$).

- Fast exchange where $k_{ex} \gg |\Delta\omega|$
In fast exchange interaction a single peak appears at a population weighted average chemical shifts.
- Intermediate exchange where $k_{ex} \approx |\Delta\omega|$
In intermediate exchange signals are severely broadened. The position and intensity of the peaks are highly uncertain, making the interpretation more complicated.
- Slow exchange $k_{ex} \ll |\Delta\omega|$
For interactions in slow exchange each state and the corresponding frequencies can be individually observed.

The most common NMR experiment for studying protein interactions is the ^1H - ^{15}N Heteronuclear quantum coherence (HSQC) spectrum. It shows all H-N correlation within a protein. These signals represent mainly the backbone amide groups, but Tryptophan, Asparagine and Glutamine side chains are also visible. The ^1H - ^{15}N HSQC is regarded as the fingerprint of a protein. To record ^1H - ^{15}N HSQC spectra ^{15}N isotope labeling of the protein of interest is essential to overcome the low natural abundance of ^{15}N nitrogen.

During the experiment the magnetization is transferred from hydrogen nuclei to attached ^{15}N nuclei. The chemical shift is evolved on the nitrogen is then transferred back to the hydrogen for detection.

Another spectrum that provides information on binding sites is the ^1H - ^{13}C HSQC. It provides correlations between a carbon and its attached protons. Titration with unlabeled binding partner causes different chemical environment of side chain atoms and as a consequence shifting peaks. Chemical shifts of side chain atoms are essential

for identification of Nuclear Overhauser Effect (NOE) crosspeaks, which are used to obtain distance information for structure determination.

Experiment

^1H - ^{15}N HSQC NMR spectra and ^1H - ^{13}C HSQC NMR spectra were recorded at 298 K either on a 700 MHz Bruker Avance III NMR spectrometer equipped with a TCI cryoprobe or on a 600 MHz Bruker Avance Neo NMR spectrometer equipped with a TXI 600S3 probehead at 298 K.

All spectra were recorded with an interscan delay of 1.0 s with 1,024 and 256 points, respectively, and 8 scans per increment. Data acquisition and processing was performed using Topspin3.5 and Topspin4.0 (Bruker).

^{15}N labeled samples were used at a concentration of either 50 μM or 100 μM as indicated in the respective figures. Titrations were performed with 1 and 2 stoichiometric equivalents of the unlabeled binding partner.

All spectra ^1H - ^{13}C HSQC NMR spectra were recorded with an interscan delay of 1.0 s with 1,024 and 400 points, respectively, and 8 scans per increment.

Buffers for the titrations were optimized during the project and are indicated in respective figure descriptions.

NMR assignment strategies

Backbone Assignment

In order to identify binding sites, affected peaks in the ^1H - ^{15}N HSQC have to be linked to the amino acid residue. This can be achieved by using triple resonance NMR experiments (also three-dimensional NMR experiments), which utilize scalar and dipolar couplings between certain nuclei to establish their connectivity. Those experiments can be divided into three categories: intra-residue, sequential, and bi-directional correlation experiments.

For sequential assignments the correlated ^1H and ^{15}N nuclei are connected in a third dimension with one or more additional nucleus ($^{13}\text{C}_\alpha$, $^{13}\text{C}_\beta$...).

^1H - ^{15}N pairs are recognized as belonging to neighboring residues when corresponding frequencies match. In this way chains of sequentially connected residues can be built, which might be interrupted by missing or unobservable NMR signals, as for example prolines. Afterwards, those chains can then be mapped to the protein sequence.

Typically, multiple triple resonance NMR experiments are combined for a protein assignment. A graphical representation of common triple resonance assignment experiments is shown in Figure 9.

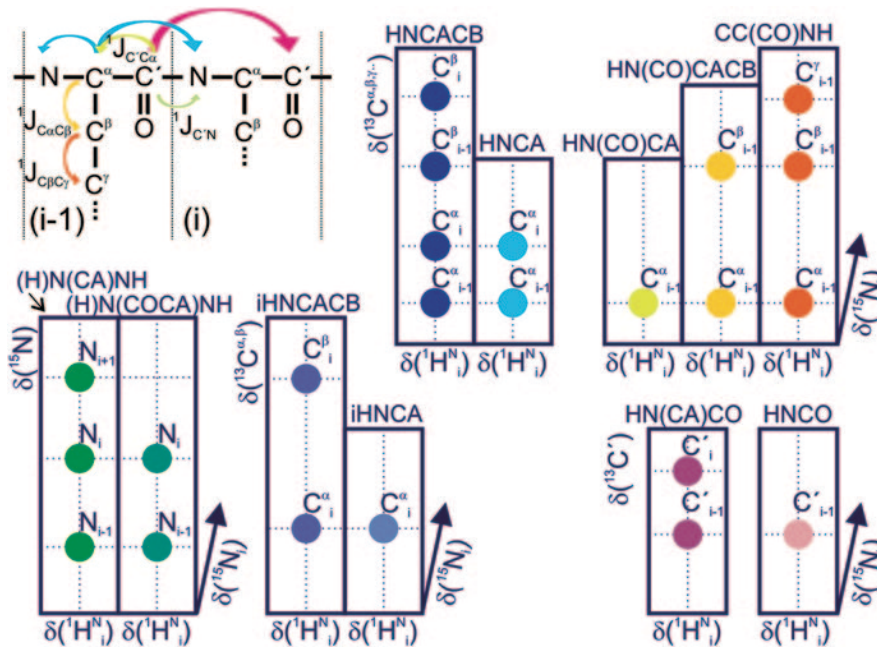


Figure 9: Overview of three-dimensional backbone assignment experiments
Reprinted by permission from Springer Nature (53)

The backbone assignment is based on two main spectra: HNCACB and CBCA(CO)NNH. The HNCACB links each NH group with the C_α and C_β chemical shift of its own residue and the preceding residue, whereas the CBCA(CO)NNH only links NH groups with the C_α C_β chemical shifts of the residue before (Figure 10).

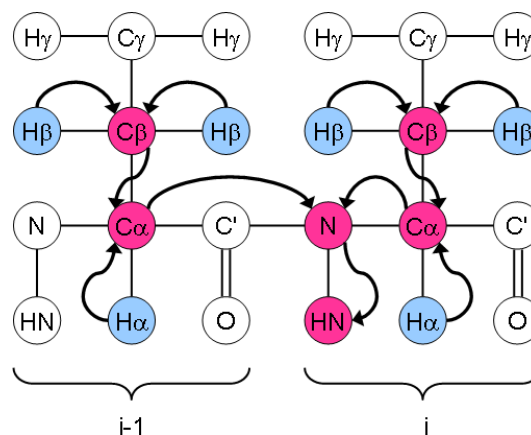


Figure 10: Magnetization transfer during an HNCACB experiment
(<http://www.protein-nmr.org.uk/solution-nmr/spectrum-descriptions/cbcanh-hncacb/> called up 28.09.2018)

In the HNCACB, the magnetization is transferred from the $^{15}\text{N}^1\text{H}$ group coming from the backbone of one given amino acid (residue i) to the $^{13}\text{C}_\alpha$ and $^{13}\text{C}_\beta$ of the side chain of itself (residue i) and those of the preceding residue (residue $i-1$) and then back to ^{15}N and ^1H for detection. Thus, for each NH group of the backbone, besides glycine, two C_α and C_β peaks are visible.

In contrast to the HNCACB, the magnetization transferred in the CBCA(CO)NNH only from C_α and C_β of residue $i-1$ to HN of residue i . This gives rise to signals of C_α and C_β of residue $i-1$ (Figure 11).

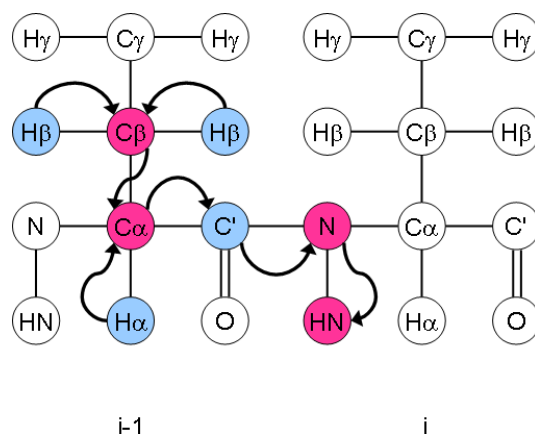


Figure 11: Magnetization transfer during an CBCA(CO)NNH experiment

(<http://www.protein-nmr.org.uk/solution-nmr/spectrum-descriptions/cbcaconh-hncocacb/> called up 28.09.2018)

Using those experiments C_α and C_β chemical shifts can be obtained, and in some characteristic cases identify the residue. Furthermore, chains of connected residues can be built (Figure 12).

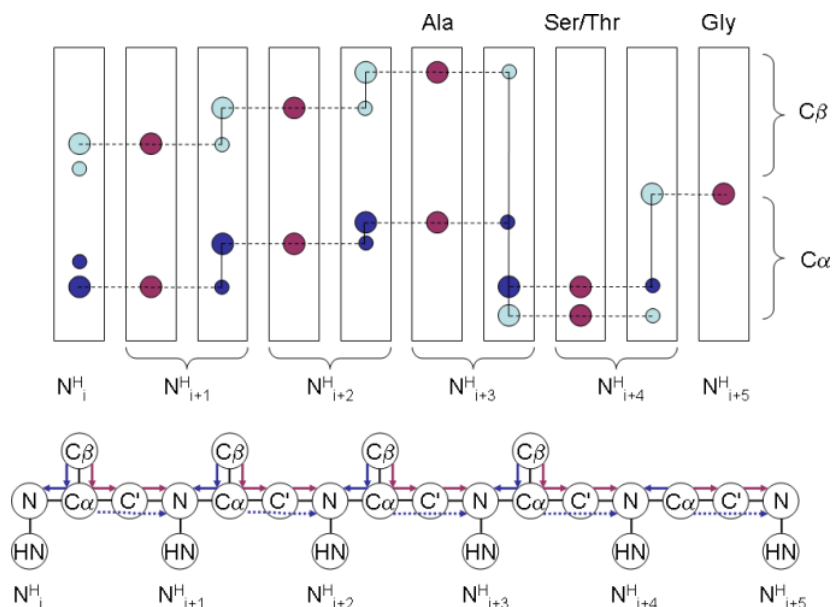


Figure 12: Schematic representation of the assignment strategy and formation of amino acid chains

(<http://www.protein-nmr.org.uk/solution-nmr/assignment-theory/triple-resonance-backbone-assignment/> called up

28.09.2018)

Side chain assignment

In a H(CCCO)NH experiment magnetization is transferred from the side-chain hydrogen nuclei to attached ^{13}C nuclei. Then magnetization is transferred between carbon nuclei via isotropic ^{13}C mixing and then transferred to the carbonyl carbon, amide nitrogen and to the amide hydrogen for detection. The chemical shift is evolved simultaneously on all carbon nuclei, as well as on the amide nitrogen and hydrogen nuclei (Figure 13).

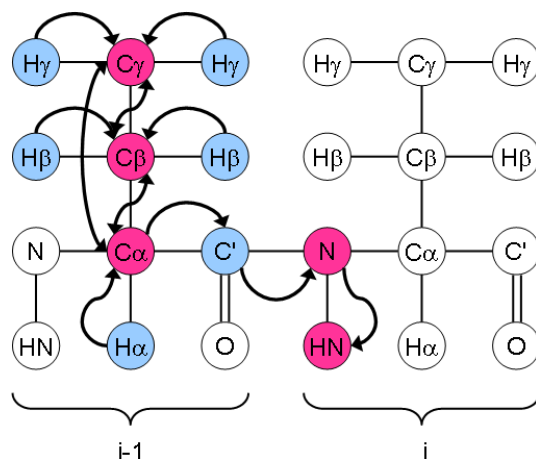


Figure 13: Magnetization transfer during a H(CCCO)NH experiment
(<http://www.protein-nmr.org.uk/solution-nmr/spectrum-descriptions/hcconh/> called up 28.09.2018)

In this spectrum signals for all carbon atoms of residue i-1 are visible.

Experiment

Three-dimensional assignment experiments of p53¹⁻⁹⁴ were conducted at a 700 MHz Bruker Avance III NMR spectrometer equipped with a TCI cryoprobe at 298 K. ^{13}C ^{15}N labeled p53¹⁻⁹⁴ was used at a concentration of 500 μM in an NMR buffer containing 50 mM NaPO_4 , 150 mM NaCl and 1 mM DTT and 10% D_2O at pH 6.5.

For p53³⁷⁻⁵⁷ the assignment experiments were measured at a 600 MHz Bruker Avance Neo NMR spectrometer equipped with a TXI 600S3 probehead at 298 K. Measurements were performed using ^{13}C ^{15}N labeled p53³⁷⁻⁵⁷ at a 700 μM in an NMR buffer containing 50 mM Sodium phosphate and 10% D_2O at pH 7.5.

Data acquisition and processing was performed with Topspin3.5 and Topspin4.0 (Bruker). Data analysis, peak picking and assignment were performed using ccpNMR (55).

NMR Molecular dynamics

Secondary Chemical Shift

The chemical shifts of the protein backbone are sensitive to the local backbone geometry and can therefore provide information on the propensity of secondary structural elements. This allows to derive secondary structure elements and dihedral angles from chemical shifts. The secondary chemical shift is dependent on the protein secondary structure and can be calculated as follows:

$$\Delta\delta = \delta_{observed} - \delta_{random\ coil}$$

Positive $^{13}\text{C}_\alpha$ values have positive secondary chemical shift values if they tend to form alpha-helical structures and negative $^{13}\text{C}_\alpha$ values if they are likely to be in a beta-stranded secondary structure.

Secondary chemical shift values can provide information of transient secondary structure elements within intrinsically disordered region, which can be characteristic for protein-protein interaction sites. Using database of machine learning approaches one can derive the dihedral angles based on the sequence, the backbone and the $^{13}\text{C}_\beta$ chemical shifts, which can be used for structural calculations.

Random coil chemical shifts were predicted using the nclDP library, which is optimized for intrinsically disordered proteins, harboring many proline residues (56)

Relaxation

Local and global molecular motions can be characterized by quantification of nuclear spin relaxation effects.

T_1 , T_2 and ^1H - ^{15}N heteronuclear NOE (HetNOE) characterize the dynamic behavior of proteins. The longitudinal relaxation time T_1 measures the decay of ^{15}N polarization, while the transverse relaxation time T_2 accounts for the loss of spin coherence. HetNOE quantifies the polarization transfer from an amide ^1H to its attached ^{15}N .

The measured ^{15}N relaxation parameters provide quantitative information on the amplitudes and time scales of motion experienced by the ^{15}N - ^1H amide group of each residue. The sensitivity of ^{15}N relaxation ranges from nano- to picoseconds.

T_2 relaxation can additionally cover slower conformational changes in the micro- to millisecond scale.

HetNOE values range from +0.9 for amide groups in rigid protein fragments to largely negative values for highly flexible disordered regions. Values for each residue indicate the degree of freedom of a particular amide group.

Information derived from HetNOE experiments can provide very useful information of the flexibility of protein regions. Regions that form secondary structures are more rigid than disordered regions. For intrinsically disordered proteins, interaction sites are often more rigid compared to other parts.

Experiment

$^1\text{H}^{15}\text{N}$ HetNOE was measured on $^{13}\text{C}^{15}\text{N}$ -labeled p53¹⁻⁹⁴ at a concentration of 500 μM . 1,024 and 256 points, respectively, and 8 scans per increment were recorded at a 700 MHz Bruker Avance III NMR spectrometer, equipped with a TCI cryoprobe at 298 K. Data acquisition and processing was performed using Topspin3.5 (Bruker). The pulse program hsqcnoef3gpsi with a saturation time of 3 seconds was used.

NMR for detection of post-translational modifications

NMR spectroscopy can be used to detect and to follow post-translational modifications. Covalent attachment of a phosphate to a serine, threonine or tyrosine changes the local arrangement and chemical environment of the related nuclei. Altered chemical environment affects the chemical shifts of nuclei, which are attached or nearby (57).

^1H and ^{15}N chemical shifts of phosphorylated residues are very characteristic, leading to chemical shift change in a well-defined area of the spectrum. This allows to track phosphorylation events and follow phosphorylation over time (57).

Phosphorylation of recombinant expressed isotope labeled proteins can be achieved either (i) using recombinant kinases or (ii) incubating the isotope-labeled protein in a cell extract, making use of the various kinases within a cell lysate (57).

Experiment:

A 200 μl pellet of human HEK293T cells was resuspended in 400 μl of lysis buffer containing Tris 50 mM pH 7.5, NaCl 150 mM, 1% Triton, 1 mM EDTA and 10 mM MgCl_2 supplemented with a cocktail of phosphatase inhibitor (preventing dephosphorylation, Roche) and protease inhibitor (preventing degradation, (Serva)). After incubation at 4°C for 30 minutes cells were centrifuged at 12 000 rpm for 30 minutes at 4°C. The supernatant contains all the soluble proteins of the cell extract including all kinases.

^{15}N labeled p53¹⁻⁹⁴ was incubated with 15 mg/ml HEK293T cell lysate for 5 minutes. Just before the measurement 10 mM adenosinotriphosphat (ATP) (Roth) was added to the sample and then a series of 20 $^1\text{H}^{15}\text{N}$ HSQC spectra was recorded, each measuring 35 minutes.

Small-Angle X-ray Scattering

Small-Angle x-ray scattering (SAXS) is a versatile and powerful method to characterize structure, flexibility and size of particles in solution. It finds applications in various fields such as material science, biophysics and structural biology.

In structural biology it is well suited for using it complementary with Electron Microscopy, X-Ray Crystallography and NMR spectroscopy in order to investigate large complexes (58).

Advantages of SAXS compared to X-Ray Crystallography is that it can be used for proteins in solution and that it is not necessary to grow crystals. This allows to study proteins in a more physiological environment. In comparison with NMR spectroscopy the benefits origin from a broad size range of proteins that can be studied (from few kDa to MDa).

However, in contrast to those techniques, it is not possible to derive an atomic resolution structure of a protein from SAXS experiments. Nevertheless, SAXS provides essential information as, overall shape (20 Angstrom resolution), molecular weight, flexibility and size (59).

Basic principle of SAXS

In SAXS a monochromatic X-ray beam irradiates a solution of macromolecules and the scattered intensity I is recorded by a two-dimensional detector.

A solution of proteins gives rise to an isotropic scattering intensity, which is the modulus of the scattering vector s , which is defined as

$$s = \frac{4\pi \sin(\theta)}{\lambda}$$

Where λ is the wavelength of the incoming radiation and 2θ is the angle between the incident and the scattered beam.

$$I(s) = \langle I(s) \rangle = \langle A(s)A^*(s) \rangle$$

$\langle \rangle$ stands for the average over all directions of the scattering vector. The scattering amplitude is the sum of all coherent waves with their phase difference φ , as consequence of elastic scattering (59).

Scattering intensity profiles usually do not provide intuitive structural information, therefore transformations of the SAXS profile $I(s)$ can be performed. Molecular weight

and radius of gyration (R_g) can be obtained from Guinier analysis of the Guinier region (typically $0 \leq qR_g \leq 1.3$) (60).

Another transformation that can even provide more information, such as shape of molecules, is the pair distance distribution function ($P(r)$) (60). Another advantage of the $P(r)$ is that it can be used as input for calculating low-resolution structure models. DAMMIF is an ab-initio method that uses $P(r)$ functions to obtain dummy atom models that correspond to the scattering profiles and provides information on the surface structure of a protein or protein complex. Dummy atoms serve as placeholder, that occupy a known position in space and have a known scattering pattern. DAMMIF tries to find the set of dummy atoms within a search volume whose accumulated scattering resembles the experimental data best (60, 61).

Experiment

For SAXS measurements, protein samples were prepared at a concentration of 5 mg/ml in a SAXS buffer containing 50mM Tris, 150mM NaCl and 1mM TCEP at a pH of 7.5. Scattering data was measured with an in-house SAXS instrument (SAXSspace, Anton Paar, Graz, Austria) equipped with a Kratky camera, a sealed X-ray tube source and a Mythen2 R 1K Detector (Dectris). 180 frames, each 1 minute of the scattering pattern were recorded. Recording short frames allows to observed sample stability throughout the measurement, which was given for all samples.

SAXS data was processed using the SAXSanalysis package (Anton Paar, version 3.0) and analyzed using the ATSAS package (version 2.8.2, Hamburg, Germany (62)). Desmearing was performed using GIFT (PCG-Software). GNOM was used to calculate forward scattering ($I(0)$), radius of gyration (R_g), the maximum distance (D_{max}) and the interatomic distance distribution ($P(r)$).

To calculate surface models based on the $P(r)$ functions DAMMIF was employed, which uses GNOM files as input (61). For each structure, 50 simulated annealing runs were and the resulting models were superimposed, averaged and filtered using DAMAVER. Matching models were then clustered by DAMCLUST.

Microscale Thermophoresis

Microscale thermophoresis (MST) is a technique to investigate biomolecular interactions. It is based on thermophoresis, the directed movement of molecular in a temperature gradient. The temperature gradient is induced by an infrared laser. During the experiment the directed movement of molecules is detected and quantified using

fluorophores. Using fluorescent labeled proteins and unlabeled binding partners stoichiometries, binding modes and binding affinities can be observed (63).

Experiment

MST requires fluorescent labeled proteins. For labeling Alexa 488 maleimide (Invitrogen) was used. 500 μ M of a 7 mM stock were used for the reaction with 50 μ M of protein. The reaction was carried out at 4°C overnight protected from light. Size exclusion chromatography was performed to separate the labeled protein from unbound fluorophore.

Concentration of the labeled protein was determined by measuring the absorbance at 495 nm corresponding to the maximum absorbance of the fluorophore (Alexxa 488).. Measurements were performed using Monolith NT.115 (NanoTemper).

Results

Expression and Purification

The set of experiments involved expression tests to find the optimal conditions for proteins expression in *E.Coli* BL21(DE3). Expression tests were performed for all protein constructs used during the study (Data not shown).

Overexpression was observed in all tested conditions (at 20°C, 25°C and 30°C) after an IPTG incubation period of 8 hours. Optimal expression conditions for all protein constructs revealed to be at 20°C after 16 hours of IPTG induction.

After expression, proteins were purified as described in the Material and Methods section. Purity of the protein solution during the purification process was investigated using SDS-PAGE. A representative SDS gel of fractions during the purification process of FOXO4⁸⁶⁻²⁰⁸ is shown in Figure 14.

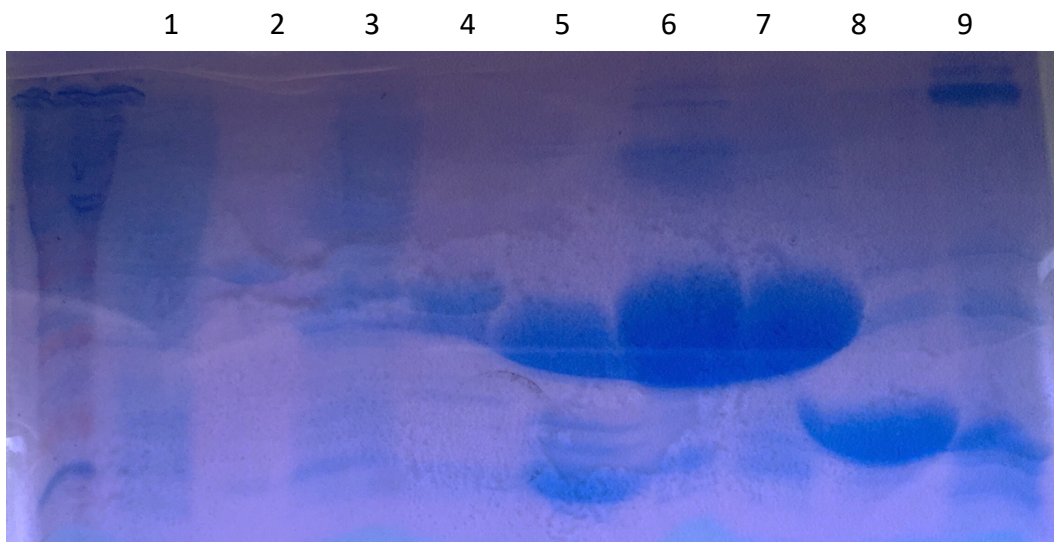


Figure 14: Expression and purification of FOXO4⁸⁶⁻²⁰⁸, FOXO4⁸⁶⁻²⁰⁸ was expressed in *E.coli* BL21(DE3) and purified Purification was controlled using SDS-PAGE. Lane 1: Lysate, Lane 2:Flow-through fraction, Lane 3: washing fraction; Lane 4: high-salt washing fraction,, Lane 5: Elution fractions of FOXO4⁸⁶⁻²⁰⁸;Lane 6: cleaved FOXO4⁸⁶⁻²⁰⁸

In the flow-through fraction in lane 1 only few FOXO4⁸⁶⁻²⁰⁸ did not bind to the Ni-NTA column, confirming the sufficient binding of the N-terminal fused His₆-proteinA tag to the nickel column. During the washing steps unspecifically bound proteins were eluted as seen in lane 3 harboring the washing fractions. The elution fraction in lanes 5 to 7 contains His₆-proteinA tagged FOXO4⁸⁶⁻²⁰⁸. The tag might change the protein structure or interaction behavior and was therefore removed using TEV protease. The fraction after cleavage is separated in lane 8. The band is about 10 kDa lower than the one of

the uncleaved His₆-proteinA tagged FOXO4⁸⁶⁻²⁰⁸ corresponding to the size His₆-proteinA tag. Further purification via size exclusion chromatography is required as there are still unspecific bands visible.

In lane 9 the elution fraction of the second nickel-step is separated showing bands for His₆-proteinA tagged TEV protease at around 20kDa and the His₆-proteinA tag at around 10 kDa.

Identification of Binding sites on p53

p53 physically interacts with FOXO4 Forkhead Domain with high nanomolar affinity

As shown by our group in the publication of Baar et al. there is physical interaction between FOXO4 and p53 and the Forkhead Domain of FOXO4 is responsible on the FOXO4 side (2). However, it is yet unknown which regions of p53 are responsible for mediating the interaction.

First, we performed the reverse experiment confirming that the interaction is also observable from p53 side, using ¹⁵N labeled p53¹⁻³¹² and titrating it with increasing amounts of unlabeled FOXO4⁸⁶⁻²⁰⁸. An overlay of the ¹H-¹⁵N HSQC spectra is shown in Figure 15. In a ¹H-¹⁵N HSQC spectrum signals of backbone amide groups, Tryptophan, Asparagine and Glutamine side chains are visible. The position in the spectrum depends on the chemical environment. In case of a binding event during the titration, the local chemical environment at the binding sites will change and affect the ¹H-¹⁵N cross peaks position of the corresponding residues. Upon addition of unlabeled FOXO4, several p53 ¹H-¹⁵N cross peaks show progressive chemical shift change indicating direct interaction between p53 and FOXO4.

Most of the affected peaks are located in a region of the spectrum characteristic for unstructured regions of proteins (between 6 and 8 ppm), suggesting that the unstructured N-terminal domain of p53 might be involved in the interaction. Upon binding, the affected p53 cross peaks are shifted from the free-state position towards a bound state in a “fast-exchange” regime on the NMR timescale indicating micromolar to high millimolar binding affinities

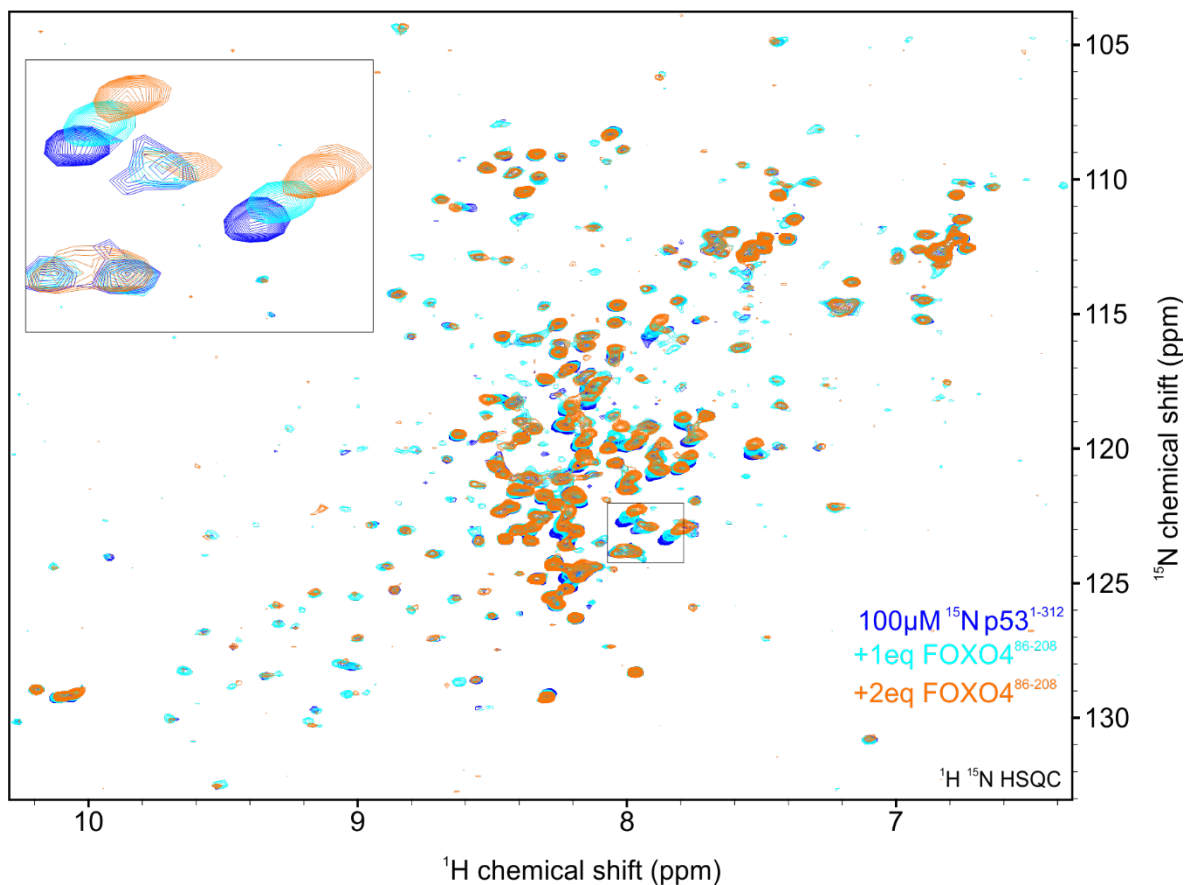


Figure 15: ^1H - ^{15}N HSQC Spectra of ^{15}N p53¹⁻³¹² titration with FOXO4⁸⁶⁻²⁰⁸
 Blue: reference spectrum of 100 μM ^{15}N p53¹⁻³¹² light blue: ^{15}N p53¹⁻³¹² in presence of 100 μM FOXO4⁸⁶⁻²⁰⁸; orange: ^{15}N p53¹⁻³¹² in presence of 200 μM FOXO4⁸⁶⁻²⁰⁸
 Measurements were recorded at 298K using a 700 MHz Bruker spectrometer, in a NMR buffer containing 50mM NaPO₄, 150mM NaCl and 2mM DTT at pH 6.5

MST was employed to precise the binding affinities corresponding to the p53 – FOXO4 complex formation.

Fluorescent labeled p53¹⁻³¹² was titrated with increasing amounts of FOXO4⁸⁶⁻²⁰⁸. The fitted binding curves of three replicates is shown in Figure 16.

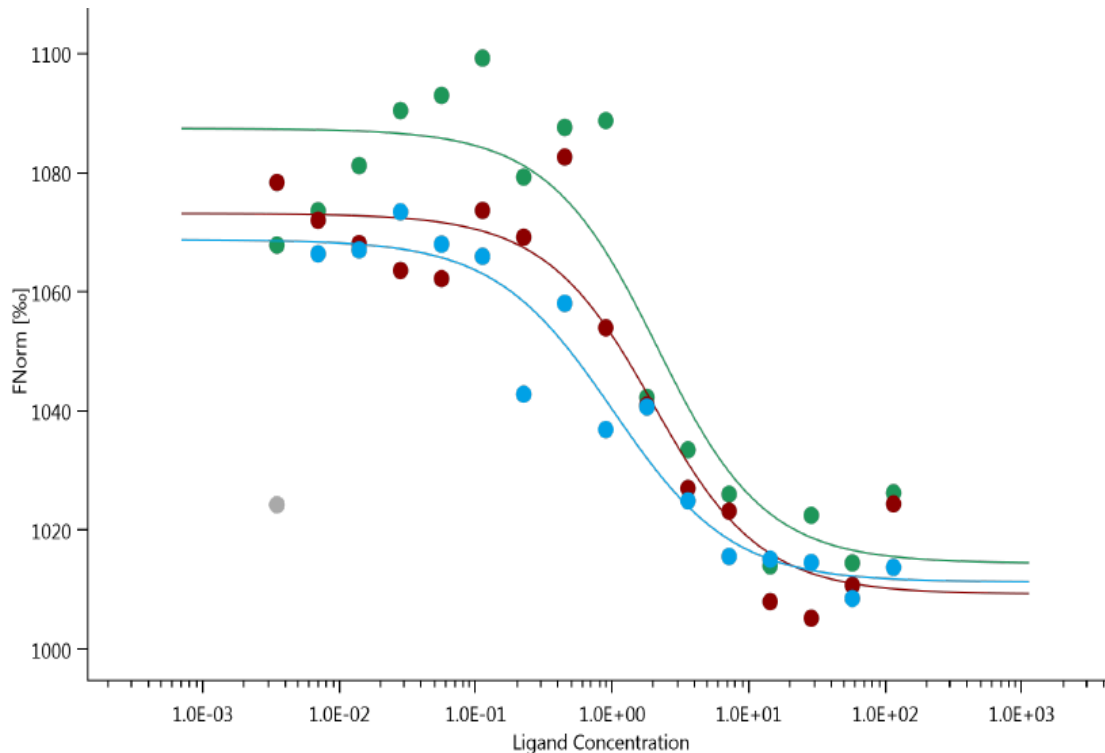


Figure 16: MST binding curve of fluorescent labeled p53¹⁻³¹² to unlabeled FOXO4⁸⁶⁻²⁰⁸

The binding affinity of p53¹⁻³¹² for FOXO4⁸⁶⁻²⁰⁸ determined by MST is 780 nM. Interactions with high nanomolar affinity are often visible in the fast-exchange regime on the NMR timescale, supporting results of NMR titrations.

The DNA Binding Domain of p53 does not physically interact with FOXO4 Forkhead Domain

In order to confirm out NMR results, suggesting that the disordered part of p53 is involved in FOXO4 binding we designed two p53 constructs corresponding either to the N-terminal disordered part (1 – 94) or the DNA-binding domain (94 -312) and tested their binding to FOXO4 using NMR.

Addition of unlabeled FOXO4⁸⁶⁻²⁰⁸ to a solution of ¹⁵N labeled p53⁹⁴⁻³¹² did not change the ¹H-¹⁵N cross peaks indicating no interaction between the DNA-binding domain of p53 and the Forkhead domain of FOXO4. An overlay of the corresponding ¹H-¹⁵N HSQC spectra is shown in Figure 17.

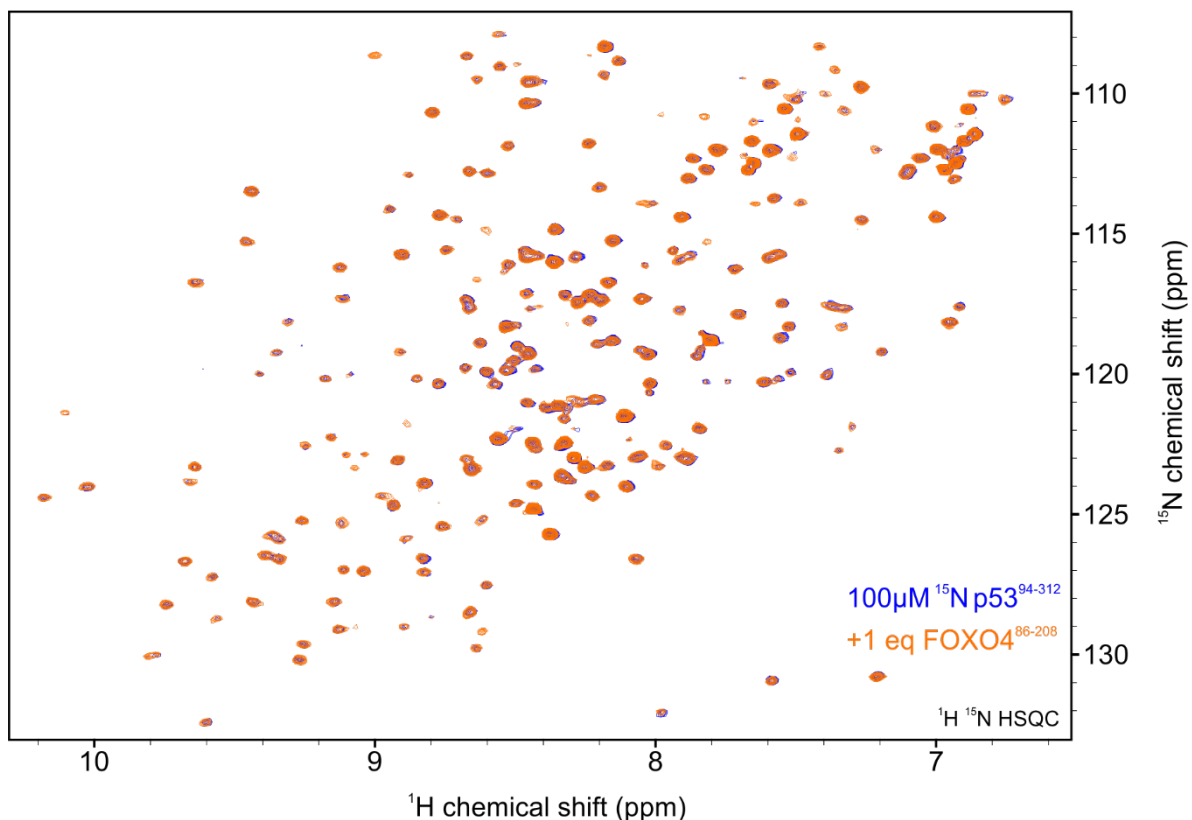


Figure 17: ^1H - ^{15}N HSQC Spectra of ^{15}N p53⁹⁴⁻³¹² titration with unlabeled FOXO4⁸⁶⁻²⁰⁸
 Blue: reference spectrum of 100 μM ^{15}N p53⁹⁴⁻³¹² orange: ^{15}N p53⁹⁴⁻³¹² in presence of 100 μM FOXO4⁸⁶⁻²⁰⁸
 Measurements were recorded at 298K using a 700 MHz Bruker spectrometer, in a NMR buffer containing 50mM NaPO₄, 150mM NaCl and 2mM DTT at pH 6.5

These results were also confirmed using MST, as there was also no binding detectable of fluorescent labeled p53⁹⁴⁻³¹² to FOXO4⁸⁶⁻²⁰⁸ (Data not shown).

Previously it was described that the p53 – FOXO3 interaction not only involves the FOXO4 Forkhead domain but also the CR3 region of FOXO3. Therefore, we wanted to test if there is a similar additional interaction between the DNA-binding domain of p53 and the CR3 region of FOXO4. Unlabeled FOXO4⁴⁶⁵⁻⁵⁰⁵ was added in excess to a solution of ^{15}N -labeled p53⁹⁴⁻³¹². An overlay of the resulting spectra is shown in Figure 18. Overall the spectra look similar and there are no chemical shift changes observable, even though the large excess of the CR3 region of FOXO4, indicating no binding event between the DNA-binding domain of p53 and the CR3 region of FOXO4.

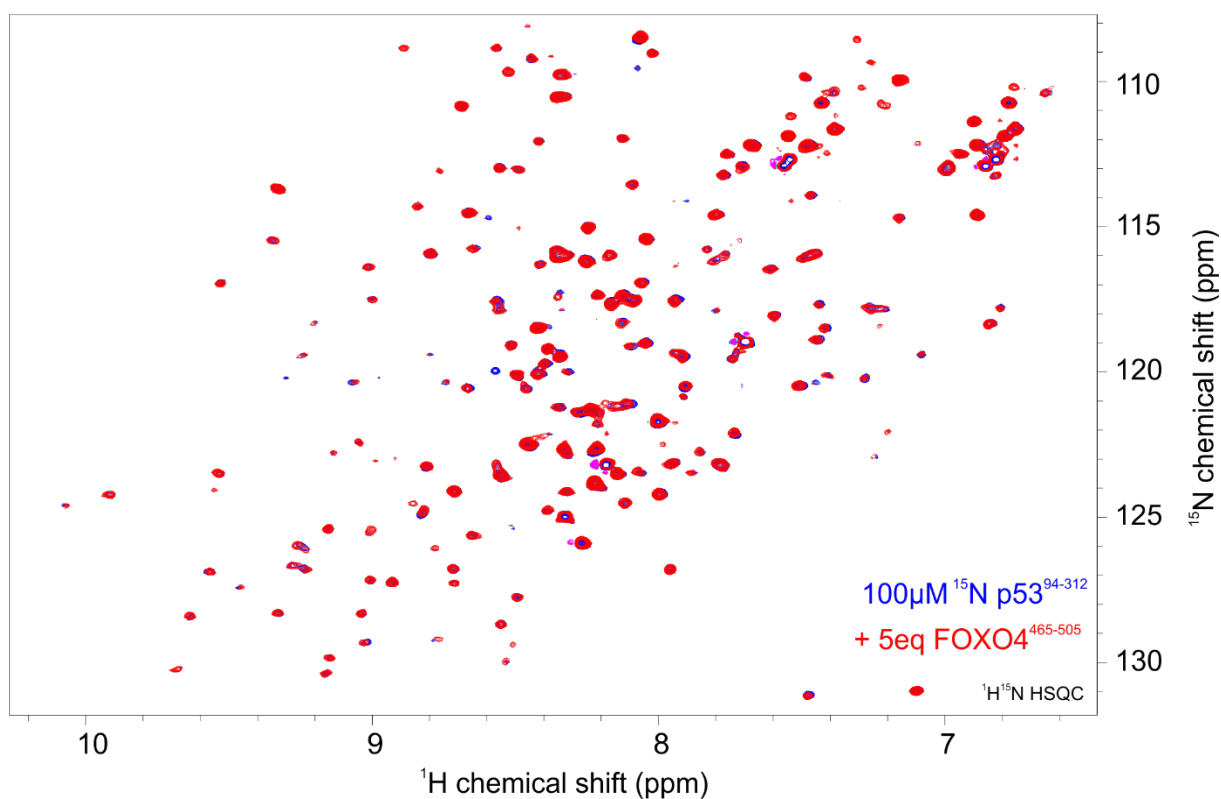


Figure 18: ^1H - ^{15}N HSQC Spectra of ^{15}N p53⁹⁴⁻³¹² titration with unlabeled FOXO4⁴⁶⁵⁻⁵⁰⁵
 Blue: reference spectrum of 100 μM ^{15}N p53⁹⁴⁻³¹² red: ^{15}N p53⁹⁴⁻³¹² in presence of 500 μM FOXO4⁴⁶⁵⁻⁵⁰⁵
 Measurements were recorded at 298K using a 700 MHz Bruker spectrometer, in a NMR buffer containing 50mM NaPO₄, 150mM NaCl and 2mM DTT at pH 6.5

These findings show that the interaction of p53 and FOXO4 is not similar to the p53 – FOXO3 interaction and strengthen the hypothesis, that the unstructured N-terminal transactivation domain of p53 is responsible FOXO4 interaction.

FOXO4 - p53 Interaction is mediated by two subdomains within the N-terminal Transactivation Domain of p53

For validation of our hypothesis and further identification of the binding sites, ^{15}N labeled p53¹⁻⁹⁴ was titrated with unlabeled FOXO4⁸⁶⁻²⁰⁸. The resulting ^1H - ^{15}N HSQC spectra of the titration are shown in an overlay in Figure 19.

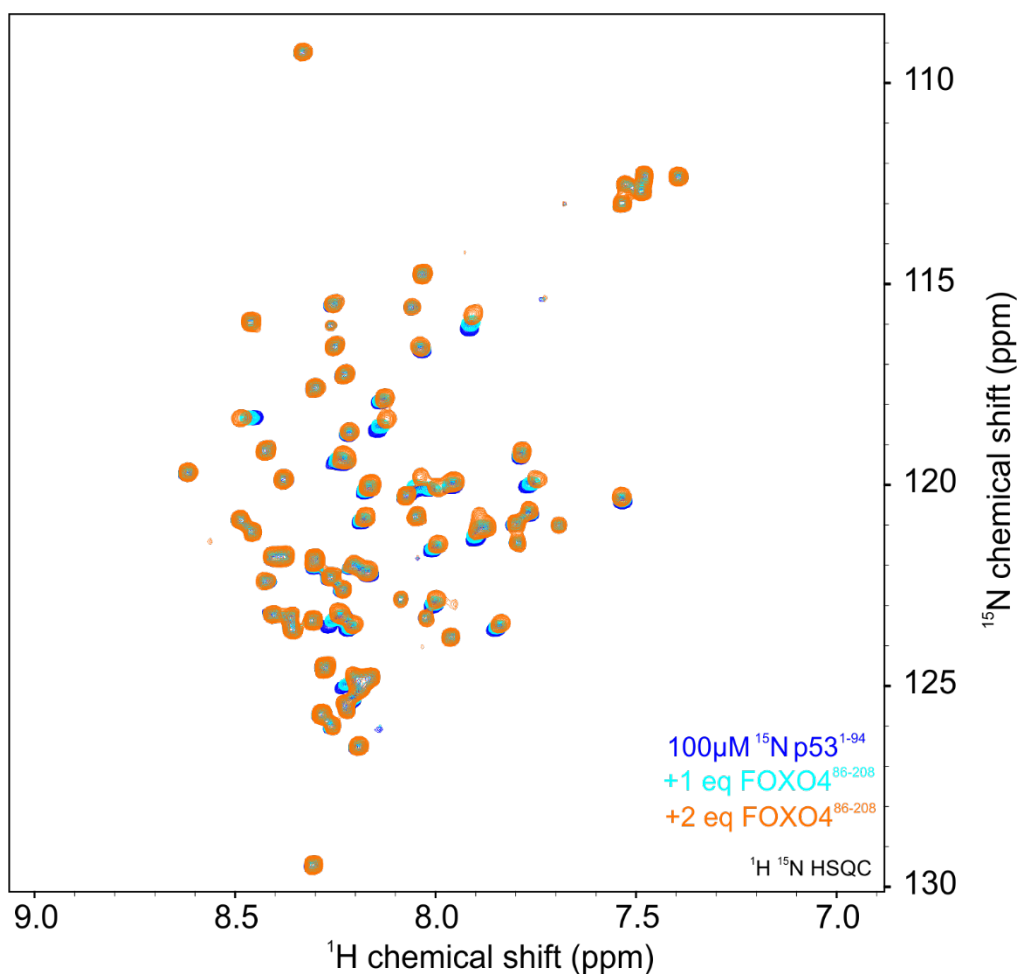


Figure 19: ^1H - ^{15}N HSQC Spectra of ^{15}N p53¹⁻⁹⁴ titration with FOXO4⁸⁶⁻²⁰⁸
 Blue: reference spectrum of 100 μM ^{15}N p53¹⁻⁹⁴ light blue: ^{15}N p53¹⁻⁹⁴ in presence of 100 μM FOXO4⁸⁶⁻²⁰⁸; orange: ^{15}N p53¹⁻⁹⁴
 in presence of 200 μM FOXO4⁸⁶⁻²⁰⁸
 Measurements were recorded at 298K using a 700 MHz Bruker spectrometer,
 in a NMR buffer containing 50mM NaPO₄, and 2mM DTT at pH 7.5

The low dispersion of signals in the proton dimension is characteristic for disordered proteins. The addition of unlabeled FOXO4⁸⁶⁻²⁰⁸ to ^{15}N p53¹⁻⁹⁴ affected the chemical environment of p53¹⁻⁹⁴ thereby changing the position of the ^1H - ^{15}N cross peaks. Shifting of the ^1H - ^{15}N cross peaks indicates that the interaction takes place in the fast-exchange regime on NMR timescale.

To confirm the interaction of p53¹⁻⁹⁴ with FOXO4⁸⁶⁻²⁰⁸ the reverse titration with ^{15}N labeled FOXO4⁸⁶⁻²⁰⁸ and unlabeled p53¹⁻⁹⁴ was performed. ^1H - ^{15}N HSQC spectra of ^{15}N FOXO4⁸⁶⁻²⁰⁸ with increasing amounts of unlabeled p53¹⁻⁹⁴ are shown in Figure 20. During the titration the binding of unlabeled p53¹⁻⁹⁴ affected the local chemical environment of ^{15}N FOXO4⁸⁶⁻²⁰⁸ and as a consequence the position of ^1H - ^{15}N cross peaks.

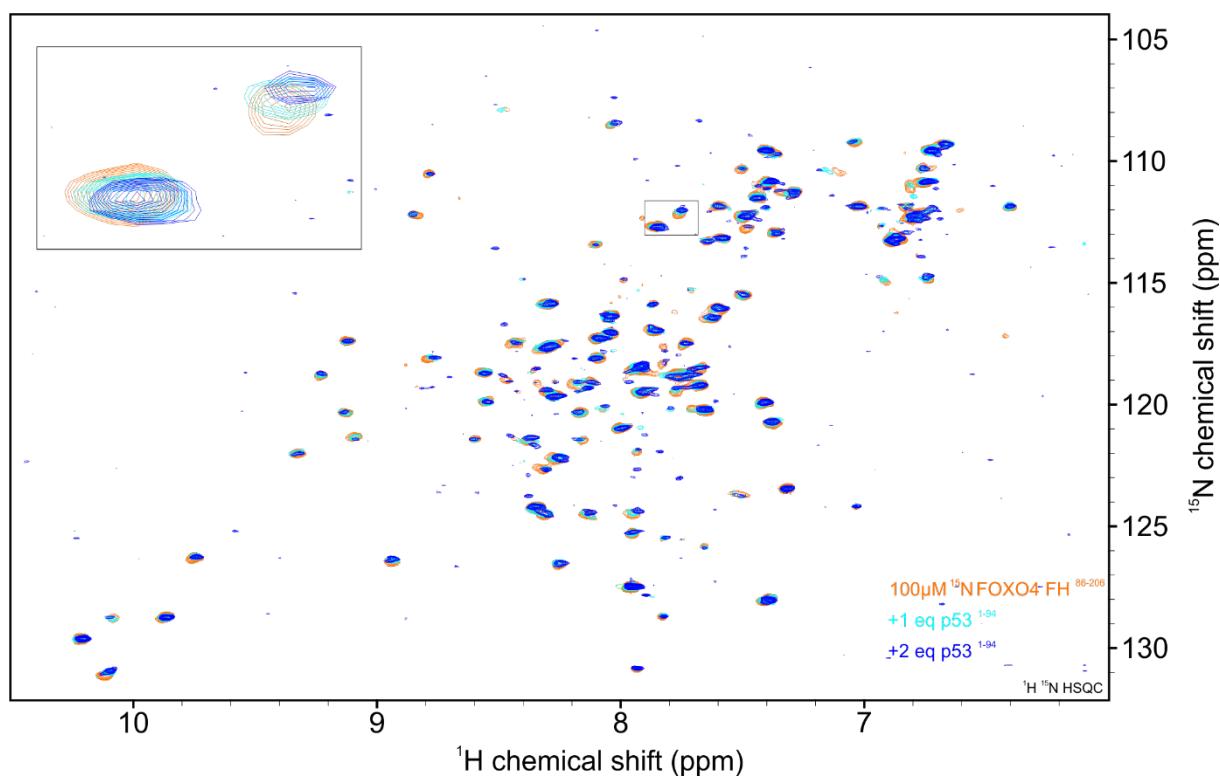


Figure 20: ^1H - ^{15}N HSQC Spectra of ^{15}N FOXO4⁸⁶⁻²⁰⁸ titration with p53¹⁻⁹⁴
 Blue: reference spectrum of 100 μM ^{15}N FOXO4⁸⁶⁻²⁰⁸; light blue: ^{15}N FOXO4⁸⁶⁻²⁰⁸ in presence of 100 μM p53¹⁻⁹⁴; orange: ^{15}N FOXO4⁸⁶⁻²⁰⁸ in presence of 200 μM p53¹⁻⁹⁴; Measurements were recorded at 298K using a 700 MHz Bruker spectrometer, in a NMR buffer containing 50mM NaPO₄, and 2mM DTT at pH 7.5

NMR spectroscopy provides the possibility of identifying exactly the residues and even atoms, which are responsible for the interaction. Three-dimensional NMR experiments are essential to assign peaks in the spectra to the corresponding amino acid residue of the protein. The assignment strategy for the backbone assignment was discussed in the methods section before. For those experiments ^{13}C , ^{15}N labeled p53¹⁻⁹⁴ was expressed and purified.

At the end 65% of the backbone amides of p53¹⁻⁹⁴ were assigned. Figure 21 shows the ^1H - ^{15}N HSQC spectrum of p53¹⁻⁹⁴ with residues assigned to the corresponding peaks. Of residues 1-60 83% backbone amides were assigned, the poly-proline region from residue 61 to 94 however, proved to be difficult, as connected chains of residues are often early interrupted by prolines. 98% of the backbone of non-proline residues between residue 1-60 were identified.

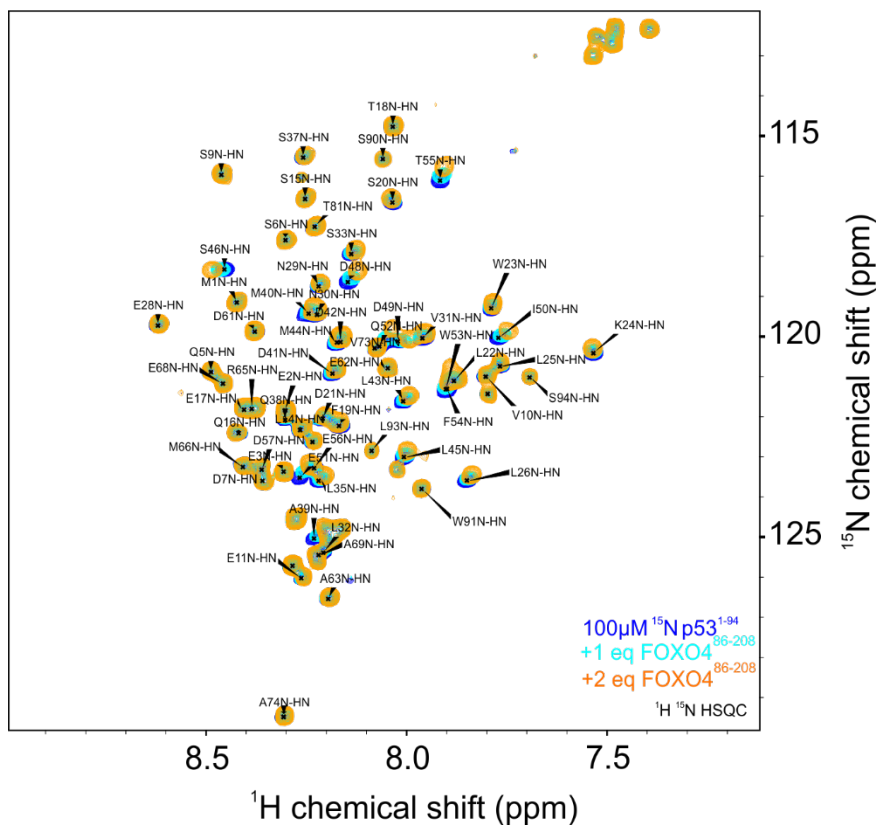


Figure 21: ^1H - ^{15}N HSQC Spectra of ^{15}N p53¹⁻⁹⁴ titration with FOXO4⁸⁶⁻²⁰⁸ including assigned peaks
Assignment experiments were measured at 298K using a 700 MHz Bruker spectrometer,
in a NMR buffer containing 50mM NaPO₄, and 2mM DTT at pH 7.5

Furthermore H_N, N_H, C_α and C_β chemical shifts of p53¹⁻⁹⁴ alone and in presence of unlabeled FOXO4⁸⁶⁻²⁰⁸ were determined. With $^1\text{H}_\text{N}$ and $^{15}\text{N}_\text{H}$ chemical shifts, the ^1H - ^{15}N normalized chemical shift perturbation for each residue can be calculated to identify the residues affected by the binding using the following formula (64):

$$\Delta\delta(\text{ppm}) = \sqrt{(\Delta\delta_\text{H})^2 + \left(\frac{\Delta\delta_\text{N}}{10}\right)^2}$$

Results are shown in Figure 22.

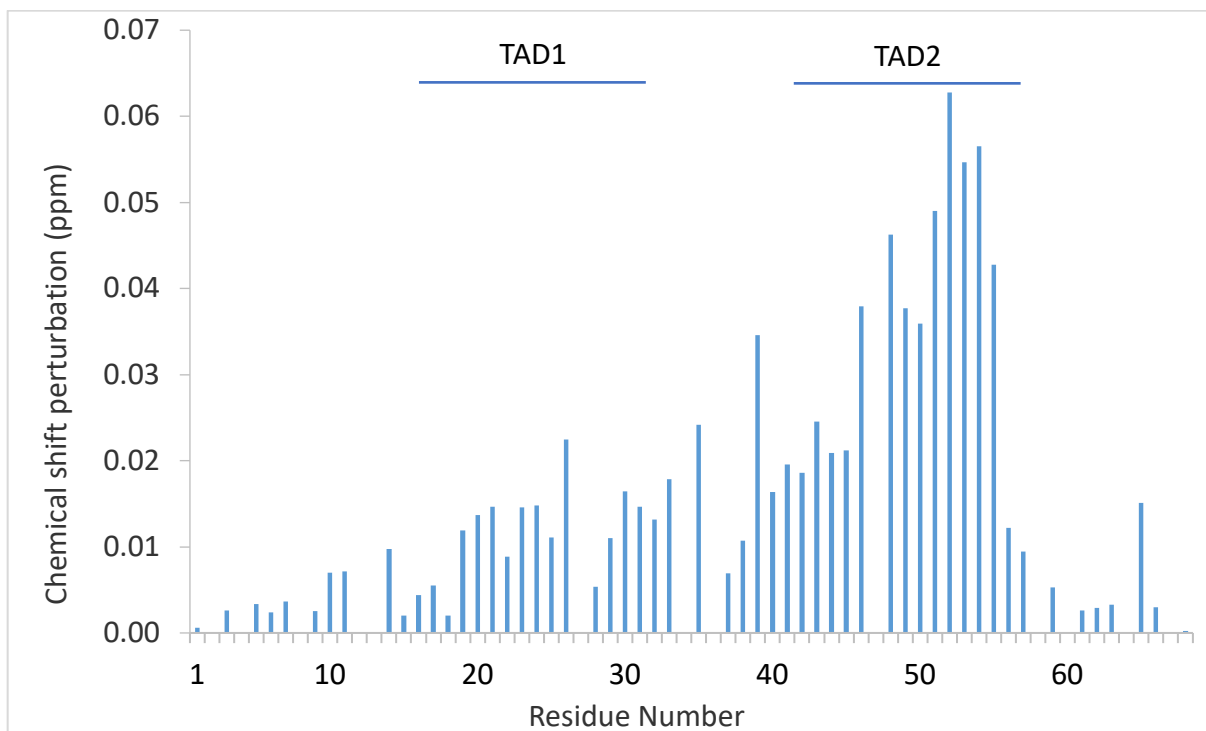


Figure 22: ^1H - ^{15}N normalized chemical shift perturbation of p53^{1-94} upon titration with FOXO4^{86-208}

^1H ^{15}N chemical shift perturbation shows two stretches of residues from 18 to 30 and from 37 to 57 which are affected by the binding event with FOXO4^{86-208} , indicating two distinct binding sites. The second binding site, corresponding to transactivation domain 2 is stronger affected, proposing that this is the main binding site.

Based on C_α and C_β chemical shifts the secondary chemical shift can be calculated. Secondary chemical shift values can be indicative for transient secondary structure elements, which are often characteristic for protein-protein interaction sites.

The results of secondary chemical shift analysis of p53^{1-94} are shown in Figure 23.

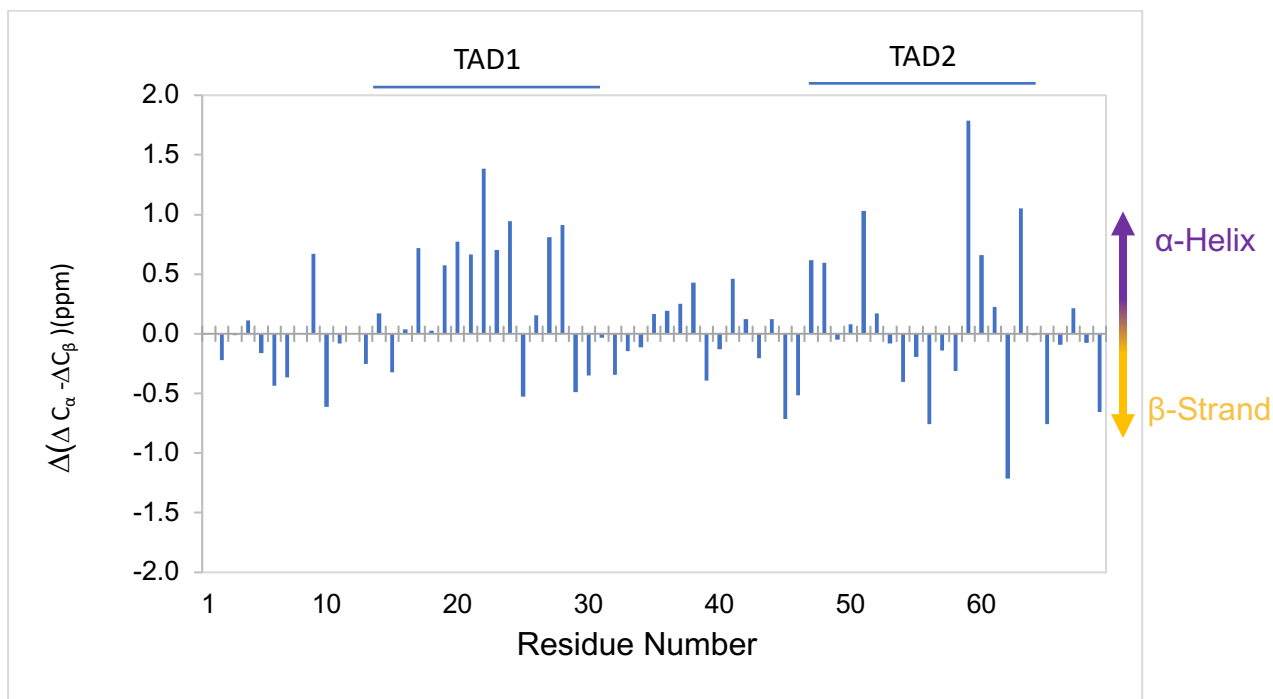


Figure 23: $\Delta(\Delta C_{\alpha} - \Delta C_{\beta})$ of the assigned residues of $^{13}C^{15}N$ labeled p53¹⁻⁹⁴

Positive values in this diagram indicate alpha helical tendencies, whereas negative values indicate that those residues are likely in a beta-stranded structure. Long stretches of positive values, as seen for residues 16 to 24, make the formation of an alpha-helix likely. These results indicate that p53¹⁻⁹⁴ harbors a motif with high alpha-helical propensity, which is characteristic for protein-protein interaction sites.

Measurement of $^1H^{15}N$ HetNOE provides information of flexibility of proteins and protein dynamics. Figure 24 shows the results of $^1H^{15}N$ HetNOE experiments of ^{15}N p53¹⁻⁹⁴. Positive values are correlated with lower flexibility and a higher rigidity of region within the protein.

Residues 16 to 24 and 48 to 55 show positive $^1H^{15}N$ HetNOE indicating lower flexibility in those regions. This is characteristic for interaction sites in a protein and might even be enhanced by formation of temporary secondary structure elements upon binding.

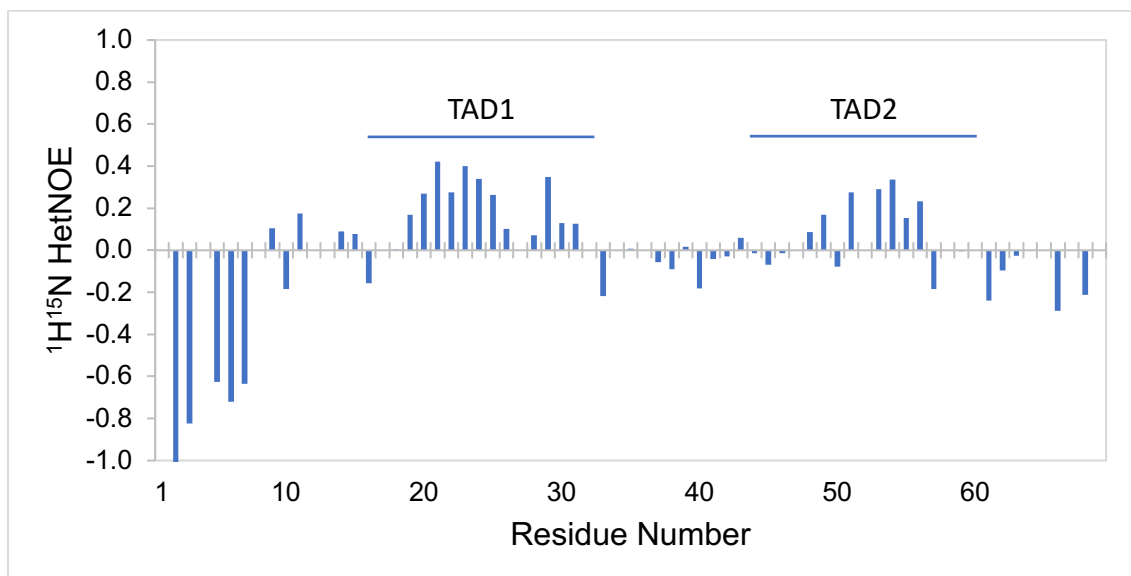


Figure 24: $^1\text{H}^{15}\text{N}$ HetNOE of ^5N p53¹⁻⁹⁴

Residues 37 to 57 are affected most by the binding of FOXO4⁸⁶⁻²⁰⁸, but also residues 16 to 24. The same stretches of residues are shown to have a lower flexibility and a high propensity for formation of an alpha-helix. Taking those results together it indicates that there are two binding sites for FOXO4⁸⁶⁻²⁰⁸ on p53 which corresponds to the two subdomains of the N-terminal transactivation domain: Transactivation domain 1 (16 to 24) and transactivation domain 2 (37-57).

The two affected domains raise the question, whether it is one molecule of FOXO4⁸⁶⁻²⁰⁸ binding to both subdomains or whether two molecules FOXO4⁸⁶⁻²⁰⁸ bind each to one of the subdomains of p53¹⁻⁹⁴.

SAXS confirms that two molecules of FOXO4 Forkhead Domain can bind to the N-terminal Transactivation Domain of p53

To assess this question, we used SAXS. SAXS provides structural information, such as Radius of Gyration, maximum diameter and molecular mass of molecules in solution, which can be used to elucidate the oligomeric state of the FOXO4 – p53 complex. Furthermore, SAXS can provide low-resolution structure models.

SAXS curves were recorded for p53¹⁻⁹⁴ and FOXO4⁸⁶⁻²⁰⁸ alone and for the 1:1 complex as well as the 1:2 complex. The SAXS curve, the calculated values and a low-resolution model of the complex are shown in Figure 25 and Table 6.

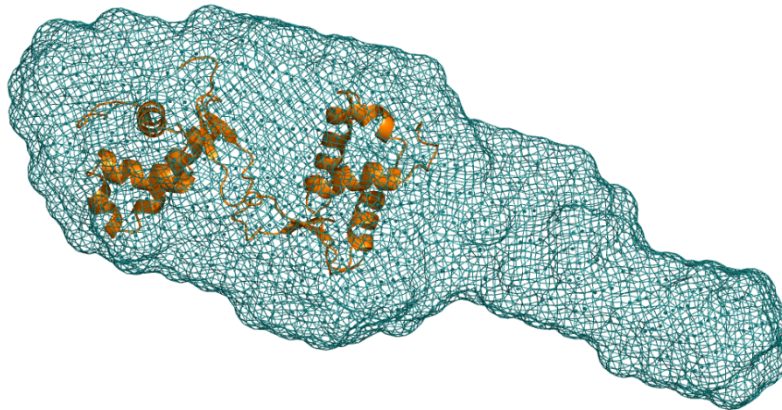
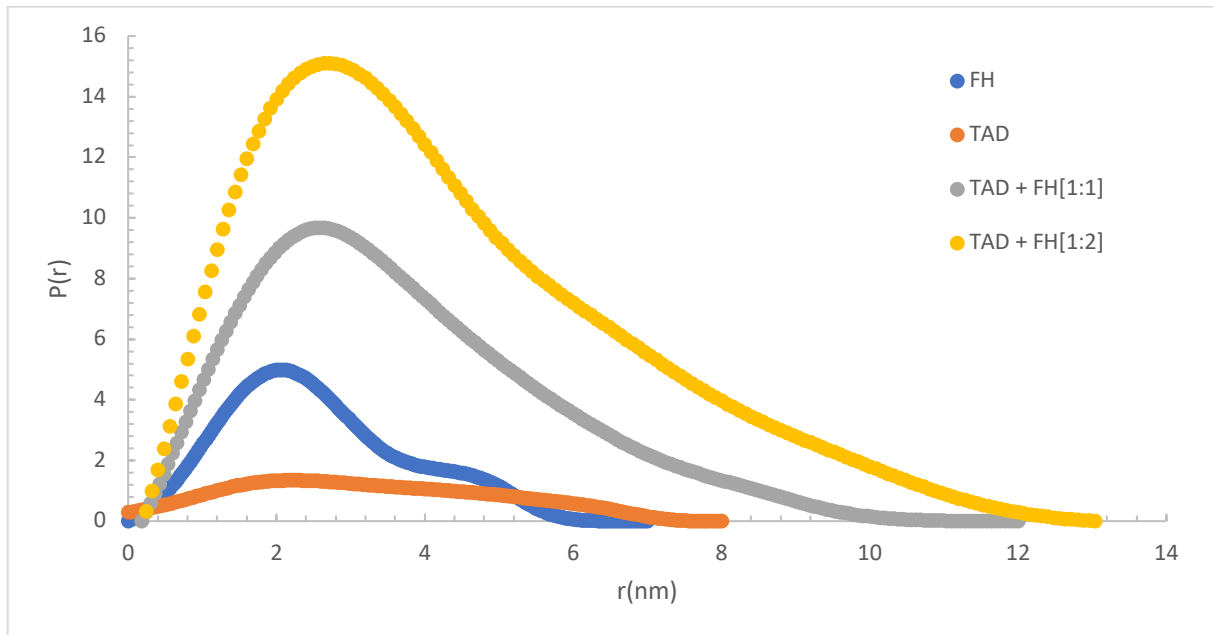


Figure 25: $P(r)$ function and surface model derived from SAXS experiments
 A) $P(r)$ of FOXO4⁸⁶⁻²⁰⁸ (orange), p53¹⁻⁹⁴ (violet) and complex of p53¹⁻⁹⁴ - FOXO4⁸⁶⁻²⁰⁸ at a ratio of 1:2 (blue); B) Surface model of p53¹⁻⁹⁴ - FOXO4⁸⁶⁻²⁰⁸ complex calculated based on $P(r)$ using DAMMIF merged with NMR structure of FOXO4 Forkhead Domain (PDB entry 1E17)

Based on the $P(r)$ function of a scattering experiment one can get indications about the overall shape of a protein. $P(r)$ functions of fully globular particles or molecules have a gaussian shape, whereas flat and elongated functions indicate elongated molecules. The observations in the scattering experiments fit well to the expectations for FOXO4⁸⁶⁻²⁰⁸, as it was previously described to be well-folded and globular, but also a elongated tail is visible. For the intrinsically disordered p53¹⁻⁹⁴ the function matches expectations as well. Scattering experiments of the p53¹⁻⁹⁴- FOXO4⁸⁶⁻²⁰⁸ complex confirmed the binding event. Furthermore, the calculated parameters listed in Table 6 indicate that there are two molecules of FOXO4⁸⁶⁻²⁰⁸ binding to one molecule of p53¹⁻⁹⁴. Also, the surface structure of calculated model based on the $p(r)$ function allows to fit two molecules of FOXO4⁸⁶⁻²⁰⁸.

Table 6: Parameters calculated from SAXS experiments

	R _g (nm)	Molecular mass (kDa)	Theoretical molecular mass (kDa)
FOXO4 ⁸⁶⁻²⁰⁸	1.9	19	13
p53 ¹⁻⁹⁴	2.5	10	10
p53 ¹⁻⁹⁴ + FOXO4 ⁸⁶⁻²⁰⁸ [1:2]	3.3	39	36

Transactivation domain 2 of p53 can individually bind FOXO4 Forkhead domain

The next question that came up was, whether cooperativity is involved in the binding event or whether both transactivation domain 1 and transactivation domain 2 can bind FOXO4⁸⁶⁻²⁰⁸ individually. To address this question, constructs only harboring transactivation domain 1 (residues 14-36) and transactivation domain 2 (residues 37-57) respectively were designed.

¹⁵N-labeled p53³⁷⁻⁵⁷ was expressed and titrated with increasing amounts of FOXO4⁸⁶⁻²⁰⁸. Overlaid spectra of this titration are shown in Figure 26.

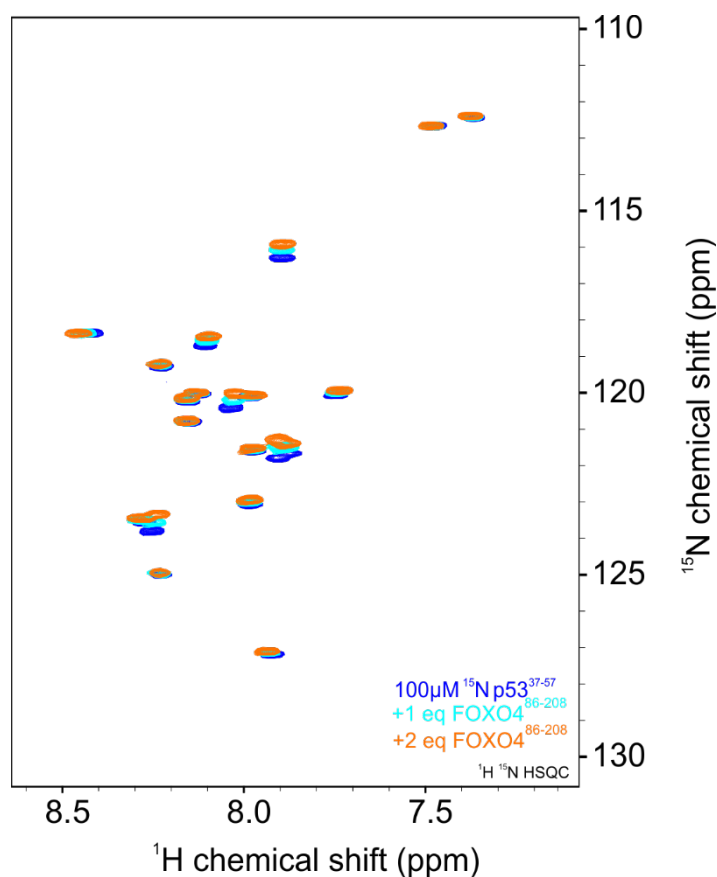


Figure 26: ^1H - ^{15}N HSQC Spectra of ^{15}N p53³⁷⁻⁵⁷ titration with FOXO4⁸⁶⁻²⁰⁸
 Blue: reference spectrum of 50 μM ^{15}N p53³⁷⁻⁵⁷; light blue: ^{15}N p53³⁷⁻⁵⁷ in presence of 50 μM FOXO4⁸⁶⁻²⁰⁸; orange: ^{15}N p53³⁷⁻⁵⁷ in presence of 100 μM FOXO4⁸⁶⁻²⁰⁸
 Measurements were recorded at 298K using a 600 MHz Bruker spectrometer, in a NMR buffer containing 50mM NaPO₄, and 2mM DTT at pH 7.5

Unlabeled FOXO4⁸⁶⁻²⁰⁸ changes the local chemical environment of the amid backbone of p53³⁷⁻⁵⁷ which is visible by changes in ^1H - ^{15}N cross peak position. The chemical shift perturbation of p53³⁷⁻⁵⁷ (Figure 27) affected signals are similar to the ones of p53¹⁻⁹⁴ (Figure 19), which shows that the affinity of p53³⁷⁻⁵⁷ for FOXO4⁸⁶⁻²⁰⁸ is comparable with the affinity of p53¹⁻⁹⁴ for FOXO4⁸⁶⁻²⁰⁸. This indicates that the Transactivation domain 2 of p53 is sufficient for binding the Forkhead domain of FOXO4.

Assignment experiments were performed to link $^1\text{H}_\text{N}$, $^{15}\text{N}_\text{H}$, $^{13}\text{C}_\alpha$ and $^{13}\text{C}_\beta$ chemical shifts of p53³⁷⁻⁵⁷ to the corresponding aminoacid residue within the sequence. All of the non-proline backbone amides were assigned. Calculation of the chemical shift perturbation (shown in Figure 27) reveals that especially residues 46 to 55 are affected by FOXO4⁸⁶⁻²⁰⁸ binding whereas the N-terminal part of the transactivation domain 2 of p53 seems not strongly involved in the interaction. These findings suggest that residues 46 to 55 of the transactivation domain 2 are crucial for FOXO4 Forkhead binding.

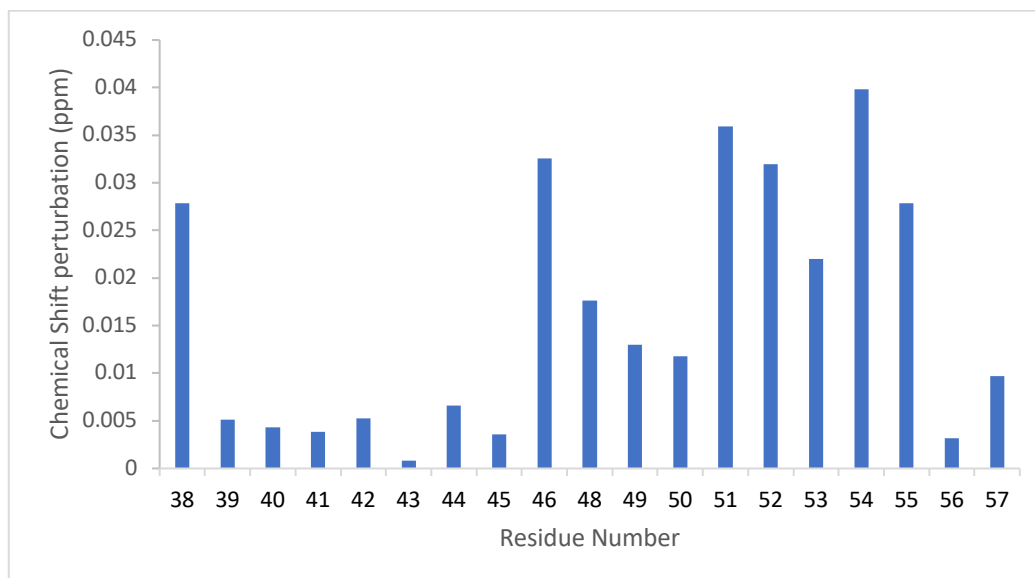


Figure 27: Chemical shift perturbation of ^{15}N p53³⁷⁻⁵⁷ upon titration with FOXO4⁸⁶⁻²⁰⁸

Regulation of FOXO4 – p53 Interaction

Serine 15 of p53 Transactivation Domain is phosphorylated in HEK293T cells

As previously described in the introduction, a complex and complicated network of regulatory mechanisms controls both p53 and FOXO4. Both proteins are often subject to post-translational modification, so we aimed to investigate which post-translational modifications happen on p53 side and if they would affect binding of FOXO4.

First, we aimed to identify post-translational modifications of ^{15}N p53¹⁻⁹⁴ using HEK293T cells. The experimental setup is described in the Material and Methods section. Figure 28 shows an overlay of ^1H - ^{15}N HSQC spectra of p53¹⁻⁹⁴ as control and after hour incubation with HEK293T cell lysate. In presence of HEK293T cell lysate overall many peaks are shifted and affected. But most striking is the appearance of an additional signal in the region characteristic for phosphorylated residues.

Theoretically, the appearance of the phosphorylated serine/threonine residue of ^{15}N p53¹⁻⁹⁴ is correlated to the disappearance of the non-phosphorylated corresponding serine/threonine peak.

Based on the backbone assignment the phosphorylated signal corresponds to Ser15 of ^{15}N p53¹⁻⁹⁴. The fact that the peak for Ser15 does not fully disappear can be explained that only a portion of the ^{15}N -labeled p53¹⁻⁹⁴ is phosphorylated and a portion is still in the unphosphorylated state. The phosphorylation is not stable as it is being dephosphorylated during the measurements.

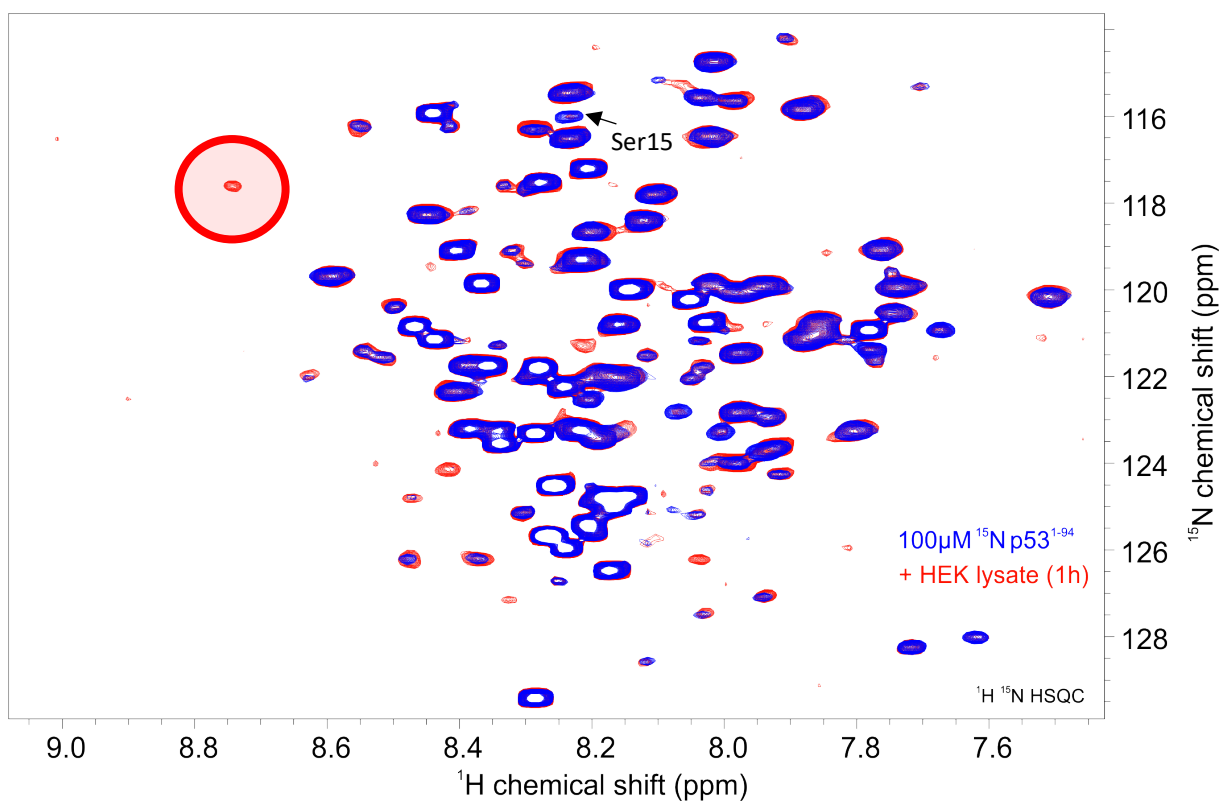


Figure 28: Phosphorylation Assay: $100\mu\text{M } ^{15}\text{N p53}^{1-94}$ in presence of HEK293T cell lysate after 1 hour of incubation
 Measurements were recorded at 298K using a 700 MHz Bruker spectrometer, in a NMR buffer containing 50mM NaPO_4 ,
 150mM NaCl and 2mM DTT at pH 6.5

The experiment was performed a second time, again with HEK293T, but in presence of phosphatase inhibitor, otherwise under the same conditions. Interestingly, this time there are two signals appearing in the region characteristic for phosphorylation. One of the peaks appears at the same site as in the first experiment, indicating phosphorylated Ser15. However, there is no clear disappearance of peaks visible, not even for Ser15, and therefore, it is not possible to link the other phosphorylation event to a residue. The spectra are shown in Figure 29.

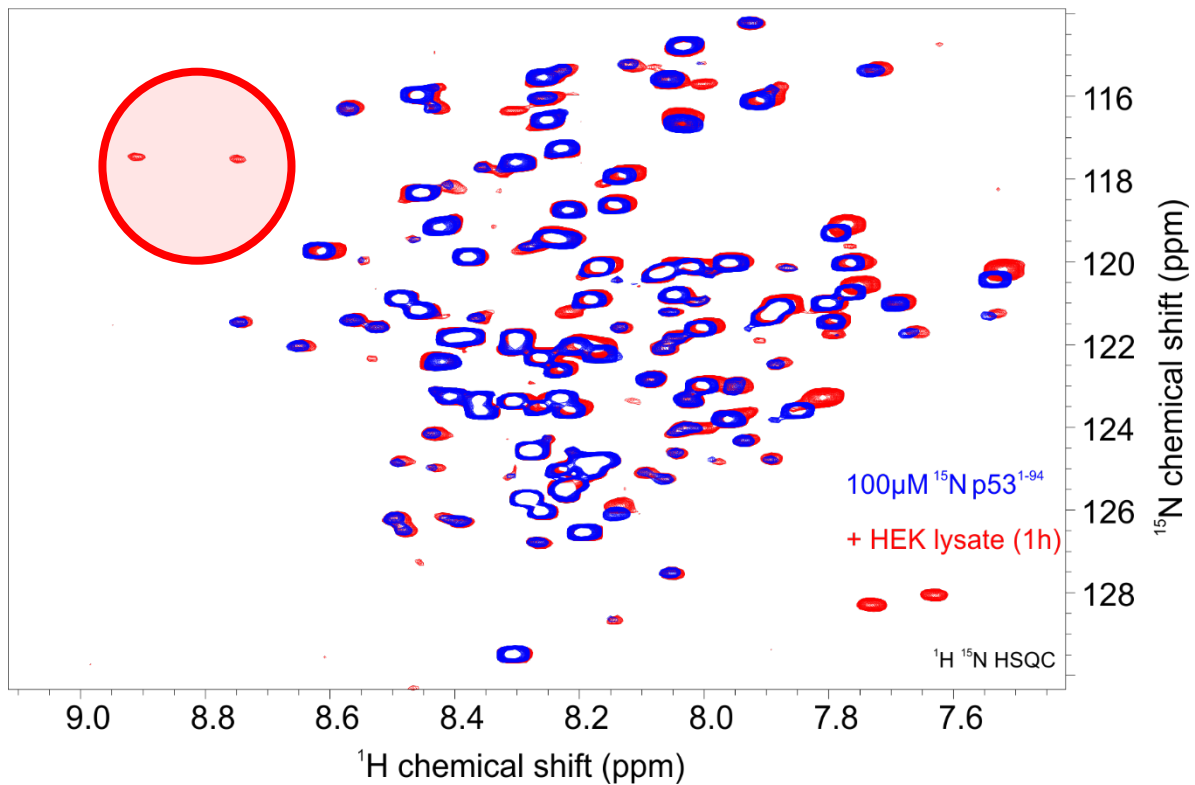


Figure 29: Phosphorylation Assay: 100 μ M 15 N p53¹⁻⁹⁴ in presence of HEK293T cell lysate after 1 hour of incubation
 Measurements were recorded at 298K using a 700 MHz Bruker spectrometer, in a NMR buffer containing 50mM NaPO₄,
 150mM NaCl and 2mM DTT at pH 6.5

Phosphorylation mimicking S46E mutation does not change binding of p53 Transactivation domain to FOXO4 Forkhead Domain

Based on the findings of the phosphorylation assay and on literature research, phosphorylation mimicking glutamate mutants of serine 15, 20, 33, 37 and 46 were designed. However, mutagenesis PCR was only successful for the S46E mutation.

Phosphorylation of serine 46 was shown to be involved in regulation of apoptosis. Given the fact that the main binding site of FOXO4 on p53 are residues 37 to 57 phosphorylation of Ser46 might change the affinity as a regulatory mechanism.

15 N labeled p53^{1-94S46E} was titrated with FOXO4⁸⁶⁻²⁰⁸. A zoom in of the titration of wild-type 15 N p53¹⁻⁹⁴ is shown Figure 30 (left panel) as a reference and a zoom in of the titration of 15 N labeled p53^{1-94S46E} is shown in Figure 30 (right panel).

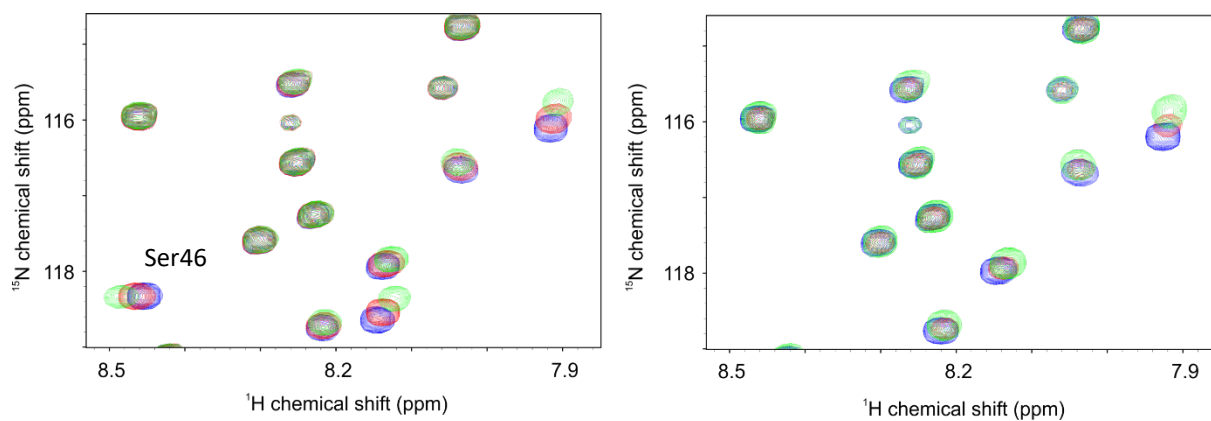


Figure 30: Zoom-in on ^1H - ^{15}N HSQC Spectra of ^{15}N p53¹⁻⁹⁴ (left) and of ^{15}N p53^{1-9 4S46E} titration with FOXO4⁸⁶⁻²⁰⁸. Blue: reference spectrum of 100 μM ^{15}N p53¹⁻⁹⁴; red: ^{15}N p53¹⁻⁹⁴ in presence of 100 μM FOXO4⁸⁶⁻²⁰⁸; green: ^{15}N p53¹⁻⁹⁴ in presence of 200 μM FOXO4⁸⁶⁻²⁰⁸.

Overall, FOXO4-induced chemical shift perturbation of ^1H - ^{15}N cross peaks are similar for wild-type p53 and the serine mutant, indicating comparable binding affinity of the phosphorylation mimicking mutant compared to wild-type p53. The disappearance of the of the ^1H - ^{15}N cross peak corresponding to Ser46 confirms the successful mutagenesis.

Discussion

Prior analysis in our laboratory demonstrated a physical interaction of p53 with the Forkhead domain of FOXO4. Based on this discovery, the group of Peter de Keizer designed a FOXO4-derived peptide in order to prevent FOXO4 – p53 complex formation in cells. Treatment with this peptide of senescent IMR90 fibroblast efficiently and selectively targets and eliminates senescent cells by promoting apoptosis. Furthermore, treatment of naturally or fast aged mice with this peptide restores their fitness, fur density and renal function. Therefore, targeting the FOXO4 – p53 interaction is seen as prominent way to cure age-related diseases and utopically to give us “eternal life”. In order to optimize the existing drug or design new ones with higher potency/selectivity molecular details of the p53 – FOXO4 interaction are required. In this way, the aim of my master thesis was to specify the yet unknown binding site of FOXO4 on p53 which is (i) prerequisite to determine the atomic 3D structure of the complex using NMR (ii) indispensable for a better understanding of the function of this binary interaction in the regulation of cellular senescence.

Using NMR and MST data we identified the N-terminal 1-94 disordered region of p53 as binding site for FOXO4 Forkhead domain. Both subdomains (ie. TAD1 and TAD2) are involved in FOXO4 binding. Nevertheless, based on the chemical shift perturbation analysis of p53¹⁻⁹⁴ upon titration with the Forkhead domain of FOXO4, it appears that the Transactivation domain 2 region binds with higher affinity than the Transactivation domain 1 and can therefore be seen as the main FOXO4 binding site. Interestingly it has been shown for FOXO3 that it is the DNA-binding domain of p53, which is responsible for interaction with FOXO3 Forkhead domain. Forkhead Domains of FOXO3 and FOXO4 are highly conserved and share high sequence identity (20). Also, the described interaction of the CR3 region of FOXO3 with p53 DNA-binding domain is not observable for FOXO4 CR3 and p53 DNA-binding domain. The different binding sites might explain the antagonistic roles of FOXO3 and FOXO4 in regulation of senescence. The FOXO3 – p53 interaction allows in principle orchestrated DNA binding by the FOXO3 Forkhead domain and the DNA-binding domain of p53, to induce apoptosis (20).

Peaks in the spectra were linked with the corresponding aminoacid residues of p53¹⁻⁹⁴ using assignment experiments. Based on the assignment of ¹H_N, ¹⁵N_H, ¹³C_α and ¹³C_β chemical shifts of p53¹⁻⁹⁴, chemical shift perturbation, ¹H¹⁵N HetNOE and the secondary chemical shift were calculated. ¹H¹⁵N HetNOE identified two rigid parts of

p53¹⁻⁹⁴ corresponding to Transactivation domain 1 and Transactivation domain 2 of p53. Calculation of the secondary chemical shift revealed two amino acid stretches which have an alpha helical propensity, again corresponding to Transactivation domain 1 and Transactivation domain 2 of p53. Both, higher rigidity and transient formation of secondary structure elements, are characteristic features of protein-protein interaction sites. ¹H¹⁵N chemical shift perturbation revealed two distinct binding sites: residues 19 to 26 of Transactivation domain 1 and residues 46 to 55 of Transactivation domain 2. The ¹H¹⁵N chemical shift perturbation furthermore indicates that the Transactivation domain 2 has higher affinity for the Forkhead domain of FOXO4 and represents the main binding site. Data obtained by SAXS experiments indicate that two molecules of FOXO4 Forkhead bind to one molecule of p53¹⁻⁹⁴ leading to the question whether both Transactivation domains can individually bind the FOXO4 Forkhead domain. Shorter constructs harboring only Transactivation domain 1 or Transactivation domain 2 respectively were designed. NMR titrations of ¹⁵N-labeled Transactivation domain 2 with unlabeled FOXO4 Forkhead show that this region of p53 is sufficient for FOXO4 Forkhead binding. Titrations using ¹⁵N-labeled Transactivation domain 1 of p53 with FOXO4 Forkhead domain have not been performed to this point, but will provide important information to understand the mechanisms of the interaction.

The intrinsically disordered N-terminal domain of p53 is a known binding site for many proteins such as CBP/p300, MDM2, TFIID and TFIIH (26). This region harbors two interaction motifs Transactivation Domain 1 and Transactivation Domain 2, which were already previously shown to form a transient alpha helical secondary structure (26). The mode of interaction varies depending on the interaction partner. MDM2 binds exclusively to Transactivation Domain 1 of p53 (65). For CBP/p300 both Transactivation Domains of p53 are responsible for the interaction. The Transactivation Domains adapt a transient secondary structure, while the N-terminal tail and the linker between Transactivation Domain 1 and Transactivation Domain 2 remain flexible (26). For the complex formation of FOXO4 and p53 it will be interesting to see, whether Transactivation domain 1 can bind FOXO4 Forkhead domain independently or if recruitment by Transactivation domain 2 is necessary.

The solution of the complex structure of p53 – FOXO4 will be very important to understand the structural biological features of the binding, because of diverse structures of Transactivation Domain 1 and Transactivation Domain 2 depending on the binding partner. The transient helix formed in p53 Transactivation Domain 2 upon

binding to CBP/p300 is shorter than in other complexes (66). Upon binding to HMGB1 via the HMG-box, the transactivation domain 2 forms a short helical turn and a longer helix (67). The different conformations and structures the N-terminal Transactivation domain can adopt upon binding are illustrated in Figure 31.

The FOXO4 – p53 interaction is because of its immense biological relevance a promising target for anti-aging intervention (2, 44, 52) and knowledge of the complex structure is crucial to develop compounds to interfere the interaction and clear senescent cells.

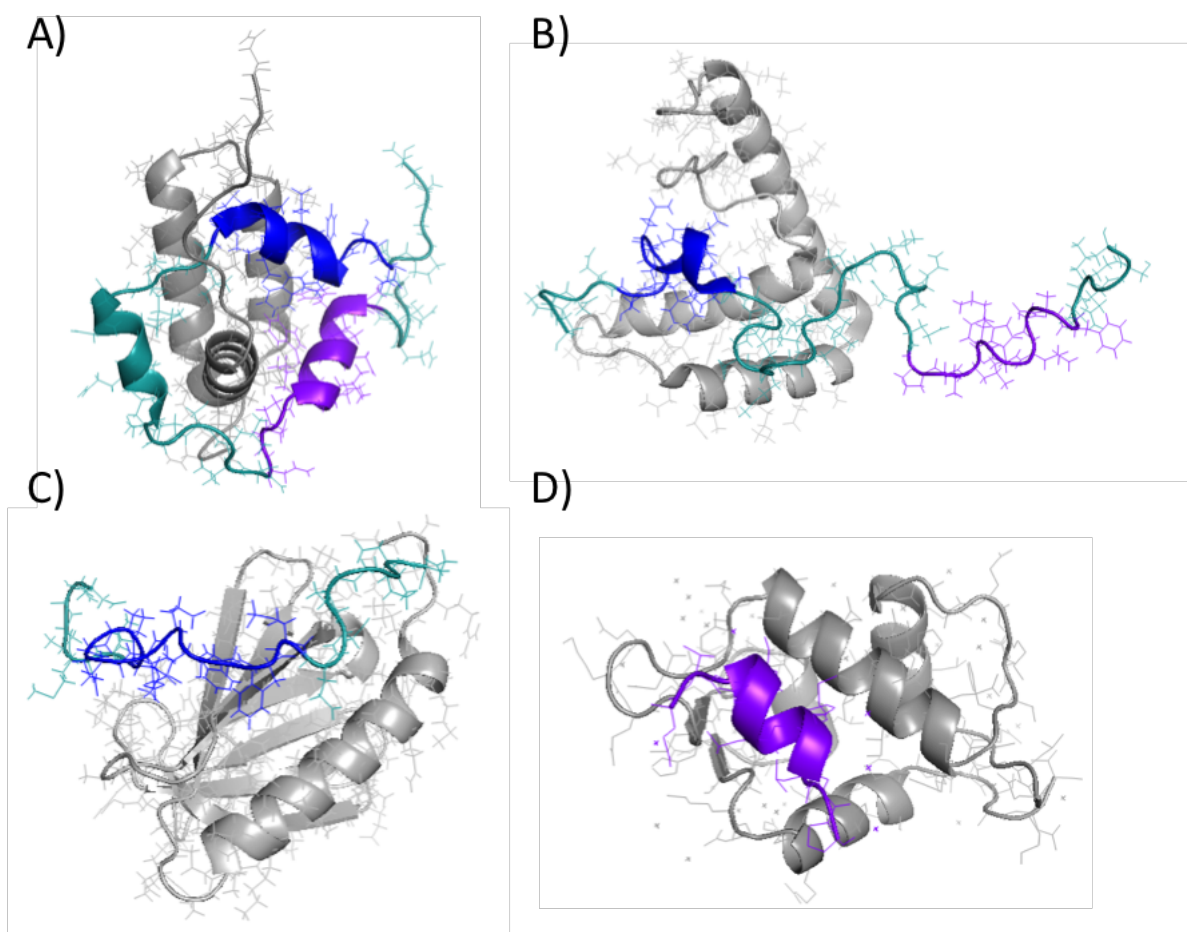


Figure 31: Complex Structures of p53 Bound to several interaction partners. Binding partners are colored grey, p53 in darkgreen and TAD1 is highlighted in violet and TAD2 is highlighted in blue.

- A) p5313-61 bound to CBP nuclear coactivator binding domain (pdb: 2L14)*
- B) p531-93 bound to HMGB1 (pdb: 2LY4)*
- C) p5341-62 bound to TFIIH (pdb: 2ruk)*
- D) p5313-29 bound to MDM2 (pdb: 1ycq)*

Both p53 and FOXO4 are tightly regulated by a complex network, including post-translational modifications and protein interaction partners.

p53 and especially the N-terminal transactivation domain is subject to many post-translational modifications such as phosphorylation of Ser15, Ser20, Ser33, Ser37 and Ser46 resulting in different effector functions (34).

In-cell phosphorylation of ^{15}N labeled p53¹⁻⁹⁴ in HEK293T cells revealed phosphorylation of Ser15. However, to unambiguously identify the phosphorylated residue backbone assignment experiments are necessary. Ser15 was described to be phosphorylated by CDK5, PRPK, AMPK, NUA1 and ATM in response to DNA damage (34). The phosphorylation stabilizes and activates p53 and p53-mediated tumor suppression (34). HEK293T cells are a cell line derived from human embryonic kidney cells and commonly used in molecular biology (68). These cells express most common human kinases but have a heterogenous, unstable karyotype and are tumorigenic (68). Phosphorylation of p53 Ser15 in HEK293T can be explained by their tumorigenic nature and the instable genome, which might activate DNA damage response. This assay in HEK293T provides a good proof of principle, but for studying senescence it will be important to use senescent cells, to have an appropriate setting, especially as there are many kinases known to phosphorylate the N-terminal Transactivation Domain of p53.

Another technique to investigate impact of post-translational modifications using NMR spectroscopy are phosphorylation mimicking mutations. We used the mutation S46E to mimic the phosphorylation of Ser46 by HIPK2 to investigate the impact on FOXO4 Forkhead binding. Titration of ^{15}N -labeled p53¹⁻⁹⁴ S46E with unlabeled FOXO4 Forkhead resulted in similar chemical shift changes compared with wild-type p53¹⁻⁹⁴. Phosphorylation of Ser46 by HIPK2, p38 MAP kinase, PKC or CDK5 was linked with induction of apoptosis (39, 40). The interaction of FOXO4 and p53 was described to promote senescence over apoptosis, therefore one might expect that phosphorylation would prevent or weaken the interaction (2). Our results show that the phosphorylation mimicking mutant S46E alone is not sufficient to decrease binding of FOXO4 Forkhead Domain. However, it was described that NORE1A forms a complex with HIPK2, inhibiting the proapoptotic phosphorylation of p53 on Ser46 and promoting the pro-senescent acetylation of p53 in HIPK2 dependent manner by recruiting acetyl transferases PCAF and CBP/p300 (16). Interestingly, the CR3 domain of FOXO3, which was also described to interact with the DNA-binding domain of p53 can also interact with CBP, regulating the transcriptional activity of FOXO3 (69).

Similarly, it is possible that FOXO4 binding to p53 transactivation domain 2 prevents HIPK2-mediated phosphorylation of Ser46, but still allows HIPK2-dependent acetylation, resulting in p21 expression and senescence. A putative representation of the different interaction pattern is shown in Figure 32.

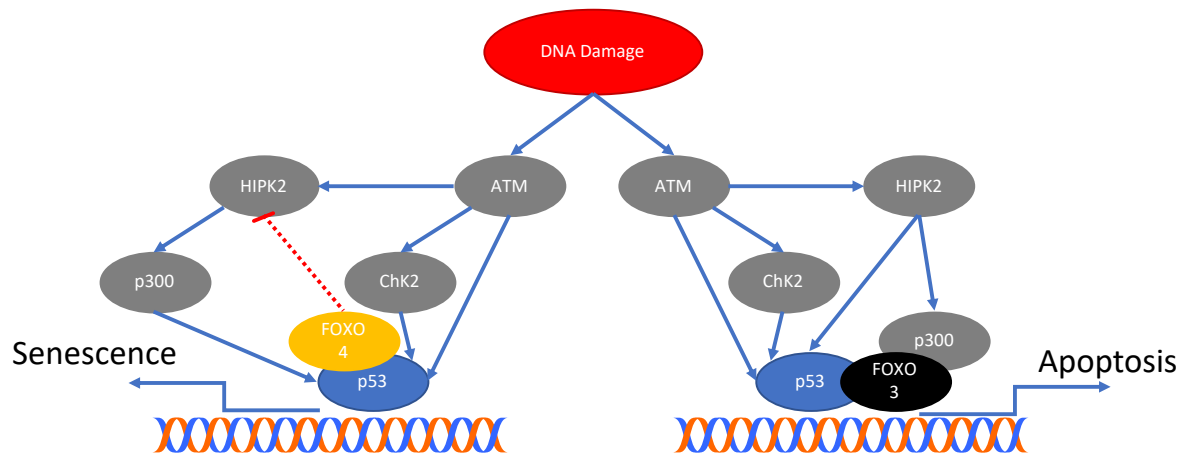


Figure 32: Putative schematic pathway of the FOXO - p53 interplay in senescence and apoptosis
 Upon DNA damage ATM is activated and in turn phosphorylates p53 and activates Chk2, which also phosphorylates p53. Those phosphorylation events stabilize p53. ATM also activates HIPK2, which phosphorylates p53 at Ser46. If p53 is bound to FOXO3 this phosphorylation site is accessible. p53 DNA-binding domain and FOXO3 Forkhead domain can cooperative induce transcription and apoptosis. The acetyl transferase CBP/p300 forms a complex with the CR3 region of FOXO3, preventing pro-senescent acetylation of p53. If p53 is bound to FOXO4 the Ser46 is not accessible for phosphorylation by HIPK2. Still HIPK2 recruits CBP/p300 which can acetylate the C-terminal regulatory domain of p53, resulting in senescence.

Finally, it should be considered that all protein constructs used in this study lack the C-terminus of p53. Full-length p53 including the tetramerization and C-terminal regulatory domain is difficult to investigate using NMR spectroscopy due to the high molecular weight. Interaction partners of p53, such as MDM2 or CBP/p300 bind to the N-terminal Transactivation domain of p53 and are still able to modify the C-terminal regulatory domain (33).

Taking together, data obtained during this study clearly identifies the N-terminal Transactivation domain of p53 as binding site for FOXO4 Forkhead domain. The N-terminus of p53 harbors two protein interaction motifs Transactivation Domain 1 and Transactivation domain 2, that are more rigid and have a propensity to form alpha-helical secondary structure elements. Main binding site for FOXO4 Forkhead domain is Transactivation domain 2 of p53 but also Transactivation domain 1 is involved in the binding, forming a complex with two molecules of FOXO4 Forkhead.

Phosphorylation mimic of p53 Ser46 does not change binding to FOXO4 Forkhead, but the binding event might interfere with the phosphorylation by HIPK2.

This study is a small step towards understanding the regulation of senescence and apoptosis via p53 – FOXO4 axis.

Unfortunately, my findings are not yet sufficient to provide eternal life.

Acknowledgements

I was allowed to write my masters thesis under supervision of Benjamin Bourgeois and Tobias Madl at the Medical University of Graz at the Gottfried Schatz Forschungszentrum.

Benjamin Bourgeois

Je tiens à vous remercier pour vos excellents conseils scientifiques et personnels, pour votre patience et surtout pour votre amitié. Je suis désolé de vous avoir causé des cheveux gris, mais je travaille sur la solution. Merci et allez les bleus.

Tobias Madl

I want to thank you for the opportunity to work at this project, to help me with your excellent expertise and especially to work with all the fantastic people in your group.

Sarah Stryeck

I want to thank you for awakening my enthusiasm in structural biology and for all technical, academical and personal advices and for being a person to look up to.

Gesa Richter

I want to thank you for being always positive minded and available for questions and guidance and for encouraging me.

Denise Prietl, Therese Macher, Anna Springer

I want to thank you for your technical support, for taking over some hands-on work in stressful times and for sharing the office with me.

Julia Sternat

I want to thank you for the time working along side you and that I could share my time during master study with you.

Barbara Hinteregger, Fangrong Zhang,

I want to thank you for the time working with you.

My parents

I want to thank you, especially my mother, for your love, patience and support.

Linda

I want to thank you for all the time on your side, for always supporting me and for being the person that you are.

Friends

I want to thank all my friends for supporting me not just in the time of my study. They were there before and I hope they will be forever there.

Each of you influenced my professional and personal life and future.
May the best of their past be the worst of your future!

Appendix

Buffers and Solutions

Gel buffer for SDS PAGE (3 x)

1 M Bis (2-hydroxyethyl)aminotris(hydroxymethyl)methane
(Sigma 98%)
pH 6.5-6.8 adjusted with HCl (12.2 M) and NaOH (5 M)

MES SDS running buffer (20 x)

1 M MES (Sigma Aldrich >99%)
1 M Trizma[®] base (Sigma Aldrich >99.8%)
2 % (w/v) SDS (Applichem Panreac 10 %)
20 mM EDTA (Alfa Aesar 99+%)
No need to adjust pH

Coomassie Staining solution

40% desalted H₂O
40% MeOH (VWR 99.9%)
10 % glacial acetic acid (Roth >99%)
Tip of a spatula of Coomassie R-250 dye powder (Thermo
Fischer)

Coomassie Destaining solution

40% desalted H₂O
40% MeOH (VWR 99.9%)
10 % glacial acetic acid (Roth >99%)

Kanamycin (1000 x; 50 mg/ml)

5 g Kanamycin (Applichem Panreac) in 100 ml of MilliQ H₂O
Filter sterilize

(Selective) LB medium

2 % (w/v) lysogeny broth (Roth)
(+ 0.1 % (v/v) Kanamycin (1000 x))

(Selective) LB Agar plates

2 % (w/v) lysogeny broth (Roth)
2 % (w/v) agar (Amresco pure, bacterial grade)
(+ 0.1 % (v/v) Kanamycin (1000 x))

10 x Salt

1 M KH_2PO_4 (VWR 99.8%)
0.5 M K_2HPO_4 (VWR 99.8%)
0.6 M Na_2HPO_4 (Applichem Panreac anhydrous >99%)
0.14 M K_2SO_4 (VWR 99-101%)
pH 7.2 adjusted with HCl (12.2 M) and NaOH (5 M)

Trace element solution

41 mM $\text{CaCl}_2 \times 2 \text{H}_2\text{O}$ (Applichem Panreac 97%)
22 mM $\text{FeSO}_4 \times 7 \text{H}_2\text{O}$ (VWR 84%)
6 mM $\text{MnCl}_2 \times 4 \text{H}_2\text{O}$ (Applichem Panreac)
3 mM $\text{CoCl}_2 \times 6 \text{H}_2\text{O}$ (Applichem Panreac)
1 mM $\text{ZnSO}_4 \times 7 \text{H}_2\text{O}$ (VWR 99.9%)
0.1 mM $\text{CuCl}_2 \times 2 \text{H}_2\text{O}$ (VWR)
0.2 mM $(\text{NH}_4)_6\text{Mo}_7\text{O}_{24} \times 4 \text{H}_2\text{O}$ (VWR 98.5%)
17 mM EDTA (Alfa Aesar 99+%)

Minimal medium

It was used for production of labeled or non-labeled proteins. In case of labeling, ^{15}N and/or ^{13}C isotopes were used.

For expression of ^{13}C -methyl-ILVM transportin-1, 100 mg of 2-Keto-3-methylbutyric acid $5\text{-}^{13}\text{C}$ (Sigma), 50 mg of 2-Ketobutyric acid $4\text{-}^{13}\text{C}$ (Sigma) and 50 mg of L-methionine-methyl- ^{13}C (Cambridge Isotope Laboratories) was added before induction.

900 ml MilliQ H_2O
100 ml 10 x Salt
5 ml Trace element solution
5 ml 1 M MgCl_2 (Alfa Aesar 99%)

1g $^{15}\text{NH}_4\text{Cl}$ (Sigma Aldrich 98%)/2 g $^{14}\text{NH}_4\text{Cl}$ (Alfa Aesar 99.5%)

2g $^{13}\text{C}_6\text{H}_{12}\text{O}_6$ (Cambridge Isotope Laboratories 99%)/

6 g $^{12}\text{C}_6\text{H}_{12}\text{O}_6$ (Roth 99%)

0.1% (w/w) Kanamycin (1000x)

Chook buffer (lysis buffer for structured proteins)

150 mM NaCl (VWR 99.6%)

50 mM Tris (VWR ultra pure)

20 % glycerol (VWR 99%)

20 mM imidazole (Millipore 99.0%)

Urea buffer (lysis buffer for disordered proteins)

150 mM NaCl (VWR 99.6%)

50 mM Tris (VWR ultra pure)

6 M Urea (Roth >99.5%)

20 M imidazole (Millipore 99.0%)

2 mM TCEP (Roth 98%)

pH 7.5 adjusted with HCl (12.2 M) and NaOH (5 M)

Buffer A

150 mM NaCl (VWR 99.6%)

50 mM Tris (VWR ultra pure)

20 mM imidazole (Millipore 99.0%)

2 mM TCEP (Roth 98%)

pH 7.5 adjusted with HCl (12.2 M) and NaOH (5 M)

Buffer A'

1 M NaCl (VWR 99.6%)

50 mM Tris (VWR ultra pure)

20 mM imidazole (Millipore 99.0%)

2 mM TCEP (Roth 98%)

pH 7.5 adjusted with HCl (12.2 M) and NaOH (5 M)

Buffer B'

1 M NaCl (VWR 99.6%)
50 mM Tris (VWR ultra pure)
500 mM imidazole (Millipore 99.0%)
2 mM TCEP (Roth 98%)
pH 7.5 adjusted with HCl (12.2 M) and NaOH (5 M)

NMR buffers

150 mM NaCl (VWR 99.6%)
50 mM NaPO₄ (VWR ultra pure)
1 mM DTT (Roth 98%)
pH 6.7 adjusted with HCl (12.2 M) and NaOH (5 M)

150 mM NaCl (VWR 99.6%)
50 mM NaPO₄ (VWR ultra pure)
1 mM DTT (Roth 98%)
pH 7.5 adjusted with HCl (12.2 M) and NaOH (5 M)

50 mM NaPO₄ (VWR ultra pure)
1 mM DTT (Roth 98%)
pH 7.5 adjusted with HCl (12.2 M) and NaOH (5 M)

SAXS buffer

150 mM NaCl (VWR 99.6%)
50 mM Tris (VWR ultra pure)
2 mM TCEP (Roth 98%)
pH 7.5 adjusted with HCl (12.2 M) and NaOH (5 M)

Bibliography

1. Martins R, Lithgow GJ, Link W. Long live FOXO: unraveling the role of FOXO proteins in aging and longevity. *Aging Cell*. 2016;15(2):196-207.
2. Baar MP, Brandt RMC, Putavet DA, Klein JDD, Derks KWJ, Bourgeois BRM, et al. Targeted Apoptosis of Senescent Cells Restores Tissue Homeostasis in Response to Chemotoxicity and Aging. *Cell*. 2017;169(1):132-47 e16.
3. Leopardi G. *Essays, Dialogues and Thoughts:(Operette Morali and Pensieri) of Giacomo Leopardi.*: G. Routledge & sons, ; 1905.
4. da Costa JP, Vitorino R, Silva GM, Vogel C, Duarte AC, Rocha-Santos T. A synopsis on aging-Theories, mechanisms and future prospects. *Ageing Res Rev*. 2016;29:90-112.
5. Lopez-Otin C, Blasco MA, Partridge L, Serrano M, Kroemer G. The hallmarks of aging. *Cell*. 2013;153(6):1194-217.
6. Hanahan D, Weinberg RA. The hallmarks of cancer. *Cell*. 2000;100(1):57-70.
7. Vaiserman AM, Lushchak OV, Koliada AK. Anti-aging pharmacology: Promises and pitfalls. *Ageing Res Rev*. 2016;31:9-35.
8. Hernandez-Segura A, Nehme J, Demaria M. Hallmarks of Cellular Senescence. *Trends Cell Biol*. 2018;28(6):436-53.
9. Kuilman T, Michaloglou C, Mooi WJ, Peeper DS. The essence of senescence. *Genes Dev*. 2010;24(22):2463-79.
10. Collado M, Blasco MA, Serrano M. Cellular senescence in cancer and aging. *Cell*. 2007;130(2):223-33.
11. Sun Y, Coppe JP, Lam EW. Cellular Senescence: The Sought or the Unwanted? *Trends Mol Med*. 2018.
12. Cawthon RM, Smith KR, O'Brien E, Sivatchenko A, Kerber RA. Association between telomere length in blood and mortality in people aged 60 years or older. *Lancet*. 2003;361(9355):393-5.
13. Ogami M, Ikura Y, Ohsawa M, Matsuo T, Kayo S, Yoshimi N, et al. Telomere shortening in human coronary artery diseases. *Arterioscler Thromb Vasc Biol*. 2004;24(3):546-50.
14. Wei W, Ji S. Cellular senescence: Molecular mechanisms and pathogenicity. *J Cell Physiol*. 2018.
15. Donninger H, Barnoud T, Clark GJ. NORE1A is a double barreled Ras senescence effector that activates p53 and Rb. *Cell Cycle*. 2016;15(17):2263-4.
16. Donninger H, Calvisi DF, Barnoud T, Clark J, Schmidt ML, Vos MD, et al. NORE1A is a Ras senescence effector that controls the apoptotic/senescent balance of p53 via HIPK2. *J Cell Biol*. 2015;208(6):777-89.
17. Acosta JC, Banito A, Wuestefeld T, Georgilis A, Janich P, Morton JP, et al. A complex secretory program orchestrated by the inflammasome controls paracrine senescence. *Nat Cell Biol*. 2013;15(8):978-90.
18. Baker DJ, Wijshake T, Tchkonia T, LeBrasseur NK, Childs BG, van de Sluis B, et al. Clearance of p16Ink4a-positive senescent cells delays ageing-associated disorders. *Nature*. 2011;479(7372):232-6.
19. Yosef R, Pilpel N, Papsimadov N, Gal H, Ovadya Y, Vadai E, et al. p21 maintains senescent cell viability under persistent DNA damage response by restraining JNK and caspase signaling. *EMBO J*. 2017;36(15):2280-95.
20. Wang F, Marshall CB, Yamamoto K, Li GY, Plevin MJ, You H, et al. Biochemical and structural characterization of an intramolecular interaction in FOXO3a and its binding with p53. *J Mol Biol*. 2008;384(3):590-603.

21. Lane DP. Cancer. p53, guardian of the genome. *Nature*. 1992;358(6381):15-6.
22. Levine AJ. p53, the cellular gatekeeper for growth and division. *Cell*. 1997;88(3):323-31.
23. Zilfou JT, Lowe SW. Tumor suppressive functions of p53. *Cold Spring Harb Perspect Biol*. 2009;1(5):a001883.
24. Levine AJ, Hu W, Feng Z. The P53 pathway: what questions remain to be explored? *Cell Death Differ*. 2006;13(6):1027-36.
25. Joerger AC, Fersht AR. Structure-function-rescue: the diverse nature of common p53 cancer mutants. *Oncogene*. 2007;26(15):2226-42.
26. Uversky VN. p53 Proteoforms and Intrinsic Disorder: An Illustration of the Protein Structure-Function Continuum Concept. *Int J Mol Sci*. 2016;17(11).
27. Vousden KH, Prives C. Blinded by the Light: The Growing Complexity of p53. *Cell*. 2009;137(3):413-31.
28. Rufini A, Tucci P, Celardo I, Melino G. Senescence and aging: the critical roles of p53. *Oncogene*. 2013;32(43):5129-43.
29. Aksoy O, Chicas A, Zeng T, Zhao Z, McCurrach M, Wang X, et al. The atypical E2F family member E2F7 couples the p53 and RB pathways during cellular senescence. *Genes Dev*. 2012;26(14):1546-57.
30. Demidenko ZN, Korotchkina LG, Gudkov AV, Blagosklonny MV. Paradoxical suppression of cellular senescence by p53. *Proc Natl Acad Sci U S A*. 2010;107(21):9660-4.
31. Leontieva OV, Gudkov AV, Blagosklonny MV. Weak p53 permits senescence during cell cycle arrest. *Cell Cycle*. 2010;9(21):4323-7.
32. Tidow H, Melero R, Mylonas E, Freund SM, Grossmann JG, Carazo JM, et al. Quaternary structures of tumor suppressor p53 and a specific p53 DNA complex. *Proc Natl Acad Sci U S A*. 2007;104(30):12324-9.
33. Meek DW. Regulation of the p53 response and its relationship to cancer. *Biochem J*. 2015;469(3):325-46.
34. Kruse JP, Gu W. Modes of p53 regulation. *Cell*. 2009;137(4):609-22.
35. Ko LJ, Shieh SY, Chen X, Jayaraman L, Tamai K, Taya Y, et al. p53 is phosphorylated by CDK7-cyclin H in a p36MAT1-dependent manner. *Mol Cell Biol*. 1997;17(12):7220-9.
36. Lees-Miller SP, Sakaguchi K, Ullrich SJ, Appella E, Anderson CW. Human DNA-activated protein kinase phosphorylates serines 15 and 37 in the amino-terminal transactivation domain of human p53. *Mol Cell Biol*. 1992;12(11):5041-9.
37. Tibbetts RS, Brumbaugh KM, Williams JM, Sarkaria JN, Cliby WA, Shieh SY, et al. A role for ATR in the DNA damage-induced phosphorylation of p53. *Genes Dev*. 1999;13(2):152-7.
38. Romanova LY, Willers H, Blagosklonny MV, Powell SN. The interaction of p53 with replication protein A mediates suppression of homologous recombination. *Oncogene*. 2004;23(56):9025-33.
39. D'Orazi G, Cecchinelli B, Bruno T, Manni I, Higashimoto Y, Saito S, et al. Homeodomain-interacting protein kinase-2 phosphorylates p53 at Ser 46 and mediates apoptosis. *Nat Cell Biol*. 2002;4(1):11-9.
40. Yoshida K, Liu H, Miki Y. Protein kinase C delta regulates Ser46 phosphorylation of p53 tumor suppressor in the apoptotic response to DNA damage. *J Biol Chem*. 2006;281(9):5734-40.
41. Li HH, Li AG, Sheppard HM, Liu X. Phosphorylation on Thr-55 by TAF1 mediates degradation of p53: a role for TAF1 in cell G1 progression. *Mol Cell*. 2004;13(6):867-78.
42. Hussain MT, K.; Mutti ,L.; Krstic-Demonacos ,M.; Schwartz ,JM. The Expanded p53 Interactome as a Predictive Model for Cancer Therapy. *GCB*. 2015;1(1).

43. Webb AE, Brunet A. FOXO transcription factors: key regulators of cellular quality control. *Trends Biochem Sci.* 2014;39(4):159-69.
44. Bourgeois B, Madl T. Regulation of cellular senescence via the FOXO4-p53 axis. *FEBS Lett.* 2018;592(12):2083-97.
45. Kenyon CJ. The genetics of ageing. *Nature.* 2010;464(7288):504-12.
46. Willcox BJ, Donlon TA, He Q, Chen R, Grove JS, Yano K, et al. FOXO3A genotype is strongly associated with human longevity. *Proc Natl Acad Sci U S A.* 2008;105(37):13987-92.
47. Anselmi CV, Malovini A, Roncarati R, Novelli V, Villa F, Condorelli G, et al. Association of the FOXO3A locus with extreme longevity in a southern Italian centenarian study. *Rejuvenation Res.* 2009;12(2):95-104.
48. Broer L, Buchman AS, Deelen J, Evans DS, Faul JD, Lunetta KL, et al. GWAS of longevity in CHARGE consortium confirms APOE and FOXO3 candidacy. *J Gerontol A Biol Sci Med Sci.* 2015;70(1):110-8.
49. Zhang X, Tang N, Hadden TJ, Rishi AK. Akt, FoxO and regulation of apoptosis. *Biochim Biophys Acta.* 2011;1813(11):1978-86.
50. de Keizer PL, Packer LM, Szypowska AA, Riedl-Polderman PE, van den Broek NJ, de Bruin A, et al. Activation of forkhead box O transcription factors by oncogenic BRAF promotes p21cip1-dependent senescence. *Cancer Res.* 2010;70(21):8526-36.
51. Wang F, Marshall CB, Ikura M. Forkhead followed by disordered tail: The intrinsically disordered regions of FOXO3a. *Intrinsically Disord Proteins.* 2015;3(1):e1056906.
52. de Keizer PL. The Fountain of Youth by Targeting Senescent Cells? *Trends Mol Med.* 2017;23(1):6-17.
53. Brutscher B, Felli IC, Gil-Caballero S, Hosek T, Kummerle R, Piai A, et al. NMR Methods for the Study of Intrinsically Disordered Proteins Structure, Dynamics, and Interactions: General Overview and Practical Guidelines. *Adv Exp Med Biol.* 2015;870:49-122.
54. Teilum K, Kunze MB, Erlendsson S, Kragelund BB. (S)Pinning down protein interactions by NMR. *Protein Sci.* 2017;26(3):436-51.
55. Vranken WF, Boucher W, Stevens TJ, Fogh RH, Pajon A, Llinas M, et al. The CCPN data model for NMR spectroscopy: development of a software pipeline. *Proteins.* 2005;59(4):687-96.
56. Tamiola K, Acar B, Mulder FA. Sequence-specific random coil chemical shifts of intrinsically disordered proteins. *J Am Chem Soc.* 2010;132(51):18000-3.
57. Selenko P, Frueh DP, Elsaesser SJ, Haas W, Gygi SP, Wagner G. In situ observation of protein phosphorylation by high-resolution NMR spectroscopy. *Nat Struct Mol Biol.* 2008;15(3):321-9.
58. Madl T, Gabel F, Sattler M. NMR and small-angle scattering-based structural analysis of protein complexes in solution. *J Struct Biol.* 2011;173(3):472-82.
59. Kachala M, Valentini E, Svergun DI. Application of SAXS for the Structural Characterization of IDPs. *Adv Exp Med Biol.* 2015;870:261-89.
60. Liu H, Zwart PH. Determining pair distance distribution function from SAXS data using parametric functionals. *J Struct Biol.* 2012;180(1):226-34.
61. Franke D, Svergun DI. DAMMIF, a program for rapid ab-initio shape determination in small-angle scattering. *J Appl Crystallogr.* 2009;42(Pt 2):342-6.
62. Franke D, Petoukhov MV, Konarev PV, Panjkovich A, Tuukkanen A, Mertens HDT, et al. ATSAS 2.8: a comprehensive data analysis suite for small-angle scattering from macromolecular solutions. *J Appl Crystallogr.* 2017;50(Pt 4):1212-25.

63. Moran Jerabek-Willemsen TA, Randy Wanner, Heide Marie Roth, Stefan Duhr,, Philipp Baaske DB. MicroScale Thermophoresis: Interaction analysis and beyond. *Journal of Molecular Structure*. 2014;1077:101-13.
64. Krishnan N, Krishnan K, Connors CR, Choy MS, Page R, Peti W, et al. PTP1B inhibition suggests a therapeutic strategy for Rett syndrome. *J Clin Invest*. 2015;125(8):3163-77.
65. Kussie PH, Gorina S, Marechal V, Elenbaas B, Moreau J, Levine AJ, et al. Structure of the MDM2 oncoprotein bound to the p53 tumor suppressor transactivation domain. *Science*. 1996;274(5289):948-53.
66. Lee CW, Martinez-Yamout MA, Dyson HJ, Wright PE. Structure of the p53 transactivation domain in complex with the nuclear receptor coactivator binding domain of CREB binding protein. *Biochemistry*. 2010;49(46):9964-71.
67. Rowell JP, Simpson KL, Stott K, Watson M, Thomas JO. HMGB1-facilitated p53 DNA binding occurs via HMG-Box/p53 transactivation domain interaction, regulated by the acidic tail. *Structure*. 2012;20(12):2014-24.
68. Stepanenko AA, Dmitrenko VV. HEK293 in cell biology and cancer research: phenotype, karyotype, tumorigenicity, and stress-induced genome-phenotype evolution. *Gene*. 2015;569(2):182-90.
69. Wang F, Marshall CB, Li GY, Yamamoto K, Mak TW, Ikura M. Synergistic interplay between promoter recognition and CBP/p300 coactivator recruitment by FOXO3a. *ACS Chem Biol*. 2009;4(12):1017-27.

Table of Figures

Figure 1: Domain architecture of p53:	18
Figure 2: Model structure of p53 ¹⁻³⁶⁰ bound to DNA.	19
Figure 3: Structures of the individual domains of p53.....	19
Figure 4: Schematic representation of p53 with selected important post-translational modification sites	21
Figure 5: Domain architecture of FOXO4:	23
Figure 6: Schematic representation of FOXO4 with post-translational modification sites	24
Figure 7: pETM-11 vector for expression of proteins containing Z-Tag in E.coli	27
Figure 8: Schematic representation of different NMR exchange regimes.	37
Figure 9: Overview of three-dimensional backbone assignment experiments	40
Figure 10: Magnetization transfer during an HNCACB experiment	40
Figure 11: Magnetization transfer during an CBCA(CO)NH experiment	41
Figure 12: Schematic representation of the assignment strategy and formation of amino acid chains	41
Figure 13: Magnetization transfer during a H(CCCO)NH experiment	42
Figure 14: Expression and purification of FOXO4 ⁸⁶⁻²⁰⁸ ,	48
Figure 15: ¹ H- ¹⁵ N HSQC Spectra of ¹⁵ N p53 ¹⁻³¹² titration with FOXO4 ⁸⁶⁻²⁰⁸	50
Figure 16: MST binding curve of fluorescent labeled p53 ¹⁻³¹² to unlabeled FOXO4 ⁸⁶⁻²⁰⁸	51
Figure 17: ¹ H- ¹⁵ N HSQC Spectra of ¹⁵ N p53 ⁹⁴⁻³¹² titration with unlabeled FOXO4 ⁸⁶⁻²⁰⁸	52
Figure 18: ¹ H- ¹⁵ N HSQC Spectra of ¹⁵ N p53 ⁹⁴⁻³¹² titration with unlabeled FOXO4 ⁴⁶⁵⁻⁵⁰⁵	53
Figure 19: ¹ H- ¹⁵ N HSQC Spectra of ¹⁵ N p53 ¹⁻⁹⁴ titration with FOXO4 ⁸⁶⁻²⁰⁸	54
Figure 20: ¹ H- ¹⁵ N HSQC Spectra of ¹⁵ N FOXO4 ⁸⁶⁻²⁰⁸ titration with p53 ¹⁻⁹⁴	55
Figure 21: ¹ H- ¹⁵ N HSQC Spectra of ¹⁵ N p53 ¹⁻⁹⁴ titration with FOXO4 ⁸⁶⁻²⁰⁸ including assigned peaks	56
Figure 22: ¹ H- ¹⁵ N normalized chemical shift perturbation of p53 ¹⁻⁹⁴ upon titration with FOXO4 ⁸⁶⁻²⁰⁸	57
Figure 23: $\Delta(\Delta C_{\alpha} - \Delta C_{\beta})$ of the assigned residues of ¹³ C ¹⁵ N labeled p53 ¹⁻⁹⁴	58
Figure 24: ¹ H ¹⁵ N HetNOE of ⁵ N p53 ¹⁻⁹⁴	59
Figure 25:P(r) function and surface model derived from SAXS experiments	60
	84

Figure 26: ^1H - ^{15}N HSQC Spectra of ^{15}N p53 ³⁷⁻⁵⁷ titration with FOXO4 ⁸⁶⁻²⁰⁸	62
Figure 27: Chemical shift perturbation of ^{15}N p53 ³⁷⁻⁵⁷ upon titration with FOXO4 ⁸⁶⁻²⁰⁸	63
Figure 28: Phosphorylation Assay: 100 μM ^{15}N p53 ¹⁻⁹⁴ in presence of HEK293T cell lysate after 1 hour of incubation.....	64
Figure 29: Phosphorylation Assay: 100 μM ^{15}N p53 ¹⁻⁹⁴ in presence of HEK293T cell lysate after 1 hour of incubation.....	65
Figure 30: Zoom-in on ^1H - ^{15}N HSQC Spectra of ^{15}N p53 ¹⁻⁹⁴ (left) and of ^{15}N p53 ^{1-9 4S46E} titration with FOXO4 ⁸⁶⁻²⁰⁸	66
Figure 31: Complex Structures of p53	69
Figure 32: Putative schematic pathway of the FOXO - p53 interplay in senescence and apoptosis	71

Abbreviations

AMPK	AMP-activated protein kinase
AP1	Activator protein 1
ATM	Ataxia Telangiectasia mutated
ATP	Adenosintriphosphat
BAX	BCL2 associated X protein
BC	Before Christ
BCL2	B-cell CLL/lymphoma 2
BIM	Bcl-2-like protein 11
BRAF	B-Raf proto-oncogene
BRCA1	Breast cancer 1
CDK	Cyclin Dependent Kinase
Chk	Checkpoint kinase
CREB	cAMP Response Element Binding Protein
DNA	Desoxyribonucleic Acid
DNA SCARS	DNA segments with chromatin alterations reinforcing senescence
DNMT	DNA Methyltransferase
dNTP	Desoxynucleoside Triphosphate
DRI	D-retro inverso
E2F7	Transcription factor E2F7
ETDA	Ethylenediaminetetraacetic acid
Ets	E26 transformation-specific
FOXO	Forkhead Box Protein
FPLC	Fast protein liquid chromatography
H2AX	H2A Histone Family Member X
HetNOE	Heteronuclear Nuclear Overhauser Effect
HIPK2	Homeodomain-interacting protein kinase 2
HSQC	Heteronuclear Quantum Coherence
IGF-1	Insulin-like growth factor 1
IPTG	isopropyl β -D-1-thiogalactopyranoside
JNK	c-Jun N-terminal kinases
Kd	dissociation constant
kDa	Kilo-Dalton
LB	Lysogeny broth
M	Molar
MDM2	Mouse double minute 2 homolog
MST	Microscale Thermophoresis
mTOR	mechanistic target of rapamycin
Ni-NTA	nickel - nitrilotriacetic acid
nm	Nanometer
NMR	Nuclear Magnetic Resonance
NOE	Nuclear Overhauser Effect

NORE1A	Ras associated domain-containing protein
OD	Optical Density
p53	Cellular Tumor Antigen p53
PAGE	Polyacrylamide Gelectrophoresis
PCR	Polymerase Chain Reaction
PI3K	Phosphatidylinositol-4,5-bisphosphate 3-kinase
PPAR γ	Peroxisome proliferator-activated receptor γ
PRAK	MAP kinase-activated protein kinase 5
PUMA	p53 upregulated modulator of apoptosis
RB	Retinoblastoma Protein
ROS	Reactive Oxygen Species
SASP	Senescence Associated Secretory Phenotype
SAXS	Small-angle X-ray Scattering
SDS	Sodium dodecyl Sulfate
SIRT1	NAD-dependent deacetylase sirtuin-1
Smad	Mothers against decapentaplegic homolog 2
Sp1	Specificity protein 1
TEV	Tobacco etch virus
TGF- β	Transforming growth factor beta
TNF- β	Tumor Necrosis Factor beta

Appendix II

Figure Licences

Figure 2:

Uversky VN. p53 Proteoforms and Intrinsic Disorder: An Illustration of the Protein Structure-Function Continuum Concept. *Int J Mol Sci.* 2016;17(11).

Licensed by CC BY 4.0

This is an open access article distributed under the Creative Commons Attribution License which permits unrestricted use, distribution, and reproduction in any medium.

Figure 8:

Teilum K, Kunze MB, Erlendsson S, Kragelund BB. (S)Pinning down protein interactions by NMR. *Protein Sci.* 2017;26(3):436-51.

Licensed by CC BY 4.0

This is an open access article distributed under the Creative Commons Attribution License which permits unrestricted use, distribution, and reproduction in any medium.

Figure 9:

Reprinted by permission from Springer Nature:

Brutscher B, Felli IC, Gil-Caballero S, Hosek T, Kummerle R, Piai A, et al. NMR Methods for the Study of Intrinsically Disordered Proteins Structure, Dynamics, and Interactions: General Overview and Practical Guidelines. *Adv Exp Med Biol.* 2015;870:49-122.

SPRINGER NATURE LICENSE TERMS AND CONDITIONS

Oct 07, 2018

This Agreement between Mr. Emil Spreitzer ("You") and Springer Nature ("Springer Nature") consists of your license details and the terms and conditions provided by Springer Nature and Copyright Clearance Center.

License Number

License date

Licensed Content Publisher Licensed Content Publication Licensed Content Title

Licensed Content Author Licensed Content Date Type of Use

Requestor type

Format Portion

Number of figures/tables/illustrations

Will you be translating?

Circulation/distribution

Author of this Springer Nature content

Title

Instructor name

Institution name

Expected presentation date Portions

Requestor Location

Billing Type Billing Address

4443520284025 Oct 07, 2018 Springer Nature Springer eBook

NMR Methods for the Study of Intrinsically Disordered Proteins Structure, Dynamics, and Interactions: General Overview and Practical Guidelines

Bernhard Brutscher, Isabella C. Felli, Sergio Gil-Caballero et al Jan 1, 2015

Thesis/Dissertation

academic/university or research institute

print and electronic figures/tables/illustrations 26

no <501 no

Regulation of Cellular Senescence Tobias Madl

Medical University Graz

Nov 2018

Figure 3.26

Mr. Emil Spreitzer Straßengelstraße 21/1

Graz, Steiermark 8051 Austria
Attn: Mr. Emil Spreitzer

Invoice

Mr. Emil Spreitzer Straßengelstraße 21/1

<https://s100.copyright.com/App/PrintableLicenseFrame.jsp?publis...2895-4403-8c30-721c4d72d5c8%20%20&targetPage=printablelicense> Seite 1 von 4

RightsLink Printable License 07.10.18, 09)56

Graz, Austria 8051 Attn: Mr. Emil Spreitzer

Total 0.00 EUR [Terms and Conditions](#)

Springer Nature Terms and Conditions for RightsLink Permissions Springer Nature Customer Service Centre GmbH (the Licensor) hereby grants you a non-exclusive, world-wide licence to reproduce the material and for the purpose and requirements specified in the attached copy of your order form, and for no other use, subject to the conditions below:

1. The Licensor warrants that it has, to the best of its knowledge, the rights to license reuse of this material. However, you should ensure that the material you are requesting is original to the Licensor and does not carry the copyright of another entity (as credited in the published version).

If the credit line on any part of the material you have requested indicates that it was reprinted or adapted with permission from another source, then you should also seek permission from that source to reuse the material.

2. Where **print only** permission has been granted for a fee, separate permission must be obtained for any additional electronic re-use.
3. Permission granted **free of charge** for material in print is also usually granted for any electronic version of that work, provided that the material is incidental to your work as a whole and that the electronic version is essentially equivalent to, or substitutes for, the print version.
4. A licence for 'post on a website' is valid for 12 months from the licence date. This licence does not cover use of full text articles on websites.
5. Where '**reuse in a dissertation/thesis**' has been selected the following terms apply: Print rights of the final author's accepted manuscript (for clarity, NOT the published version) for up to 100 copies, electronic rights for use only on a personal website or institutional repository as defined by the Sherpa guideline (www.sherpa.ac.uk/romeo/).
6. Permission granted for books and journals is granted for the lifetime of the first edition and does not apply to second and subsequent editions (except where the first edition permission was granted free of charge or for signatories to the STM Permissions Guidelines <http://www.stm-assoc.org/copyright-legal-affairs/permissions/permissions-guidelines/>), and does not apply for editions in other languages unless additional translation rights have been granted separately in the licence.
7. Rights for additional components such as custom editions and derivatives require additional permission and may be subject to an additional fee. Please apply to

Journalpermissions@springernature.com/bookpermissions@springernature.com for these rights.

8. The Licensor's permission must be acknowledged next to the licensed material in print. In electronic form, this acknowledgement must be visible at the same time as the figures/tables/illustrations or abstract, and must be hyperlinked to the journal/book's homepage. Our required acknowledgement format is in the Appendix below.
9. Use of the material for incidental promotional use, minor editing privileges (this does not include cropping, adapting, omitting material or any other changes that affect the meaning, intention or moral rights of the author) and copies for the disabled are permitted under this licence.

<https://s100.copyright.com/App/PrintableLicenseFrame.jsp?publi...-2895-4403-8c30-721c4d72d5c8%20%20&targetPage=printablelicense> Seite 2 von 4

RightsLink Printable License 07.10.18, 09)56

10. Minor adaptations of single figures (changes of format, colour and style) do not require the Licensor's approval. However, the adaptation should be credited as shown in Appendix below.

Appendix — Acknowledgements:

For Journal Content:

Reprinted by permission from [**the Licensor**]: [**Journal Publisher** (e.g. Nature/Springer/Palgrave)] [**JOURNAL NAME**] [**REFERENCE CITATION** (Article name, Author(s) Name), [**COPYRIGHT**] (year of publication)]

For Advance Online Publication papers:

Reprinted by permission from [**the Licensor**]: [**Journal Publisher** (e.g. Nature/Springer/Palgrave)] [**JOURNAL NAME**] [**REFERENCE CITATION** (Article name, Author(s) Name), [**COPYRIGHT**] (year of publication), advance online publication, day month year (doi: 10.1038/sj.[**JOURNAL ACRONYM**].)]

For Adaptations/Translations:

Adapted/Translated by permission from [**the Licensor**]: [**Journal Publisher** (e.g. Nature/Springer/Palgrave)] [**JOURNAL NAME**] [**REFERENCE CITATION** (Article name, Author(s) Name), [**COPYRIGHT**] (year of publication)]

Note: For any republication from the British Journal of Cancer, the following credit line style applies:

Reprinted/adapted/translated by permission from [**the Licensor**]: on behalf of Cancer Research UK: : [**Journal Publisher** (e.g. Nature/Springer/Palgrave)] [**JOURNAL NAME**] [**REFERENCE CITATION** (Article name, Author(s) Name), [**COPYRIGHT**] (year of publication)]

For Advance Online Publication papers:

Reprinted by permission from The [**the Licensor**]: on behalf of Cancer Research UK: [**Journal Publisher** (e.g. Nature/Springer/Palgrave)] [**JOURNAL NAME**] [**REFERENCE CITATION** (Article name, Author(s) Name), [**COPYRIGHT**] (year

of publication), advance online publication, day month year (doi: 10.1038/sj.
[JOURNAL ACRONYM])

For Book content:

Reprinted/adapted by permission from [**the Licensor**]: [**Book Publisher** (e.g. Palgrave Macmillan, Springer etc) [**Book Title**] by [**Book author(s)**] [**COPYRIGHT**] (year of publication)

Other Conditions: Version 1.1

Questions? customercare@copyright.com or +1-855-239-3415 (toll free in the US) or +1-978-646-2777.